Aus dem Zentrum für Kinder- und Jugendmedizin
der Universität zu Köln
Direktor: Universitätsprofessor Dr. med. J. Dötsch

The role of matrix metalloproteinase-12 (MMP-12) in hyperoxia-induced lung injury in a mouse model of bronchopulmonary dysplasia

Inaugural-Dissertation
zur Erlangung der Doktorwürde
der Medizinischen Fakultät
der Universität zu Köln

vorgelegt von
Pınar Haznedar-Karakaya
aus Çankaya (Ankara)/Türkei

promoviert am 08. März 2023

Gedruckt mit Genehmigung der Medizinischen Fakultät der Universität zu Köln
2023

Dekan: Universitätsprofessor Dr. med. G. R. Fink
1. Gutachter: Universitätsprofessor Dr. med. Dr. nat. med. M. A. Alejandre Alcázar
2. Gutachterin: Professorin Dr. med. P. Moinzadeh

Erklärung

Ich erkläre hiermit, dass ich die vorliegende Dissertationsschrift ohne unzulässige Hilfe Dritter und ohne Benutzung anderer als der angegebenen Hilfsmittel angefertigt habe; die aus fremden Quellen direkt oder indirekt übernommenen Gedanken sind als solche kenntlich gemacht.

Bei der Auswahl und Auswertung des Materials sowie bei der Herstellung des Manuskriptes habe ich die Unterstützung von Jun.-Prof. Dr. Dr. nat. med. Miguel A. Alejandre Alcázar, von Dr. nat. med. Dharmesh Hirani, von Frau Dr. med. vet. Katharina Dinger und von Frau Christina Vohlen erhalten.

Weitere Personen waren an der Erstellung der vorliegenden Arbeit nicht beteiligt. Insbesondere habe ich nicht die Hilfe einer Promotionsberaterin/eines Promotionsberaters in Anspruch genommen. Dritte haben von mir weder unmittelbar noch mittelbar geldwerte Leistungen für Arbeiten erhalten, die im Zusammenhang mit dem Inhalt der vorgelegten Dissertationsschrift stehen.

Die Dissertationsschrift wurde von mir bisher weder im Inland noch im Ausland in gleicher oder ähnlicher Form einer anderen Prüfungsbehörde vorgelegt.

Die in dieser Arbeit angegebenen Experimente sind nach entsprechender Anleitung durch Herrn Dr. nat. med. Dharmesh Hirani und Frau Dr. med. vet. Katharina Dinger von mir selbst ausgeführt worden.

Die dieser Arbeit zugrunde liegenden Experimente sind von mir mit Unterstützung von Biologielaborantin Frau Christina Vohlen und der biologisch-technischen Assistentin Frau Rebecca Wilke durchgeführt worden

Erklärung zur guten wissenschaftlichen Praxis:

Ich erkläre hiermit, dass ich die Ordnung zur Sicherung guter wissenschaftlicher Praxis und zum Umgang mit wissenschaftlichem Fehlverhalten (Amtliche Mitteilung der Universität zu Köln am 132/2020) der Universität zu Köln gelesen habe und verpflichte mich hiermit, die dort genannten Vorgaben bei allen wissenschaftlichen Tätigkeiten zu beachten und umzusetzen.

Köln, den 26.10.2022 ..... (Pınar Haznedar-Karakaya)

Acknowledgements

Foremost, I would like to express my sincere gratitude to my advisor Prof. Dr. M. A. Alejandre Alcázar for giving me the opportunity to work on this project, for his unlimited support and guidance of my doctorate study and research, and valuable feedback helping me to grow as a scientist and clinician.

I would like to highlight two truly exceptional people from AG Alcázar: Dr. Dharmesh Hirani and Christina Vohlen. Thank you for your intensive support and valuable advice, as well as numerous instructions in the use of the necessary equipment and procedures. I would also like to extend my thanks to my fellow labmates for making my doctorate study a real fun experience.

A special thanks to my two best friends: Duygu Gerceker and Ipek Oralalp. Thank you for always being there for me and motivating me to accomplish my personal goals.

Finally, I am deeply grateful to my husband and my cat for their unconditional and endless support, encouragement, and warmest of hugs. You are the reason I keep pushing. I would also like to thank my parents and my brother for supporting me through medical school, residency, and throughout the years of this study in Germany and through the process of writing this thesis.

To Mert, Nil, and Igor

Table of Contents

Abbreviation list

AEC	Alveolar epithelial cell
Aq5	Aquaporin-5
Arg1	Arginase-1
BAL	Bronchoalveolar lavage
BPD	Bronchopulmonary dysplasia
cDNA	Complementary DNA
Col-1	Collagen type 1
Col-3	Collagen type 3
COPD	Chronic obstructive pulmonary disease
Ct	Cycle threshold
CTGF	Connective tissue growth factor
CXCL-10	C-X-C motif chemokine 10
DEPC	Diethyl dicarbonate
dNTP	Deoxyribonucleoside triphosphate
dUTP	Deoxyuridin triphosphate
ECM	Extracellular matrix
EDTA	Ethylenediaminetetraacetic acid
Eln	Elastin
EMT	Epithelial mesenchymal transition
EtOH	Ethanol
GAPDH	Glyceraldehyde 3-phosphate dehydrogenase
HCL	Hydrochloric acid
H&E	Hematoxylin and eosin
HYX	Hyperoxia
Hz	Hertz
IL	Interleukin
M1	Classically activated macrophages
M2	Alternatively activated macrophages
MFAP4	Microfibrillar-associated protein 4
MLI	Mean linear intercept
MMP	Matrix metalloproteinase

NOX	Normoxia
Oligo-dt-primer	Oligodeoxytimidine primer
PAI-1	Plasminogen activator inhibitor-1
PCNA	Proliferating cell nuclear antigen
PCR	Polymerase chain reaction
PECAM-1	Platelet endothelial cell adhesion molecule 1
PSR	Picrosirius Red
pStat3	Phosphorylated Stat3
qRT-PCR	Real-Time Quantitative Reverse Transcription PCR
RDS	Respiratory distress syndrome
Rpm	Rotation per minute
RT	Room temperature
SA	Surface area
SDS	Sodium dodecyl sulfate
SEM	Standard error of the mean
SNAI1	Zinc finger protein 1(Snail)
SNAI2	Zinc finger protein 2(Slug)
STAT1	Signal transducer and activator of transcription 1
STAT3	Signal transducer and activator of transcription 3
SMAD2/3	Mothers against decapentaplegic homolog 2/3
SP	Surfactant protein
ST	Septal thickness
TAMRA	Carboxytetramethylrhodamine
TGF- β	Transforming growth factor-β
TLR-4	Toll-like receptor 4
VEGF	Vascular endothelial growth factor
WT	Wild type
α-SMA	α-smooth muscle actin
βME	β-Mercaptoethanol

1. Abstract

Premature infants who are exposed to prolonged oxygen (O_2) therapy often develop Bronchopulmonary Dysplasia (BPD), a chronic inflammatory lung disease characterized by reduced alveolar formation and matrix remodelling. Matrix metalloproteinase-12 (MMP-12) is an important regulator of the extracellular matrix (ECM) and involved in the pathogenesis of lung diseases, e.g., chronic obstructive pulmonary disease (COPD) and emphysema. Since MMP-12 regulates elastic fibers, inflammation, and angiogenesis, we hypothesized that MMP-12 deficiency enables alveolar growth in hyperoxia-induced neonatal lung injury as a model of BPD. Specifically, we investigated the role of MMP-12 in (1) alveolar structure and pulmonary angiogenesis, (2) extracellular matrix metabolism as well as (3) macrophage activation.

To address these research questions, newborn wildtype mice (WT) and MMP-12 deficient mice ($MMP12^{-/-}$) were exposed to either hyperoxia (85% O_2) or normoxia (21% O_2) from postnatal day 1 (P1) to P14. Starting at P15 all animals were exposed to 21% O_2 for recovery. At P28, lungs were excised *en bloc* and the tissue samples were either snap-frozen in liquid nitrogen or pressure-fixed in paraformaldehyde for molecular and biochemical investigations as well as quantitative histomorphometry and immunostainings.

(1) Quantitative histomorphometric analyses revealed that lungs of WT animals had reduced alveolar and microvascular formation after hyperoxia; however, these pathological changes were significantly attenuated in $MMP12^{-/-}$ mice when compared to WT. (2) The assessment of elastic fibers and collagen showed that the distorted elastic fibers and the increase of collagen observed in WT animals after hyperoxia and indictive for fibrotic processes, were mitigated in lungs of $MMP12^{-/-}$ mice. In addition to these morphological improvements, the loss of MMP-12 promoted the gene expressions of surfactant proteins (*Stfpb, Stfpc*) and prevented the activation of TGF-β signalling under hyperoxia. (3) Finally, $MMP12^{-/-}$ mice were protected from macrophage influx after hyperoxia.
In summary, the present study demonstrates that loss of MMP-12 enables alveolar and microvsascular formation, attenuates matrix remodelling and mitigates inflammation in neonatal lungs after hyperoxia, offering a possible new therapeutic target to treat BPD.

Zusammenfassung

Frühgeborene, die einer längeren Sauerstofftherapie (O_2) ausgesetzt sind, entwickeln häufig eine bronchopulmonale Dysplasie (BPD), eine chronische entzündliche Lungenerkrankung, die durch eine verminderte Alveolenbildung und einen Bindegewebsumbau gekennzeichnet ist. Matrix-Metalloproteinase-12 (MMP-12) ist ein wichtiger Regulator der extrazellulären Matrix (ECM) und an der Pathogenese von Lungenkrankheiten, z. B. der chronisch obstruktiven Lungenerkrankung (COPD) und des Emphysems, beteiligt. Da MMP-12 elastische Fasern, Entzündung und die Angiogenese reguliert, untersuchten wir die Hypothese, dass ein MMP-12-Mangel das alveoläre Wachstum bei einer durch Hyperoxie verursachten neonatalen Lungenschädigung als Modell für BPD ermöglicht. Konkret untersuchten wir die Rolle von MMP-12 bei (1) der Alveolenbildung und der pulmonalen Angiogenese, (2) der ECM, sowie (3) der Makrophagenaktivierung.

Um diese Forschungsfragen zu beantworten, wurden neugeborene Wildtyp-Mäuse (WT) und MMP-12-defiziente Mäuse ($MMP12^{-/-}$) entweder Hyperoxie (85% O_2) oder Normoxie (21% O_2) vom postnatalen Tag 1 (P1) bis P14 ausgesetzt. Ab P15 wurden alle Tiere zur Erholung unter 21% O_2 gehalten. An P28 wurden die Lungen *en bloc* exzidiert und entweder in flüssigem Stickstoff schockgefroren oder mit Paraformaldehyd druckfixiert, um molekulare und biochemische Untersuchungen sowie quantitative Histomorphometrie und Immunfärbungen durchzuführen.

(1) Quantitative histomorphometrische Analysen zeigten, dass in Lungen von WT-Tieren nach Hyperoxie eine reduzierte alveoläre und mikrovaskuläre Ausbildung; diese pathologischen Veränderungen waren jedoch bei $MMP12^{-/-}$ Mäusen im Vergleich zu WT signifikant abgeschwächt. (2) Die Untersuchung der elastischen Fasern und des Kollagens zeigte, dass die gestörten elastischen Fasern und die Zunahme des Kollagens in Lungen von $MMP12^{-/-}$ Mäusen nach Hyperoxie im Vergleich zu WT-Tieren abgeschwächt waren. Zusätzlich zu diesen morphologischen Verbesserungen förderte der Verlust von MMP-12 die Expression von Genen, die für Surfactant-Proteine kodieren, und verhinderte die Aktivierung des TGF-β-Signalwegs unter Hyperoxie. (3) Zudem waren $MMP12^{-/-}$ Mäuse vor dem Einstrom von Makrophagen nach Hyperoxie geschützt.

Zusammenfassend zeigt die vorliegende Studie, dass der Verlust von MMP-12 unter Hyperoxie die Alveolen- und Mikrogefäßbildung ermöglicht, den Matrixumbau abschwächt und die

Entzündung in der neonatalen Lunge mildert. Somit stellt MMP12 einen möglichen neuen therapeutischen Angriffspunkt zur Behandlung der BPD dar.

2. Introduction

2.1 Lung Development

2.1.1 Physiological Lung Development

The development of a healthy lung consists of two phases: structural and functional. The first phase is structural development, which is also referred to as lung growth, and the second is functional development which comprises of biochemical development of the surfactant proteins (lung maturation). The lung growth begins around the 4th gestational week. From the 4th to 7th week, the development of the primitive lung bud from the laryngotracheal sulcus can be observed, as a projection of the midline endoderm; whereas, cartilage, muscles, connective tissue, and vessels begin to develop from the mesoderm [1]. Lung organogenesis, developmental stages as well as signaling pathways and biological processes are conserved in humans and most rodents (e.g., mice, rats). Structural lung growth is divided into five developmental stages (Figure 1). The explanation of lung development that follows is based on human lung development.

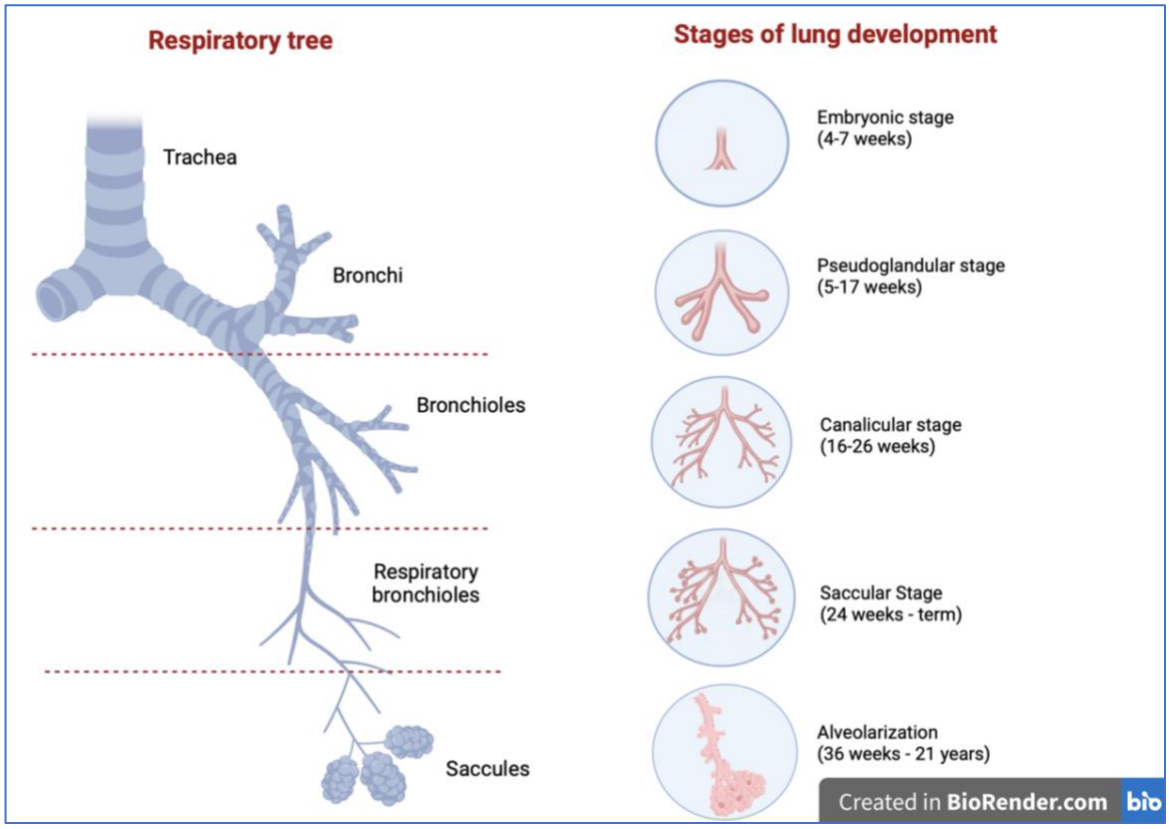

Figure 1. Schematic depiction of lung development and maturation

2.1.1.1 Embryonic Stage

The embryonic stage can be observed from the 4th to 7th gestation week, in which right and left lungs appear as two independent outpouchings and are located at both sides of the anlage of the trachea. During this time, the anlage of the two main bronchi develops from the lung bud at the lower end of the laryngotracheal groove [2]. Further dividing and branching, also referred to as branching morphogenesis; development of pulmonary artery and veins in the form of an avascular bud, occur also in this stage. At the end of the embryonic period, the first appendices of the segmental bronchial appear [1].

2.1.1.2 Pseudoglandular Stage

The pseudoglandular stage is between the 5th and 17th gestational weeks, where the formation of the bronchial tree first can be observed. During this stage, almost all of the branches of the conducting (non-respiratory) airways and approximately 70% of the future respiratory tree develop [3].

2.1.1.3 Canalicular Stage

The canalicular stage takes place between the 16th to 26th weeks. This stage comprises the transformation of distal non-respiratory bronchioles (terminal bronchioles) into primitive respiratory bronchioles and to the alveolar duct. As a result of widening distal air spaces, a ‘canaliculus’ is formed and an enhanced capillary density is observed at the same time due to intensive angiogenesis. This leads to close contact between alveolar epithelium and mesenchymal capillaries to form the future ‘air-blood barriers.’ The differentiation of the parenchymal epithelium into type I and type II alveolar epithelial cells (AEC) begins at this stage. AECIs are the primary structural cells of the alveoli and enable the gas exchange through their thin membrane-like formation. AECIIs are in charge of surfactant synthesis [1,2]. Another key function of AECIIs is to act as progenitor cells in the lungs, where they proliferate and develop into AECIs in response to lung injury [4,5].

2.1.1.4 Saccular Stage

The saccular stage encompasses the period from 24 weeks to 38 weeks. During this time, the alveolar duct system grows extensively, and the surface area of the air spaces increases resulting in a significant expansion for the future gas exchange region. Alveoli can be recognized at 32 weeks but more prominent by 36 weeks. Mesenchymal cells also undergo differentiation, producing extracellular matrix, including collagens, and components of elastic fibers. Vascular-alveolar duct arteries and the vascular tree grow in length and diameter during this stage [1,6].

2.1.1.5 Alveolar Stage

The indication of the alveolar stage is the recognition of secondary septa in the terminal airway followed by the formation of the definitive cup-shaped alveoli. Microvascular maturation also occurs during this period. Double capillary layers that are found in the secondary septa merge into one layer, which contribute to the formation of the thinner gas exchange regions [7]. Alveolarization begins shortly before birth and continues beyond 3 years of age. During postnatal development, the alveoli continue to subdivide through a process of septation resulting in a consecutive increase of the gas exchange surface area [1].

2.1.2 Continued Alveolarization During Lung Development

Alveolarization is the last stage of lung development, in which the most distal parts of the lung are formed and maturated. In rats and mice, alveolarization is a postnatal process, whereas, in humans, it begins just before birth. Therefore, mice and rodents are an ideal model to study adverse postnatal influences (e.g., oxygen or mechanical ventilation) on immature (premature) lungs. In humans, at birth, a newborn has approximately 50 million alveoli. The number of alveoli continues to increase six times by the age of eight years [2]. Alveoli are responsible for the gas exchange, which is the key physiological function of the lungs. This procedure requires a proper formation of the delicate alveolar structure. Due to malformations or destructions, this delicate structure of the alveoli can be damaged and diseases such as bronchopulmonary dysplasia (BPD) may occur.

Alveolarization is a three-phase process: The first phase is the secondary septation, which is characterized by the formation of new alveolar septa within the terminal sacs. The second phase

is the extensive remodeling of the capillary network around the alveoli. Finally, the third phase is the growth of all lung components; which takes place after two years of age [6,8].

The simple and effective alveolar structure begins to form in the saccular stage of lung development, in which the air sacs are lined with an epithelial layer that originates from the foregut endoderm. This structure consists of two types of cells: AECIs and alveolar AECIIs. AECI is flattened, thin cells that cover about 95% of the alveolar surface area, which represent the site of gas exchange. AECII cells are rather cuboidal and found in the alveolar corners. They acquire stem cell properties; they can divide and repair the damaged epithelium in need, as well as secrete surfactant which decreases the surface tension of alveoli [5,9].

The extracellular matrix (ECM) is another key player which is involved in alveolar formation and maturation. The ECM consists of a group of molecules that are secreted by the cells encircling them. They provide mechanical support, tissue elasticity, and integrity. An important molecule of ECM is elastin, which is the central molecule for proper assembly of elastic fibers during the alveolar growth with the goal to form a network for future alveoli and blood vessels [10]. It is shown that during the secondary septation, elastin expression increases, which plays an important role in the formation of alveoli. Secondary crests are in part formed by elastic fibers, which are mainly a network of cross-linked elastin and fibrillin. This assembly further interacts with other accessory molecules, such as microfibril-associated proteins, fibulins, and emilins. Together with the deposition of elastic fibers, collagen fibers that are interwoven at the secondary crests also play a role in this process [11,12].

The alveolar septal transformation also involves epithelial, endothelial, and mesenchymal (e.g., myofibroblasts, lipofibroblasts, fibroblasts) cells [13]. Mesenchymal cells play a central role in alveolarization. Myofibroblasts are contractile cells and are the primary secretary source of the ECM [14]. Lipofibroblasts are found adjacent to AECIIs and contain lipids (e.g., triglycerides, cholesterol esters) that maintain epithelial cell homeostasis (e.g., surfactant synthesis, protection against oxidative stress) [15].

Smooth muscle cell precursors, elastic fibers, and collagen fibrils migrate and accumulate to the appropriate location of the emerging alveolar septa while myofibroblast cells synthesize and store elastin. Expansion of the epithelial and endothelial components and apoptosis of myofibroblasts leads to thinning of the alveolar septa. Although most of the septa are immature at the beginning

of the formation due to the double-layered capillary network; their thinning takes place simultaneously with the capillary remodeling of a double-layered capillary network towards a simple circuit. Eventually, the new septum consists of alveolar epithelial cells, basal lamina, and endothelial cells. AECs line the alveoli and, together with the basement membrane and the capillary endothelial cell, form the diffusion path for gas exchange [7].

2.1.3 Mechanisms Involved in Lung Development

The respiratory system develops from a series of complex events which is controlled by various factors. The elements of lung development include physical and chemical factors, such as intraluminal hydraulic pressure, relative hypoxia or calcium concentration as well as transcription factors, growth factors, and various other signaling molecules that regulate epithelial-mesenchymal interactions by paracrine and autocrine mechanisms [9]. These growth/transcription factors and/or signaling molecules are genetically programmed to be expressed properly and appropriately to control normal lung formation at the right time. However, the same factors not only regulate lung development but also play a critical role in lung injury, repair, and fibrosis [16].

2.1.3.1 Transcription Factors

Transcription factors are intracellular proteins that are found in the nucleus and regulate gene expression of dynamic processes such as development and injury/repair of the lung. Notable transcription factors include, e.g., insulin-like growth factor-1, forkhead box transcription factor family, and GATA binding protein-6, which have roles in regulating the expression of genes involved in cell growth, proliferation, and differentiation [17].

2.1.3.2 Growth Factors

Peptide growth factors and other molecules in their signal pathways play important regulatory roles in controlling different stages of lung morphogenesis such as lung bud formation, branching morphogenesis, and formation of the capillary network. Many of these factors are not only a part of the developmental processes but also play a role in lung injury, repair, or lung pathologies such as pulmonary fibrosis. The expressions of their target genes are often controlled by transcription factors [18].

The transforming growth factor-β (TGF-β) superfamily consists of numerous structurally similar polypeptides such as TGF-β isoforms, activin, bone morphogenetic proteins, growth, and

differentiation factors. TGF-β is a pleiotropic factor that has the function of regulating biological processes and mechanisms such as development, tissue regeneration, immune responses, or tumorigenesis. It is shown through transgenic mouse models that TGF-β is evolutionarily conserved and plays an important role in lung organogenesis and homeostasis. TGF-β also has a pivotal role in branching morphogenesis and alveolarization [19].

Another important group of endothelial growth factors is the vascular endothelial growth factor (VEGF) family, which has been identified as a key driver of angiogenesis, vasculogenesis, and lymphangiogenesis. VEGF stimulates vascular growth in the developing lung while also contributing in the formation of the alveolar capillary network [20].

2.1.3.3 Extracellular Matrix

Extracellular matrix (ECM) is a multifunctional network of structurally, mechanically, and biochemically heterogeneous components which consists of an interstitial matrix and a basement membrane. It appoints an anchorage for cells, regulates communication within the cell, and helps the formation of a tissue scaffold; and is continuously remodeled as the lung continues to grow. The protein content comprises collagen, elastin, fibrillin, fibulin, glycoproteins, and integrin receptors of ECM components [11].

The most abundant protein present in the interstitial ECM is collagen, which can be found around the bronchi, blood vessels, and alveolar septa. The abundance of collagen offers a delicate interstitial network that helps the process of alveolarization. The expression of elastin is actively regulated during the alveolarization period. The pronounced expression, however, occurs during the secondary septation, the time when the alveolarization is at its peak point. Fibrillins act as elastin binding glycoproteins and regulate the proper formation of elastic fibers by mediating protein-protein interactions between EMC proteins, fibulins, and emilins. Cross-linked elastin and fibrillin microfibrils make up elastic fibers.[11].

The mechanical properties of the ECM are primarily determined by macromolecular collagen, elastin, and proteoglycans; in addtiiton, adhesion proteins help in the binding of cells to the ECM. The degradation of ECM molecules is important for growth processes and wound healing. [21]. A group of endopeptidases known as matrix metalloproteinases (MMPs) play an important role in this process, as they are capable of breaking down the components of the ECM and basement membrane as well as remodeling. MMPs are important regulators of tissue homeostasis and

immunity and play an important role in a variety of cell biological processes. Different MMPs degrade different components of the ECM; for example, MMP-2 and 9 degrade basement membrane collagen, fibronectin, or elastin, whereas MMP-1 and 8 target fibrillar collagen. [22].

2.1.3.4 Cell-Cell Interactions

One of the key functions of epithelium and endothelium is to form a diffusion barrier, such as the one found in the blood-air barrier in which interactions between lung epithelial cells and microvascular endothelial cells occur. These single-layer cell layers are essential to minimize leakage of blood plasma and blood cells into the pulmonary interface. Cell-cell contacts require adhesion proteins that bind to each other to form an intracellular cytoskeleton. These proteins not only have a structural function but also allow intracellular signal transduction and regulation of transcription [23].

2.2 Bronchopulmonary Dysplasia

2.2.1 Definition of Bronchopulmonary Dysplasia

Bronchopulmonary Dysplasia (BPD) is a chronic inflammatory lung disease that is commonly seen in preterm infants who need prolonged oxygen therapy and/or mechanical ventilation due to acute respiratory failure (Figure 2). The morbidity and risk of developing BPD remain high and the rate of incidence lies by 40 percent for very preterm infants (< 32 weeks of gestation), despite improvements in neonatal medicine and increased survival of very preterm infants [24,25].

BPD was first described by Northway and colleagues in 1967, which is today referred to as *'Classical BPD',* as a disease that occurs in moderately premature infants (32 – 34 weeks of gestation) with surfactant deficiency whose lungs are adversely affected due to high concentrations of oxygen and ventilation-induced volutrauma. The *'New BPD'* emerged with the use of antenatal steroids, postnatal surfactant and current neonatal treatment, diet, and respiratory management being predominant, showing signs of milder pulmonary sequelae with less fibrosis but histopathological evidence of arrested lung development [26].

The newer criteria for BPD is as follows according to the National Institute of Health (USA) for neonates treated with more than 21% oxygen for at least 28 days (Table 1):

Table 1. Classification and criteria of BPD.

Mild	Moderate	Severe
Breathing room air at 36 weeks' post-menstrual age or discharge (whichever comes first) for babies born before 32 weeks	Need for <30% oxygen at 36 weeks' postmenstrual age, or discharge (whichever comes first) for babies born before 32 weeks	Need for >30% oxygen, with or without positive pressure ventilation or continuous positive pressure at 36 weeks' postmenstrual age, or discharge (whichever comes first) for babies born before 32 weeks
Breathing room air by 56 days' postnatal age, or discharge (whichever comes first) for babies born after 32 weeks' gestation	Need for <30% oxygen to 56 days' postnatal age, or discharge (whichever comes first) for babies born after 32 weeks' gestation	Need for >30% oxygen with or without positive pressure ventilation or continuous positive pressure at 56 days' postnatal age, or discharge (whichever comes first) for babies born after 32 weeks' gestation

2.2.2 Epidemiology

The latest global estimates show that approximately 5% to 18% of all live births globally were preterm (< 37 weeks of gestation) and can be further classified as very preterm (< 32 weeks of gestation) and extremely preterm (< 28 weeks of gestation) [27]. Very preterm infants are born during the saccular stage of lung development. During this stage, infants do not have a definitive structure of alveoli for gas exchange and can only produce limited amounts of surfactant. Today, BPD is still one of the most common complications of prematurity and can have a significant impact on lifelong pulmonary function and pulmonary sequelae, and adverse neurodevelopmental outcomes [25].

Despite the discussion about the trend of the incidence of BPD, the risk of developing BPD remains inversely related to gestational age and birth weight. Although major treatment advances are now available, the incidence is still above 30% in preterm infants who are born before the 30th week of gestation. Even though the mortality rate of preterm infants younger than 32-week-gestational age has been dramatically decreased with the development of neonatal medicine, the morbidity of these infants has increased. Studies show that 40-50% of surviving preterm infants develop and suffer from BPD, also referred to as neonatal chronic lung disease [26]. The prevalence

of BPD, as well as mortality and morbidity rate, varies between clinics and institutions. This disparity is most likely due to differences in newborn birthweights, diagnostic criteria, and non-standardized therapies amongst study populations [28].

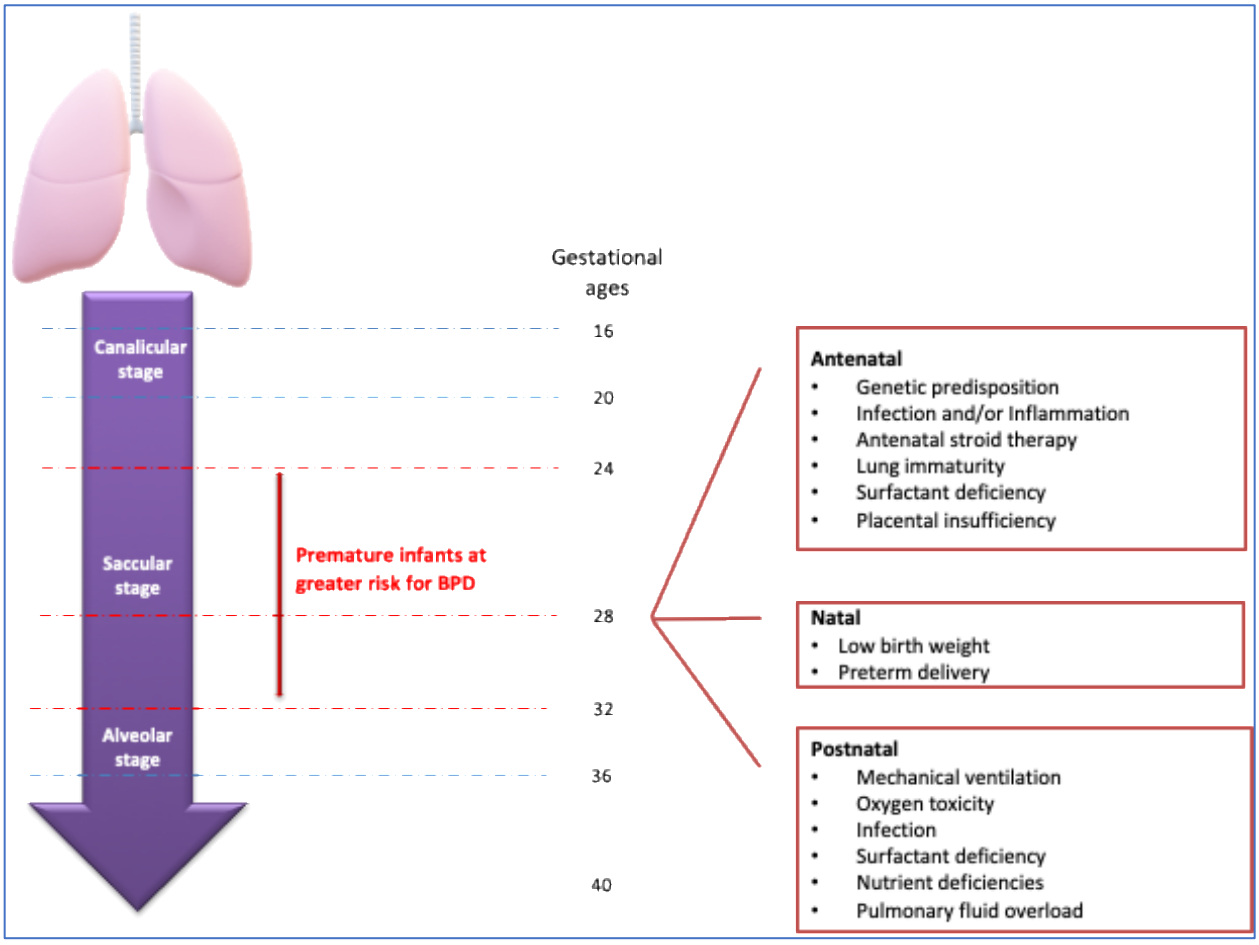

Figure 2. Risk factors for developing bronchopulmonary dysplasia (BPD)

2.3 Pathophysiology of Bronchopulmonary Dysplasia

2.3.1 Histopathology and Classification of Bronchopulmonary Dysplasia

The clinical picture of '*classic* BPD', initially described by Northway et al., occurred in children with moderately immature lungs who were artificially ventilated with high oxygen concentrations and pressure over a long period due to respiratory distress syndrome (RDS). This form of BPD was characterized by severe damage to the epithelium of the airways, alternating between over-inflated and atelectatic areas, hyperplasia of the bronchial smooth muscles, and fibroproliferative changes [29]. On the other hand, the '*new* BPD' is characterized

by less airway damage but decreased alveolar and microvascular growth as a consequence of the increasing immaturity of the lung at birth due to a low gestational week, resulting in a global decrease in alveolar number and gas exchange surface area (Table 2). The phenotype in BPD is the outcome of a complex multifactorial process in which various pre- and postnatal factors venture normal development in the premature lung (e.g., cell proliferation, inflammation and fibrotic process, oxidative stress, infection, microvascular development). These infants, who have a genetic susceptibility to problematic lung development, are generally exposed to a variety of injurious substances or courses of treatment before and/or after birth leading to direct airway and parenchymal damage [30].

Table 2. Differences between classical and new BPD

Classical BPD	New BPD
Altered inflation pattern of atelectasis and overinflation	Decreased, large and simplified alveoli (alveolar hypoplasia, decreased acinar complexity)
Severe airway epithelial lesions (hyperplasia, squamous metaplasia)	Decreased, dysmorphic capillaries
Airway smooth muscle hyperplasia	Variable interstitial fibroproliferation
Extensive fibroproliferation	Less severe, arterial/arteriolar vascular lesions
Prominent vascular hypertensive lesions	Negligible airway epithelial lesions
Decreased internal surface area and alveoli	Variable airway smooth muscle hyperplasia

Classical BPD is characterized by fibroproliferative airway changes and parenchymal fibrosis, whereas new BPD is characterized by vessel and alveolar hypoplasia. Both types of BPD have decreased alveolar formation, decreased lung growth, and increased vascular pulmonary resistance, resulting in structural changes similar to those seen in emphysema and chronic obstructive pulmonary disease (COPD). Premature infants are at a higher risk of BPD due to the disruption of lung growth before the alveolar stage. Structural changes such as larger alveoli, thicker interstitia, widened air spaces, decreased radial alveolar count, or decreased secondary crests are observed as a result of the disruption of normal development. This alveolar growth arrest is intimately linked to a reduction in the pulmonary vasculature. It has been shown that impaired vascularization is one of the main reasons for the pathogenesis of BPD. [30,31].

2.3.2 Interrupted Lung Development due to Hyperoxia in Newborns

Premature infants frequently have difficulty breathing due to their immature lungs. Therefore, supplementary oxygen, with or without ventilatory support, is administered to maintain an oxygen-rich environment. Moreover, ventilatory support (e.g., mechanical ventilator) is also often used in order to help the lungs to expand and decrease the work of breathing. These measures, however, may have a negative impact on lung development as higher levels of oxygen lead to oxygen toxicity [32].

Inflammation and fibrosis are shown to play an important role in hyperoxia-induced lung injury in newborns. Increased oxygen concentration generates reactive oxygen species (ROS), which rapidly react with adjacent biological molecules (e.g., lipids, proteins, nucleic acids) causing structural and functional damage. The imbalance between ROS and antioxidant capacities further causes an influx of inflammatory cells into the lung, resulting in inflammation, irregular collagen deposition, and capillary hyperpermeability [33]. Numerous signaling pathways are also activated, resulting in apoptosis and necrosis. All of these conditions contribute to the formation of irreversible changes within the alveolar space, and thus abnormal lung development [33].

2.3.3 Constituents of Impaired Alveolarization in BPD

When a child is born < 32 weeks' of gestation, the lung is in the saccular stage of development. During this stage, alveolar saccules have not developed into functional alveoli, nor has the blood capillary network expanded. Moreover, surfactant protein system is not mature enough to function. However, the molecular mechanisms leading to BPD have not been clearly understood. It is suggested that the interaction between key signaling mechanisms that link inflammation, remodeling of the extracellular matrix, and apoptosis facilitate the development of the disease (Figure 3) [16].

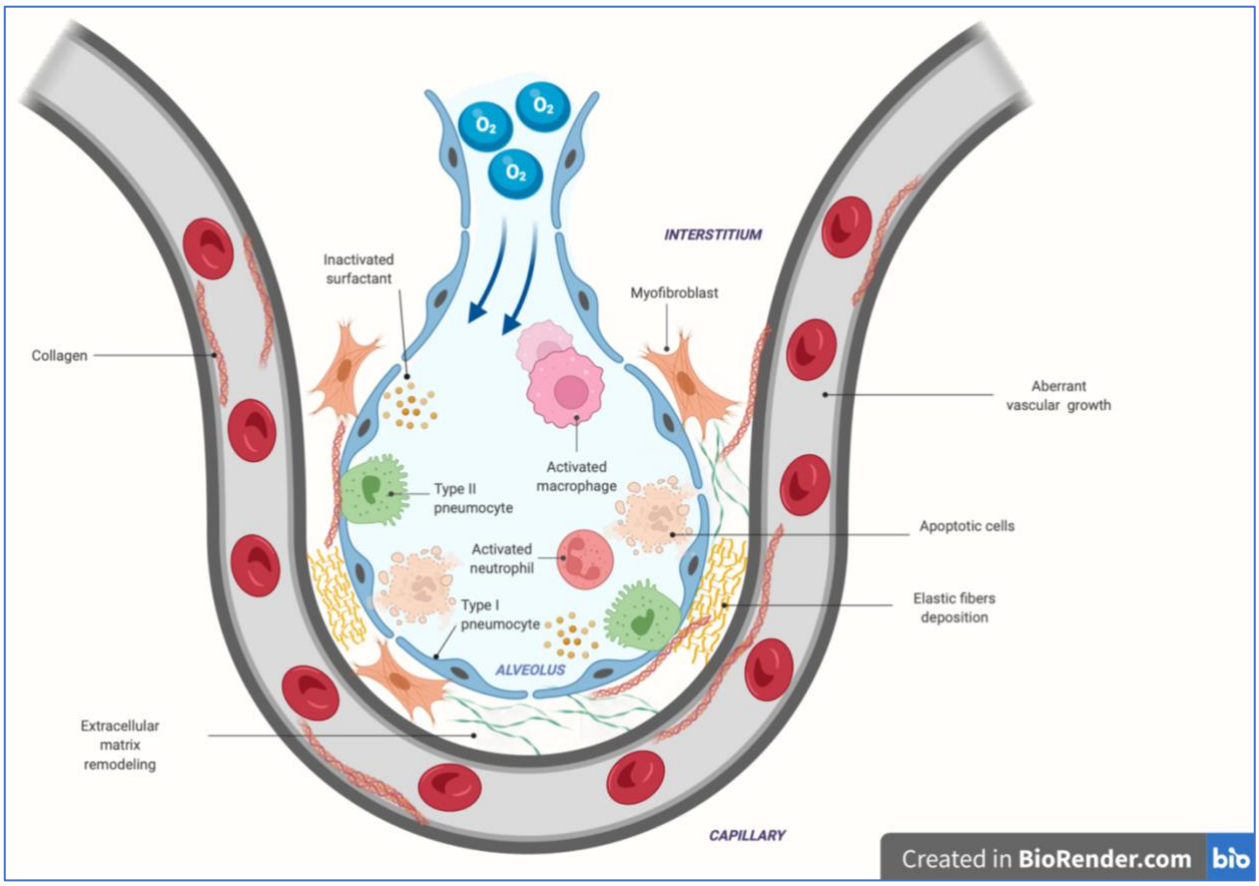

Figure 3. Constituents of Impaired Alveolarization in BPD

2.3.3.1 Aberrant Vessel Growth

Histopathology of new BPD includes abnormalities in the lung microvasculature, in addition to alveolar simplification. According to autopsy results of preterm infants dying from BPD, there is a significant drop in endothelial-specific marker CD31, indicating a decrease in vascular density. In addition, pulmonary capillaries were found to be dilated and located within the thick septum rather than the alveolar wall [34].

Vascular endothelial growth factor (VEGF) is essential for the normal formation and development of blood vessels. The expression increases in the early stages of lung development and decreases to adult levels in the final stages of alveolarization. Various animal studies have shown that using specific antibodies or knock-out mice with decreased VEGF expression impairs the alveolarization. Aside from promoting angiogenesis, VEGF preserves and improves alveolarization in the lungs of the animal models [34,35].

VEGF promotes neovascularization and thus attributes developed airways and blood vessels at the end of branching airways, but overexpression in the embryonic process contributes to disrupted airway morphology and type I cell differentiation [36]. In preterm infants who developed BPD, VEGF levels were found to be lower compared to the infants in control group [31]. Various animal studies show suppressed VEGF expression due to intense or prolonged mechanical ventilation, oxygen therapy, or exposure to endotoxins [34]. In contrast, treatment with VEGF promotes alveolarization and protects from BPD [20].

2.3.3.2 The Extracellular Matrix and Remodeling

Extracellular matrix is an important player in lung growth because it serves as a structure for the alveoli and vessels of the developing lung. In cases of abnormal ECM turnover or impaired structural organization, BPD progression is induced. In lungs of infants with BPD, abnormalities such as increased elastin degradation, perturbed elastin deposition, and defective septation can be observed. [35].

According to previous *in vitro* research, animal experiments, and observations, there is an unfavorable balance between proteases and their inhibitors in preterm newborns with BPD [37,38]. Although protease secretion, such as matrix metalloproteinase (MMP) -2 and -9, is required for cell migration and physiological ECM remodeling, overexpression results in the initiation of pathological processes, destroying the intact alveolar-capillary interface via enhanced ECM breakdown [35].

TGF-β superfamily is also closely connected to the changes in the ECM. TGF- β promotes IL-6 secretion, which acts as a growth factor that is involved in inflammation, immune regulation, hematopoiesis, and oncogenesis when stimulated by various conditions such as hyperoxia. [39]. IL-6 further regulates protease production after the metabolism of the disrupted matrix, such as MMP-14 [40]. In addition, in a mouse model of lung injury, the absence of IL-6 is associated with a reduced MMP-12 response to inflammation [41]. MMP's are responsible for the natural growth and branching morphogenesis of lungs under normal circumstances. Certain MMPs (i.e., MMP-9, MMP-12) can, however, be over-expressed during pathological conditions, such as hyperoxia [42]. In the event of lung injury, MMP-12 is upregulated and mediates the influx of neutrophils into the inflamed lung tissue. MMP-12 is also secreted by macrophages in response to their activation [42].

2.3.3.3 TGF-β Superfamily Signaling

TGF-β an important protein for lung organogenesis and homeostasis, is secreted into the ECM in an inactive form and bound to its latent binding proteins, which then bind to other ECM proteins, such as fibrillin 1 and 5, to promote elastogenesis in the developing lung. TGF-β release is observed as a result of ECM remodeling and a secretion by inflammatory cells [16].

Various cellular processes (e.g., ECM remodeling, alveolar epithelial cell differentiation, fibroblast activation) are directed by TGF-β. This pleiotropic factor is required for alveolarization and also plays an important role during the branching morphogenesis of the lung [19]. Mainly being secreted by neutrophils and macrophages; overexpression of TGF-β impairs matrix remodeling and cellular composition which can be observed in various pulmonary diseases including lung cancer [16,19] and idiopathic lung fibrosis [43].

TGF-β can bind to its receptor and mediate intracellular signaling via Suppressor of Mothers Against Decapentaplegic (Smad) protein activation, which then nuclearizes and regulates the expression of several target genes (Figure 4). TGF-β-mediated biological functions such as fibroblast to myofibroblast differentiation [44] and transcription of the α2(I) collagen gene [45] require Smad protein phosphorylation. In the developing lung, Smad1 and 7 are involved in promoting the branching whereas Smad2, 3, and 4 have an inhibitory effect on the process [32].

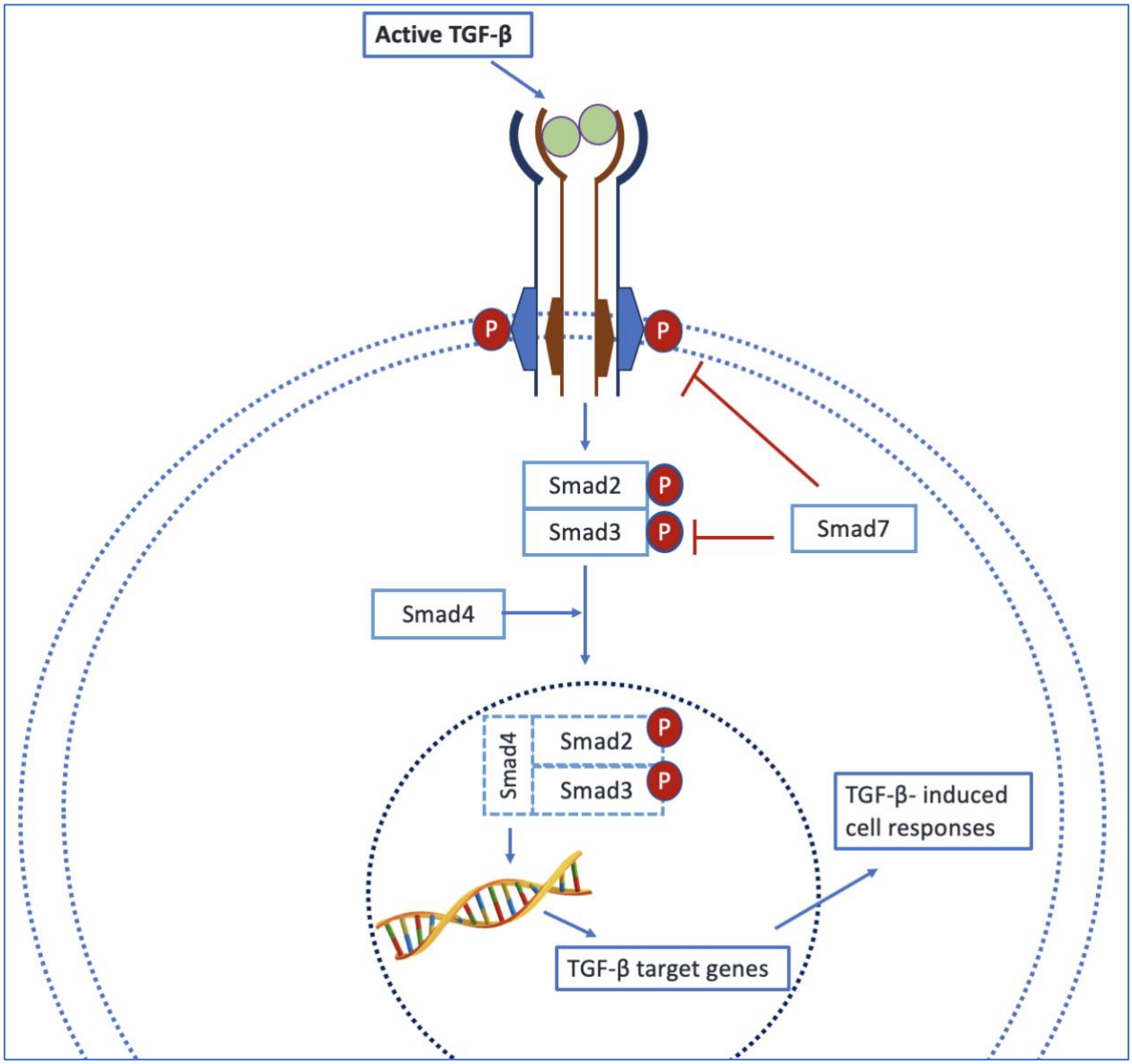

Figure 4. TGF-β signaling pathway

2.3.3.4 Organization of Collagen and Elastin

Collagen and elastin fibers are the primary components of lung connective tissue. As the lung grows normally, elastin and collagen deposition increase, and cross-linking of both components is a critical step in ECM maturation, providing stability and functionality [46]. However, the fiber network is significantly harmed as a result of prolonged hyperoxia, which causes thickening of the alveolar septa, changes in collagen and elastic fiber density, and deposition of collagen and elastic fibers [47].

Throughout pulmonary development, the amount of parenchymal collagen increases, allowing normal septation in the presence of a fine and complex collagen network. Type I and III collagens are primarily found in the bronchi, blood vessels, and alveolar septa [48], suggesting an increase in abundance during pulmonary development. Chronic lung disease disrupts lung growth, resulting in a thicker layer of collagen surrounding saccule walls, a wider interstitium, and an increase in the size and quantity of collagen fibers [49]. In clinical trials, the affected newborns (i.e., newborns who develop BPD) exhibit more collagen-positive cells, higher levels of collagen fibrils, and a specific rise in the collagen I/collagen III ratio. Collagen development is also influenced by growth factors, primarily by TGF- β, under physiological and pathological conditions [11,47].

The formation of new interalveolar walls, known as alveolar septa, is an essential step in increasing the blood-gas interface and meeting the respiratory requirements. Elastin is of great importance in septation, as the normal production and deposition of elastin play a key role in the proper development of alveoli. Conducting airways and alveolar ducts, as well as conducting vessels and developing septa, contain elastin fibers [11]. While elastin is typically deposited at the tips of the forming septa [50], its organization is severely disrupted in animal models of BPD [47]. This abnormal deposition is recognized in the walls of thickened septa as being shorter in length and having a tortuous aspect [51]. According to new studies, Elastin (*Eln)* gene is upregulated in animal models of BPD, and recent data supports that both the gene expression and the stability of *Eln* mRNA are increased by TGF-β [11,46,47].

2.3.3.5 Epithelial-Mesenchymal Transition

The epithelial-mesenchymal transition (EMT) is a physiological process that occurs during embryonic development, in which epithelial cells acquire characteristics of fibroblast-type mesenchymal cells. Although EMT is frequently reversible, it can also occur as a result of microenvironmental changes such as oxygen toxicity or carcinogenesis [52].
While multiple extracellular ligands, including CTGF, insulin-like growth factor-2, nuclear factor-kB, and Wnt regulate EMT [53], TGF-β is the primary regulator as evidenced by the literature [54]. TGF-β induces phosphorylation of two receptors, activating Smad2 and Smad3, both form a complex with Smad4. The Smad complex then inhibits E-cadherin expression via the transcription factors Snail1 and 2 [55]. These transcription factors promote the expression of mesenchymal characteristics through α-smooth muscle actin (α-SMA), vimentin, collagen, and metalloproteinases. TGF-β can also cause loss of epithelial cell markers such as aquaporin-5 [56].

Under physiological conditions, in response to a wide range of pathological insults, EMT allows epithelial cells to differentiate into fibroblastoid cells which are required for tissue regeneration, healing and remodeling [57]. However, EMT can persist beyond the inflammatory process, resulting in pathological fibrosis. As previously stated, hyperoxia results in increased ROS production which subsequently activates TGF-β, possibly leading to alveolar EMT. AECs undergo EMT in response to TGF-β1 *in vitro,* as well as converting to fibroblasts and myofibroblasts, contributing thereby significantly to lung fibrogenesis, *in vivo* [58].

2.3.3.6 Inflammation and Macrophage Polarization

Prolonged exposure to high oxygen levels recruits inflammatory cells to the lung, which affect alveolarization and distal pulmonary vascular development of the lungs. Hyperoxia further stimulates the release of chemotactic factors in the lung, increasing and amplifying the influx of inflammatory cells and exacerbating the inflammation [59]. In hyperoxia-exposed newborn rats, neutrophil-induced airway inflammation promotes the arrest of alveolarization whereas inhibiting neutrophil influx preserves alveolar development [60].

The mononuclear phagocytic immune system is made up by bone marrow derived monocytes that circulate in the blood and seed various tissues, such as the lungs, and differentiate into tissue-resident macrophages [61]. Macrophages are a vital component of the primary innate immune response that perform several specialized functions. They are the most abundant group of immune cells that are present in the lungs under homeostatic conditions. Macrophages are capable of acquiring well-defined phenotypes through phenotypic polarization in response to variegated environmental signals. This process is essential for a quick and successful initial response and a good resolution of the inflammatory process. Upon activation, macrophages are classified into categories: M1-like macrophages and M2-like macrophages. M1-like macrophages are highly effective in producing abundant pro-inflammatory cytokines, while M2-like macrophages commonly control inflammation [62].

Hyperoxia has been shown to aggravate M1-like phenotype-induced inflammation while suppressing the M2-like phenotype [63]. These CD68 positive alveolar macrophages contribute to the persistence of inflammation by producing more pro-inflammatory cytokines. In addition, under hyperoxic conditions, macrophages and neutrophils both secrete MMP-12 in response to activation, resulting in a vicious cycle [42]. It has been shown that infants who are developing BPD

did have higher rates of macrophages in their BAL fluid, compared to infants who recovered from RDS [64].

2.4 The Role of Matrix Metalloproteinase-12 in Lung Development

Metalloproteinases are a group of proteases and members of the metzincin superfamily whose primary function is degrading both ECM and basement membrane components. Recent studies indicate that by contributing to homeostasis and engaging in many physiological processes, they further serve as regulators of extracellular tissue networks [65]. MMPs also regulate the release or activation of various bioactive molecules such as chemokines, cytokines, and growth factors, and thus play a role in many processes such as bone remodeling, angiogenesis, wound healing, and apoptosis [22]. In addition, MMPs have been shown to function within the tumor microenvironment. MMPs facilitate the infiltration and migration of malignant cell metastatic traits during EMT. Increased release and activation of MMPs lead to ECM breakdown and promote infiltration and metastasis [66].

MMP-12 is a 54 kDa secretory proteinase that is predominantly expressed in alveolar macrophages and was first detected by Werb and Gordon in 1975. MMP-12 is responsible for the ability to degrade basement membrane structures like elastin, type IV collagen, fibronectin, laminin, gelatin, vitronectin, entactin, heparin, and chondroitin sulfate both *in vitro* and *in vivo* [67].

The pro-inflammatory role and the functions in chronic airway remodeling of MMP-12 have been largely studied [68]. MMP-12 overexpression is reported in BAL and bronchial biopsies of patients recovering from chronic obstructive pulmonary disease [69]. In addition, MMP-12 is present in higher concentrations in smokers' sputum and is associated with a decrease in lung function [70].

Increased MMP-12 expression in the lower airways can contribute to elastin degradation, resulting in elastin fragments that can trigger increased macrophage recruitment in mice and cultured human cells [71]. Furthermore, there is evidence that MMP-12 plays a role in lung inflammation and emphysema progression in preclinical rodent models [72]. On the other hand, MMP-12 deficient mice have a significant reduction in their airway inflammation profile after allergen-induced lung damage [73]. In 1997, Hautamaki et al. showed that MMP-12$^{-/-}$ mice were resistant to cigarette smoke-induced emphysema. Additionally, MMP-12$^{-/-}$ mice failed to accumulate macrophages in the BAL [74]. Although MMP-12 is the proteinase most strongly implicated in mouse models of

emphysema, studies of its expression in humans with COPD have reached inconclusive results. [75].

TGF-β1 plays a crucial role in the control of elastase–antielastase equilibrium, which contributes to ECM homeostasis. In mouse models, dysregulation of TGF-β1 signaling results in significantly increased levels of MMP-12 and an age-related emphysematous phenotype. In particular, the serum concentration of TGF-β1 is inversely associated with emphysema severity. These studies indicate that functional changes in activation of TGF-β are closely linked to emphysema based on MMP-12, yet the mechanism behind this process has to be investigated [76,77].

2.5 Hypotheses and Objectives

Prior studies of the Alcazar laboratory at the University Children's Hospital Cologne showed that exposure of newborn mice to increased oxygen levels causes an arrest of alveolar development [78,79]. Quantitative histomorhometric analysis revealed a significantly reduced alveolar formation and thickening of the alveolar septum, indicative of fibroproliferative processes following hyperoxia. In addition, assessment of proteolytic activity using zymography showed a 2-3-fold increase in MMP-2 activity in lungs of newborn mice exposed to hyperoxia until postnatal day 28 (P28). Moreover, measurement of gene expression demonstrated a up to 6-fold increase of *Mmp12* mRNA in neonatal lungs after hyperoxia at P28.

MMP-12 expression is closely linked to TGF-β signaling. Additionally, MMP-12 is a pro-inflammatory mediator, whose expression is induced by granulocyte-macrophage colony-stimulating factor (GM-CSF). Furthermore, elevated expression of MMP-12 was related to pathologies such as inflammation-associated atherosclerosis, aortic dissection, retinopathy, intracerebral hemorrhage, peripheral vascular injury, arterial stiffening, obstructive pulmonary disease, or deep vein thrombosis [80].

Based on the preceding findings and current knowledge, we hypothesized that;

MMP-12 deficiency enables alveolar growth and microvascular formation in hyperoxia-induced neoanatal lung injury as a model of BPD through modulation of ECM metabolism and inflammatory response.

In order to test this hypothesis, I pursued four specific aims using wildtype (WT) and Mmp12 knockout mice ($MMP12^{-/-}$) exposed to prolonged hyperoxia as an experimental model of BPD:

- Investigating the role of MMP-12 on the alveolar structure and pulmonary angiogenesis using MMP-12 knock-out mice: quantitative structural analysis of alveoli and microvessels
- Analysis of the functional role of MMP-12 in alveolar and vascular development: expression of epithelial and endothelial cell markers
- Investigating the role of MMP-12 on matrix remodeling (i.e., elastic fibers, collagen), matrix markers, and TGF-β signaling activation and regulation
- Identification of lung inflammatory response (i.e., macrophage count) and macrophage activation (PCRs for M1- like and M2-like phenotyphes) under hyperoxia

The findings will help to clarify the functional role of MMP-12 in the pathogenesis of BPD, as well as promote the development of novel therapeutic targets or the development and administration of novel therapeutic drugs in the field of neonatal lung diseases.

3. Materials and Methods

3.1 Materials

3.1.1 Equipment

Device	Manufacturer
4s3 semi-auto heat sealer	4titude
7500 Real-time PCR System	Applied Biosystems
Bag sealer FS 3604	Severin
Balance ES320A	Precisa
Bead Mill MM 400	Retsch
BioDocAnalyze Darkhood BDA digital	Biometra
Centrifuge 5424 R	Eppendorf
Centrifuge 5804 R	Eppendorf
Centrifuge Rotina 420 R	Hettich
Centrifuge Z216 MK	Hermle
ChemiDoc XRS+ Imaging system	Bio-Rad Laboratories GmbH
Cold plate COP 30	Medite
Heat chamber UM400	Memmert
Heating block TK-23	Hettich
Infinite M 200 Pro Nanoquant	Tecan
Magnetic stirrer Ikamag Reo	Ika
Microscope BX43	Olympus
Microtome Jung Biocut 2030	Leica
PerfectBlue™ Doppel-Gelsystem Twin (S; M; ExW S)	Peqlab
PerfectBlue™ 'Semi-Dry'-Blotter, Sedec™	Peqlab
Power Supply EV231	Peqlab
Rocker shaker MR-12	Biosan
Sonification device Sonoplus SH 70 G	Bandelin
SPROUT Micro-Centrifuge	LabScientific
Vortexer VTX-3000	LMS Laboratory & Medical
Water bath TFB55	Medite

3.1.2 Consumables

Item	Manufacturer
96 well plate	4titude
Amersham™ Protran® 0.45 µM NC membrane (4675.1)	Roth
Glass coverslips (#631-1573)	VWR Collection
Superfrost plus adhesion slides	Thermo Scientific
Whatman Paper 1.5 mm (#A126.1)	Roth

3.1.3 Chemicals

Substance	Manufacturer
100 bp DNA ladder	Thermo Fisher Scientific
30% Acrylamide/Bisacrylamide Mix	Roth
4% Paraformaldehyde (PFA)	Roth
Agarose	Sigma
APS	Applichem
Bromophenol blue	Roth
BSA	Roth
CHAPS	Calbiochem
Chloroform (>99%)	Roth
DNase I	Sigma
dNTP Mix (10 mM each)	Thermo Fisher Scientific
DPBS, no calcium, no magnesium	Gibco
EDTA stop solution	Promega
Neomount	Merck
Ethanol (EtOH) (>99.8%)	Roth
Eosin 0,5 %	Roth
Ethanol (EtOH) (70%)	Chemsolute
Glacial acetic acid	Roth
Glycerol	Sigma
GoTaq® qPCR Master Mix, 2X	Promega
Halt™ Protease Inhibitor Cocktail (100X)	Thermo Fisher Scientific
Weigert´s Resorcin Fuchsin	Waldeck
Hydrochloric acid (HCl)	Roth
Isopropanol (>99,8%)	Roth
Mayer's hematoxylin	Roth
Methanol	Roth
Milk powder, blocking grade	Roth
MMLV reverse transcriptase	Promega
MMLV-buffer 5x	Promega
My Taq HS Red Mix	Bioline
NaCl	Roth
Neoclear	Merck
Oligo dT-Primer (5'TTTTTTTTTTTTTTT3')	Eurofins/MWG

PageRuler™ Prestained Protein Ladder, 10 to 180 kDa	Thermo Fisher Scientific
PBS	Merck
Platinum qPCR Supermix –UDG with Rox	Invitrogen
Proteinase K	Fermentas
Ponceau S	Roth
Random-Primer	Roche
Recombinant RnasinI RNase Inhibitor	Promega
RQ1 DNase 10X Reaction Buffer	Promega
RQ1 RNase-Free DNase	Promega
SDS	Roth
Picrosirius Red	Dianova
Taq DNA Polymerase	Invitrogen
TEMED	Roth
TRI Reagent	Sigma-Aldrich
Trichloroacetic acid	Roth
Tris	Roth
Tween-20	Sigma
Xylol	Roth
β-Mercaptoethanol (βME)	Roth

3.1.4 Buffers and Solutions

Solution	**Ingredients**
SDS-PAGE separation gel buffer	1.5 M Tris pH 8.8
SDS-PAGE separation gel (8-12%)	8-12% Acrylamide 0.1% APS 0.1% SDS 260 mM Tris 0.004% TEMED
SDS-PAGE stacking gel buffer	0.5 M Tris pH 6.8
SDS-PAGE stacking gel (4%)	4% Acrylamide 0.1% APS 0.1% SDS 0.004% TEMED 160 mM Tris

SDS-PAGE loading dye (5x, 20 mL)	0.0205% SDS 0.026% Bromophenol blue 10% Glycerol 25% βME 500 mM TRIS
SDS-PAGE Laemmli-buffer (10x)	1.92 M Glycine 0.25 M Tris 10% SDS
Towbin buffer (10x) for semi-dry blotting	1.92 M Glycine 0.25 M Tris
Transfer buffer for semi-dry blotting	10% Towbin buffer 10% Methanol
Ponceau staining solution	0.2% Ponceau S 3% Trichloroacetic acid
TBST	0.1 M NaCl 10 mM Tris 0.1% Tween-20 pH 7.5
Blocking solution	5% Milk powder 2% BSA in TBST
Antibody dilution solution 1	5% Milk powder in TBST
Antibody dilution solution 2	5% BSA in TBST
Stripping buffer	62.5 mM Tris 2% SDS pH 6.7 0.7% βME (added directly before usage)
CHAPS buffer for protein isolation	50 mM Tris 20 mM CHAPS pH 7.5 1% Halt protease inhibitor cocktail (added directly before usage)

3.1.5 Kits

Kit	Manufacturer
Amersham ECL Prime Western Blotting Detection Reagent	GE Healthcare
Pierce™ BCA Protein Assay Kit	Thermo Fisher Scientific

3.1.6 Antibodies

Primary Antibody	Manufacturer	Order number
Aquaporin 5	Sigma	A4979
Caspase 3	Cell Signaling	9661
CD31	Abcam	ab28364
PAI-1	Cell Signaling	11907
PCNA	Dako	M0879
Phospho-STAT3 (Tyr705) XP®	Cell Signaling	9145
Smooth muscle actin	Santa Cruz	sc53142
Surfactant protein C	Santa Cruz	sc7705
STAT3	Cell Signaling	9139
SMAD 2/3	Cell Signaling	3102
VE-Cadherin	Abcam	ab33168
β-Actin	Cell Signaling	3700
Secondary Antibody		
Anti-mouse IgG, HRP-linked	Cell Signaling	7076
Anti-rabbit IgG, HRP-linked	Cell Signaling	7074
Anti-rat IgG, HRP-linked	Cell Signaling	7077

3.1.7 Primers

Primers for SYBR Green I qPCR

Fbn1 **(Fibrillin 1)**	for	GGTCAATGCAACGATCGAAA
	rev	AGTGTGACAAAGGCAGTAGAAGCTT
Col1a1 **(Collagen 1a1)**	for	GCAGTGCTGTTGCGATCTTG
	rev	CAGAGGGACAGAGCACAGCTT
Col3a1 **(Collagen 3a1)**	for	GGTGGTTTTCAGTTCAGCTATGG
	rev	TTTTTGCAGTGGTATGTAATGTTCTG
Fbln5 **(Fibullin 5)**	for	TACATCCTACTCAGGCCCATACC
	rev	GTTGCCTTCATCCATCTGATACC
Vim	for	CCCTGAACCTGAGAGAAACTAACC

(Vimentin)	rev	GTCTCATTGATCACCTGTCCATCT
Sfpta **(Surfactant protein a)**	for	TCAAACATCAGATTCTGCAAACAA
	rev	TGACTGCCCATTGGTGGAA
Sfptb **(Surfactant protein b)**	for	CTGCTGGCTTTGCAGAACTCT
	rev	GAGGACAAGGCCACAGACTAGCT
Sfptc **(Surfactant protein c)**	for	CCTCGTTGTCGTGGTGATTGTA
	rev	GCTCATCTCAAGGACCATCTCAGT
Sfptd **(Surfactant protein d)**	for	CAGCAGATGGAGGCCTTAAAA
	rev	GGGAACAATGCAGCTTTCTGA
Des **(Desmin)**	for	GGAGAGCAGGATCAACCTTCCT
	rev	CACTGTCTTTTTGGTATGGACTTCA
Snai1 **(Zinc finger protein, SNAIL)**	for	CTGCAACCGTGCTTTTGCT
	rev	CTGGCACTGGTATCTCTTCACATC
Snai2 **(Zinc finger protein, SLUG)**	for	CCTCACCTCGGGAGCATACA
	rev	GGCCACTGGGTAAAGGAGAGT
Il13 **(Interleukin-13)**	for	GCTTATTGAGGAGCTGAGCAACA
	rev	CCAGGTCCACACTCCATACCA
Il14 **(Interleukin-14)**	for	GGAGATGGATGTGCCAAACG
	rev	GCACCTTGGAAGCCCTACAG
Tlr4 **(Toll like receptor-4)**	for	GGTGAGAAATGAGCTGGTAAAGAATT
	rev	GCAATGGCTACACCAGGAATAAA
Il6 **(Interleukin-6)**	for	ACAAAGCCAGAGTCCTTCAGAGA
	rev	CCTTCTGTGACTCCAGCTTATCTGT
Il10 **(Interleukin-10)**	for	GGCGCTGTCATCGATTTCTC
	rev	CACCTTGGTCTTGGAGCTTATTAAA
Arg1 **(Arginase 1)**	for	ACCCTGACCTATGTGTCATTTGG
	rev	TGGTACATCTGGGAACTTTCCTTT

Primers for TaqMan qPCR

Serpine1 **(PAI-1)**	for	GCTGGCTATGCTGCAGATGAC
	rev	TGCCCTTCTCATTGACTTTGAA
	probe	AAAACCCGGCGGCAGATCCA
Vegfa **(Vasclar endothelial growth factor A)**	for	AGAAGTCCCATGAAGTGATCAAGTT
	rev	CACAGGACGGCTTGAAGATGT
	probe	TACCAGCGAAGCTACTGCCGTCCGAT
Eln **(Elastin)**	for	CTACGGACTGCCCTATACCAATG
	rev	CACCATACTTGGCTGCTTTAGCT
	probe	CAAGGCTGGCTACCCAACAGGGACA
Acta2 **(Alpha smooth muscle actin)**	for	ACATCAGGGAGTAATGGTTGGAAT
	rev	GGTGCCAGATCTTTTCCATGTC

	probe	CGATAGAACACGGCATCATCACCAACTG
Fbn2 **(Fibrillin2)**	for	CAACACCGTGGGAAGCTATTTT
	rev	TCCAGCCCTCTGATCAATGC
	probe	TCTCTGTCCCCGTGGCTTCGTAACC
Fbln4 **(Fibulin 4, EFEMP2)**	for	AGATCCGTTCTGGAAACACACA
	rev	CTCCAGGTCCAGCACGTACTC
	probe	CATTAGGCAAATCAACAATGTCAGCGCC
Cdh1 **(E-Cadherin)**	for	CAGTCATAGGGAGCTGTCTACCAAA
	rev	GGGTACACGCTGGGAAACAT
	probe	CACCACCACCGCGACCCTGC
Aqp5 **(Aquaporin 5)**	for	TCACTGGGTCTTCTGGGTAGGA
	rev	CTGGCTCATATGTGCCTTTGAC
	probe	TACTTCTACTTGCTTTTCCCCTCCTCGCTG
Mfap4 **(Microfibril associated protein 4)**	for	GGTGGTTCCCATCTCTCCTATG
	rev	GGCCCGACGAATTTTCATCT
	probe	AAAGGCTTCTATTACTCCCTCAAGCGCACG
Ctgf **(Connective tissue growth factor)**	for	CATTAAGAAGGGCAAAAAGTGCAT
	rev	TGCAGCCAGAAAGCTCAAACT
	probe	CGGACACCTAAAATCGCCAAGCCTG
18S **rRNA (*18S* ribosomal RNA)**	for	AGATCCCAGACTGGTTCCTG
	rev	TTGTTGTCTAGACCGTTGGC
	probe	CAGAACCTGGCTGTACTTCCCATCC
Actb ***(Beta actin)***	for	TGACAGGATGCAGAAGGAGATTACT
	rev	GCCACCGATCCACACAGAGT
	probe	ATCAAGATCATTGCTCCTCCTGAGCGC
Gapdh **(Glyceraldehyde-3 phosphate dehydrogenase)**	for	ATGTGTCCGTCGTGGATCTGA
	rev	TGCCTGCTTCACCACCTTCT
	probe	CCGCCTGGAGAAACCTGCCAAGTATG

3.1.8 Software

Software	**Manufacturer**
cellSens	Olympus
ImageJ	Wayne Rasband
Prism 6.0	GraphPad

3.2 Methods

3.2.1 Murine Models of Hyperoxia-Induced Lung Injury

All animal procedures were performed under German regulations and legal requirements and were approved by the local government authorities (LANUV; Nordrhein-Westfalen; 2015.A120, 2020.A095).

In this doctoral thesis, the murine model of neonatal hyperoxia-induced lung injury is studied. As our specific aim was to investigate the effects of MMP-12, we examined the lung tissues of wild-type mice (C57BL/6J) and MMP-12 knock-out (MMP12$^{-/-}$) mice (B6.129X-*Mmp12*^{tm1Sds}/J; kindly provided by Prof. Dr. Marcus Mall, Charité, Berlin, Germany) [81].

Because that homozygous MMP-12$^{-/-}$ mice lack the relevant gene in both alleles, they are deficient of MMP-12. Wild-type (WT) mice served as the control group (Figure 5). The steps of tissue preparation are as follows:

- Housing adult and neonatal C57BL/6J mice, and genetically modified mice (MMP-12$^{-/-}$) in humidity and temperature-controlled rooms on a 12:12-h light-dark cycle. *Ad libitum* access to food and water.
- WT mice and MMP12$^{-/-}$ mice were each mated separately. The newborn mice were weighed within the first 6-12 hours after the birth and randomized to the dams of the corresponding genetic background.
- Newborn mice were exposed to either 85% O_2 or 21% O_2 from postnatal day 1 (P1) to P14. The oxygen exposure was performed in 90 x 42 x 38cm plexiglass chambers and continuously ventilated (Biospherix) at a rate of 3.5 l/min. O_2 concentrations were monitored using a miniox II monitor (Catalyst Research, Owing Mills, MD).
- Nursing dams were rotated every 24 h between hyperoxia and normoxia litters to exclude any toxic O_2-related effect on the dams.
- Starting from P15 all animals were exposed to 21% O_2 until P28.
- At P28 (mature lung), mice were killed deeply anesthetized with intraperitoneal injection of Ketamine (100mg/kg) and Xylazine (5mg/kg) and subsequently exsanguinated by aortic transection.

- Heart and lungs were excised *en bloc.* Fixation of lungs were performed at 20cmH_20 pressure with 4% (mass/vol) paraformaldehyde in phosphate-buffered saline (PBS; 20mM Tris HCl, 137 mM NaCl, pH 7.6)
- Labeling and storage of frozen samples at -80°C
    - Wildtype mice exposed to 21% O_2: WT^{NOX}
    - Wildtype mice exposed to 85% O_2: WT^{HYX}
    - MMP-12 deficient mice exposed to 21% O_2: $MMP12^{-/-NOX}$
    - MMP-12 deficient mice exposed to 85% O_2: $MMP12^{-/-HYX}$

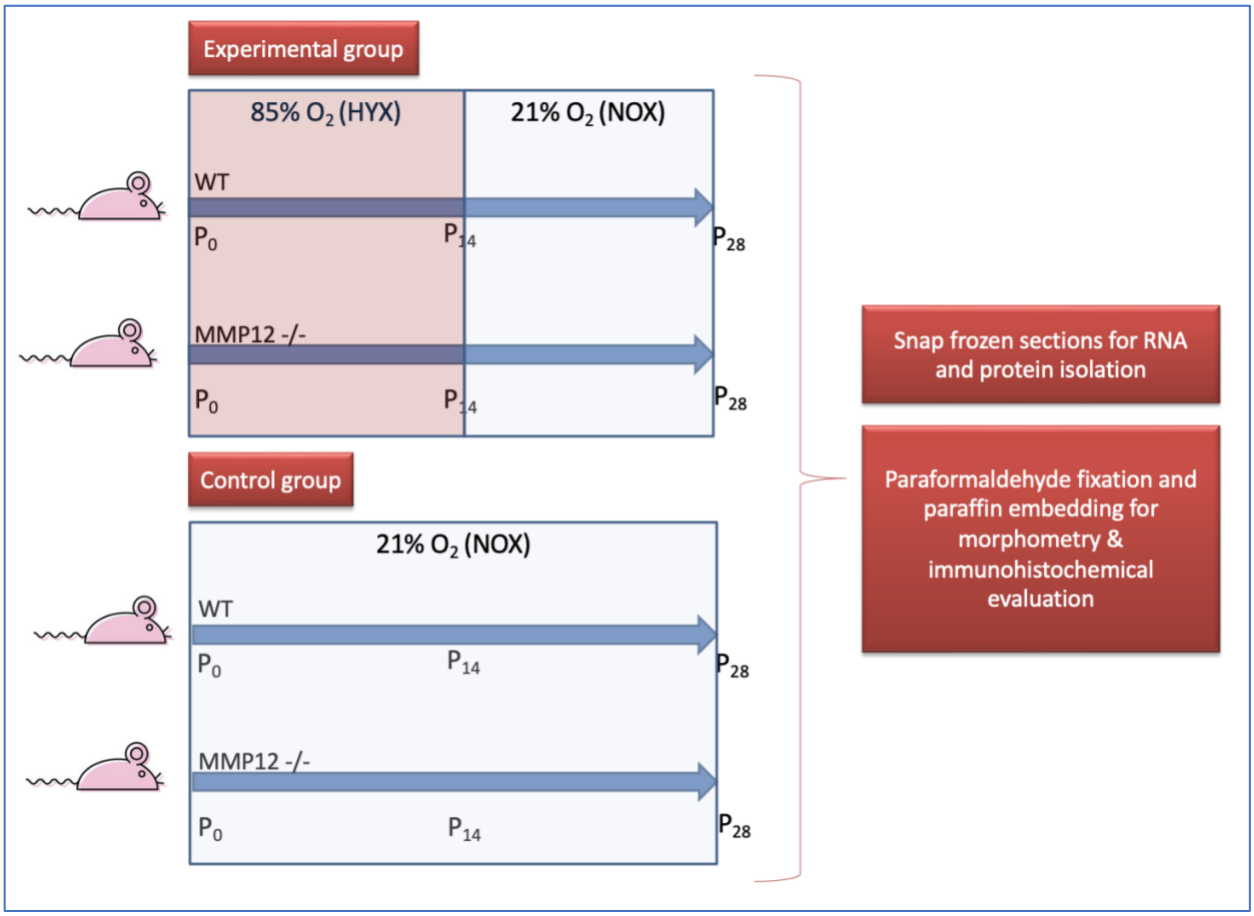

Figure 5. Experimental mouse models

Because the lung maturation, alveolarization, and vascularization are complete in mice at the age of four weeks, they were sacrificed on P28. These experiments were carried out by Jun.-Prof. Dr. Dr. Miguel A. Alejandre Alcázar (Department of Pediatric and Adolescent Medicine, University Hospital Cologne).

Tissue Preparation: At P28, ketamine (100 mg/kg) and xylazine (5 mg/kg) are injected intraperitoneally to euthanize the offspring. After aortic exsanguination and thoracotomy, lungs were excised and wet lung weight was measured. One lung was immediately snap-frozen for further molecular assessment while the other lung was inflated through the trachea and pressure-fixed in 4% (mass/vol) paraformaldehyde (PFA) at 20 cmH_2O in phosphate-buffered saline (PBS) then stored at 4°C overnigh for further quantitative histomorphometric analysis and immunostaining.

Paraffin Sections of the Lung Tissue: For histologic analysis, samples thoroughly infiltrated with wax were immediately cooled down using a cooling plate (Leica EG 1150C). Paraffin blocks on a cooling plate were cooled for sectioning and then clamped into a microtome. 3 µm tissue sections were cut and floated in a water bath on the surface of the water to flatten out and avoid compressions. Isotropic uniform random (IUR) sections were generated by the "Orientator" method [82]. Using this procedure, the three-dimensional orientation of the tissue sample section plane is randomized. Three sets of thirty slices (3 µm) were cut. Sections were mounted on poly-l-lysine-coated glass slides (25x75x10mm) and labeled, which were then mounted on a slide rack. The slide rack was put in an oven to allow sections to dry overnight at 40°C.

3.2.2 Hematoxylin-Eosin Staining

Hematoxylin and eosin (H&E) stains are used as a routine staining method for morphological studies on formalin-fixed tissues. They have been used for a long time as they can display a broad range of cytoplasmic, nuclear, and extracellular matrix features. Hematoxylin has a deep blue-purple color and stains nucleic acids, thus the nuclei. Eosin is pink and stains proteins nonspecifically thereby showing shades in the extracellular matrix and cytoplasm [83].
H&E staining protocol is applied with the following steps:

- Deparaffinization of the sections: 10 minutes in Neoclear, repeated three times
- Hydration: The tissue sections pass through decreasing concentration of alcohol baths and distilled water (100%, 90%, 80%, 70%, water); one minute each
- The tissue sections are stained in Hematoxylin (Meyer's Hematoxylin, Roth) for 3 minutes
- The tissue sections are rinsed shortly in distilled water and then washed in running tap water for 5 minutes until sections "blue"
- The tissue sections are rinsed shortly in distilled again followed by 0,5% Eosin (Roth) staining for 6 minutes

- Dehydration in increasing concentration series of alcohol (70%, 80%, 90%, 100%) one minute each and then the tissue sections are cleared in neoclear, repeated three times
- The tissue sections are mounted with “Neomount” (Merck)

3.2.3 Picrosirius Red Staining

Picrosirius red (PSR) staining is a widely used histological technique to assess the distribution of collagen and networks in paraffin-embedded tissue parts. PSR dyes are the first choice for quantitative analysis of fibrosis in various tissues because they react specifically to most collagen types [84]. Under normal conditions, PSR-stained collagen appears red under light microscopy. PSR staining is applied with the following steps:

- Deparaffinization of the sections: 10 minutes in Neoclear, repeated three times
- Hydration: The tissue sections pass through decreasing concentration series of alcohol baths and distilled water (100%, 90%, 80%, 70%, water); one minute each
- The tissue sections are rinsed shortly in distilled water for one minute
- Incubation of the tissue sections in adequate amounts (i.e., amounts that completely cover the sections) of Phosphomolybdic Acid Solution (0.2%) for 1-5 minutes.
- The slides are dipped once in distilled water.
- The tissue sections are stained in adequate amounts of (i.e., amounts that completely cover the sections) PSR solution for 60-90 minutes.
- The tissue sections are rinsed shortly in two changes of Acetic Acid Solution.
- Dehydration in two changes of 100% ethanol 30 seconds each and then the tissue sections are cleared in Neoclear twice for 30 seconds.
- The tissue sections are mounted with “Neomount” (Merck).

3.2.4 Hart’s Staining

Modified Hart’s Staining is one of the histological methods used to determine elastic fibers and elastogenesis in paraffin-embedded tissue sections. Hart’s staining is based on a standardized protocol, which is used in our research laboratory of the Children’s Hospital Cologne. After a successfully performed Hart’s Staining, the elastic fibers appear in blue-black whereas the remaining tissue has a pale-yellow color[85] .

Hart’s Staining is applied with the following steps:

- Deparaffinization of the sections: 10 minutes in Neoclear, repeated three times
- Hydration: The tissue sections pass through decreasing concentration series of alcohol baths (100%, 90%, 80%, 70%); one minute each and then rinsed one minute in distilled water
- The tissue sections are stained with adequate Hart's solution (1 volume of Weigert's resorcin fuchsin + 9 volumes of 1% hydrochloric acid in 70% ethanol) overnight
- The next day, tissue sections are briefly rinsed in 96% ethanol and shortly differentiated with 1% HCL-Alcohol (990ml 70% Alcohol + 10 ml 25% HCL) to remove the excess solution
- The sections are washed in tap water and then distilled water one minute each
- Counterstaining of the sections with tartrazine (0,5% in 0,25% acetic acid)
- The tissue sections are rinsed shortly in 96% ethanol
- Dehydration in 96% ethanol for one minute and 100% ethanol for two minutes, then the tissue sections are cleared in Neoclear, repeated three times
- The tissue sections are mounted with "Neomount" (Merck)

3.2.5 Quantitative Histomorphometric Analysis of Alveolarization

The quantitative histomorphometric study of alveolarization is calculated using the H&E-stained lung sections. Each group (WT^{NOX}, WT^{HYX}, $MMP12^{-/-NOX}$, $MMP12^{-/-HYX}$) consists of five animals. For each animal, 4 IUR sectioned slides have been selected randomly, stained and scanned. The analysis is carried by light microscopy, slide scanner (Leica SCN400), and Cell D 3.4 Olympus Soft Image Solutions (Olympus, Hamburg, Germany). Lung tissue sections with large airways or vessels and atelectatic areas were avoided when imaging.

The lung sections underwent four assessments: mean linear intercept (MLI), radial alveolar count (RAC), average surface area of a single alveolus (surface of a single alveolus; SA), and septal thickness (ST), on sections stained with hematoxylin-eosin. All analyzes were carried out by a blinded investigator.

The MLI was determined to measure the level of alveolarization and is a surrogate parameter for calculating the number of alveoli accurately. The MLI or 'Chord Length' refers to the mean free distance between gas exchange surfaces (alveolar septa). The method is based on a grid analysis in which the degree of alveolarization is determined by the number of intersections of the gas exchange surface with the grid [82]. Determination of the MLI was carried out with the software

CellSens (CellSens B.V, Den Haag, The Netherlands). The program creates a virtual grid over the image sections so that the intersections with the alveolar septa can automatically be determined by the program and presented in a table. The number of points of intersection is calculated on the gridlines and is proportional to the degree of alveolarization. To evaluate MLI, up to ten fields of view per lung section were taken for each scanned section.

The alveolar number per terminal respiratory unit was determined by evaluating the RAC as described by Emery and Mithal [86]. A total of four sections per animal containing the terminal respiratory unit were chosen. A line was drawn from the middle of each terminal respiratory unit to the nearest septum for each tissue segment below the 20x objective. The number of alveoli crossed by the line was counted and the average number of alveoli per lung segment was determined. For measurements, the ImageJ (Wayne Rasband) software was used,all values were recorded in an Excel table, and the mean value for each segment has been determined.

The measurement of the average surface area of a single alveolus and of the septal thickness was carried out using the ImageJ (Wayne Rasband) software. For septal thickness, up to 10 random images were taken with 20x magnification and 10 random septae per field of view were manually measured. For alveolar surface area measurements, up to 10 photos were taken at 20x objective, 10 alveoli were randomly selected; the diameter of each alveolus was measured manually and used to calculate the surface area of an alveolus [$4 \times \Pi \times r^2$].

3.2.6 Quantitative Analysis of Collagen

The quantitative analysis of Collagen abundance as an indicator of fibrosis was performed using the PSR stained lung sections. Four random tissue sections per animal were selected and were stained to show collagen abundance with PSR. After staining, collagen appears red on a light yellow background in bright-field microscopy. To analyze collagen content, we took up to ten images per tissue section randomly using a 20x objective. The collagen density of the tissue was measured using Cell D 3.4 Olympus Soft Imaging Solutions (Olympus, Hamburg, Germany) and related to the total lung tissue.

3.2.7 Quantitative Analysis of Elastic Fibers

The quantitative analysis of elastic fibers and the abundance of elastin were calculated using modified Hart's-stained lung sections. Four random tissue sections per animal were selected and were stained with Hart's elastic stain and counterstained with tartrazine to show elastin. After

staining, elastic fibers appear blue-black on a yellow background. To analyze elastic fiber content, we took up to ten images per tissue section. Elastic fiber density of the alveoli was measured using Cell D 3.4 Olympus Soft Imaging Solutions (Olympus, Hamburg, Germany) and related to total lung tissue.

3.2.8 Determination of Inflammation via Macrophage Staining

Considering that both M1-like and M2-like macrophages have important roles in the inflammatory processes, specific CD68 staining was performed at the laboratory of Pathology Institute, University Hospital Cologne in order to identify the number of inflammatory cells. CD68 is a glycosylated type I membrane protein found in the granules of macrophages and widely used to determine their presence. After CD68 staining, macrophages appear brown throughout the lung tissue. The whole number of macrophages per slide was quantified and adjusted to a standard tissue area of 100μm^2. All measurements are recorded in an Excel table and the mean value for each segment was calculated.

3.2.9 RNA Isolation

The RNA isolation procedure is based on a standardized protocol, which is used in our research laboratory of the Children's Hospital Cologne [87]. Isolation of RNA from lung tissue was performed as depicted in Table 3.

The principle of RNA isolation is based on the extraction of nucleic acids by guanidine, thiocyanate, sodium acetate, phenol, and chloroform. Centrifugation gives rise to an upper aqueous phase, an interphase, and a lower organic phase; the upper aqueous phase contains the RNA, which is pipetted off.

The RNA is isolated in line with the following steps:

- 0,5 ml TRI reagent is added to 50 mg tissue samples.
- Tissue samples are homogenized using a bead mill (20 sec, 30 Hz) and vortexed.
- Incubation of the samples at room temperature (RT) for 5 minutes.
- 100 µL of chloroform is added to each sample and the samples are vortexed for 15 seconds and incubated for 3 minutes at RT.
- The samples are centrifuged (15 min, 12000 rpm, 4°C) until three-phase separation occurs.
- The clear aqueous RNA containing upper layer is transferred to a fresh tube.

- The white interphase, which contains the DNA, and the pink organic bottom phase are discarded.
- 250 µL isopropanol is added to each tube for RNA precipitation, the samples are mixed and are incubated on ice for 20 minutes
- The samples are centrifuged (15 min, 15000 rpm, 4°C), the supernatants are discarded
- The pellets are washed twice with 75% EtOH to improve the purity of the RNA and centrifuged (5 min, 15000 rpm, 4°C)
- EtOH is removed and the pellets are air-dried for 30 minutes.

Table 3. Protocol: RNA isolation

Step	Reagent	Vol (µl)	Time (min)	Temp (°C)
1	Tri Reagent addition	500	5	RT
2	Chloroform addition	100	3	RT
3	Centrifugation (12000 rpm)	-	15	4
4	Phase separation	-	-	RT
5	Isopropanol addition	250	20	4
6	Centrifugation (15000 rpm)	-	15	4
7	Disposal of supernatant	-	-	RT
8	Washing with EtOH	500	-	RT
9	Centrifugation (15000 rpm)	-	10	4
10	Washing with EtOH	500	-	RT
11	Centrifugation (15000 rpm)	-	10	4
12	Pellet drying	-	30	RT
13	DEPC-treated H_20 addition	20-50	-	4

3.2.10 Determination of RNA Quantity and Quality

The RNA concentration was determined spectrophotometrically. This method allows the comparability of the samples to each other. The measurement of the concentration in µg/µL allows the use of the same concentration of each sample for subsequent cDNA synthesis. Likewise, possible impurities are identified. The spectrophotometer measures the optical density at different wavelengths. The absorption maximum of RNA is at a wavelength of 260nm.

As a final step, crystallized RNA was calibrated with H_2O treated with DEPC 20-50 µL (Volume depending on pellet size). A 260/280 nm ratio using the Infinite® M200 PRO NanoQuant (Tecan) was used to determine the RNA concentration and purity. The resulting value should be between

1.8 and 2.0 for a maximum 1 µg/µL concentration If the value is lower, this indicates contamination of the sample by proteins or phenol. The RNA was preserved at -80°C before further use.

3.2.11 Complementary Synthesis of DNA

The method of converting mRNA to generate complementary DNA (cDNA) is a reverse transcription using the enzyme reverse transcriptase. The procedure shown in Table 4 was performed for the synthesis of cDNA. For the procedure, an equivalent quantity of 1 µg RNA of each sample was used.

The cDNA is synthesized in keeping with the following steps:

- The samples are incubated with DNase (15 min, RT) to prevent potential genomic DNA contamination.
- DNase activity is stopped by adding EDTA and the samples are incubated for 15 minutes at 65°C.
- The samples are mixed along with Random and oligo-dT primers (mRNA-specific; 0.5 µg/µL) and are incubated at 70°C for 5 minutes for annealing of the primers and cooled down on ice for one minute.
- The samples are mixed with a “mastermix” containing Moloney Murine Leukemia Virus Reverse Transcriptase (MMLV RT), dNTPs, RNase inhibitor (rRNasin), and an MMLV buffer to synthesize the template-based cDNA at 37°C for 1 hour and cooled down on ice for one minute.
- cDNA samples are stored at -20°C for further use.

Table 4. Protocol: cDNA synthesis

Step	Reagent	Vol(µl)	Time (min)	Temp(°C)
1	10xDNAse I-buffer (1 µL) DNase (RQ1 / Promega) (1 µL)	2	15	RT
2	25 mM EDTA (stop solution) (1 µL)	1	15	65
3	Random primer (0.3 µg) oligo dT primer (16T) (0.2 µg) DEPC-treated H, O (4 µL)	5	5	70
4	-	-	1	on ice
5	5x MMLV-buffer (5 µL) dNTP mix (10 mM) (1.25 µL) RNase inhibitor (rRNasin, Promega, 40 U / µL (0.5 µL) MMLV (Promega, 200 U / µL) (1 µL)	10	60	37

	DEPC-treated H_2O (2.25 µL)			
6	-	-	1	on ice

3.2.12 Polymerase Chain Reaction (PCR)

PCR is a method that is used to multiply the DNA. The principle of PCR was developed by the American Kary Mullis [88]. Primers, nucleotides, Mg^{+2} ions, DNA polymerase, and buffer solution are added to the DNA sample that is to be tested. An exponential replication of the DNA is achieved through cyclic repetition, as in natural replication. This procedure is divided into three stages:

Denaturation: In the first phase, denaturation is performed by heating the double-stranded DNA to 95°C. Hydrogen bonds linking the two DNA strands are broken up, yielding two single-stranded DNA molecules. In the next step, the temperature is lowered to the optimal temperature for the primer so that it can bind to the complementary regions of the DNA.

Annealing: Primers that bind to both strands and serve as starting points for the DNA polymerase are used for the amplification of a particular DNA sequence. Primers are oligonucleotides that are complementary to the selected segment of the gene.

Elongation: The last step is the phase of elongation in which the DNA polymerase binds to the primers from the 5' to the 3' end and synthesizes the new DNA strand. The amplification takes place with the aid of DNA polymerase, a buffer solution, Mg^{+2} ions, and deoxyribonucleotide triphosphates (dNTPs). A phospho-diester bond binds the nucleotides. Mg^{+2} ions serve as a cofactor in the catalysis of these bonds. The DNA polymerase recognizes and integrates complexes of nucleotides and Mg^{+2} ions. The buffer solution should maintain an acceptable chemical environment. DNA replication is exponential [88].

3.2.13 Quantitative Real Time PCR

Real-time PCR is a replication method for nucleic acids that is based on the principle of conventional PCR, which at the same time, enables the quantification of the DNA produced. (a) The TaqMan and (b) SYBR Green methods were used to perform quantitative gene expression analysis. The TaqMan method is based on the activity of a Taq polymerase enzyme's exonuclease and dual-labeled oligonucleotide, whereas the SYBR Green method is based on the binding of a fluorescent dye to double-stranded deoxyribonucleic acid, resulting in the emission of green light [89].

(a) In the TaqMan method, a third sequence-specific oligonucleotide, known as a probe, is used in addition to the two primers. The probe is chosen to anneal within the target sequence in the 3'-5'DNA strand. It has a quencher on one end and a fluorescent reporter dye on the other. In our experiment, carboxytetramethylrhodamine (TAMRA) was used as a quencher, covalently binding to the probe's 3' end. 6-FAM-phosphoramidite (FAM), which is covalently bound to the 5' end of the probe, is used as the reporter fluorescent dye. As long as both the reporter and the quencher are on the probe, the fluorescence emitted by FAM is quenched by the quencher. During the PCR cycle, the polymerase synthesizes the complementary DNA strand, degrading the TaqMan probe. Degradation of the probe releases FAM, therefore its proximity with TAMRA is discontinued. Because the quenching effect is relieved, the fluorescence signal increases and can be measured [90].

(b) The fluorescent dye SYBR Green I is used in the SYBR Green-I method, which inserts nonspecifically into double-stranded DNA. A slow increase in temperature at the end of the amplification cycles leads to the denaturation of the newly synthesized DNA segments. As a result, the previously stored SYBR green I is released, and a change in fluorescence can be detected photometrically. The intensity of fluorescence increases proportionally to the amount of target DNA present [91]. A disadvantage of this method is the lower specificity when compared to the TaqMan method. When the melting curve and SYBR green PCR results indicated that the primers were not amplifying specifically, the more specific TaqMan method was used to achieve maximum specificity.

To perform quantitative RT-PCR, SYBR Green mixes, TaqMan mixes, and DNA samples were prepared as depicted in table 5 and table 6 using a 96-well plate. The plate is then sealed with foil and centrifuged (1200 rpm at 20°C) for 3 minutes. Subsequently, the plates were placed in the thermocycler for analysis.

The configuration of the 7500 Real-Time PCR System (Applied Biosystems) was prepared based on the RT-PCR method using Applied Biosystems 7500 Real-Time PCR software (Thermo Fisher Scientific). SYBR Green I fluorescent dye was used to select the reporter "SYBR" and the quencher "none," while the TaqMan probe was used to select the reporter "FAM" and the quencher "TAMRA." Primer Express software was used to generate exon-specific primers and probes, which were then pre-adjusted to 100 M before use.

Statistical evaluation of qRT-PCR results*:* For relative quantification reference genes, so-called housekeeping genes are used. These genes are expressed independently of cell type, cell stage, and external influences. This expression should, therefore, not vary in response to experimental treatment. The housekeeping gene serves as the foundation for the investigation of the target gene.

By using the $\Delta\Delta C_t$*-method*, the relationship between expressions of the target sequence and housekeeping gene was determined. As shown in Equation 1, the *Ct* values of both samples and controls were normalized to the *Ct* values of the housekeeping gene β-Actin of the respective probe. The relative change in gene expression is calculated according to the formula $2^{-\Delta\Delta C_t}$. Finally, GraphPad Prism 7 (GraphPad Software, LLC) software was used to statistically evaluate and graphically display the mRNA expression values for the respective genes.

Table 5. RT-PCR sample mixture and cycle program (SYBR green method)

Component	(µl)
Go Taq qPCR Master mix	10
HPLC grade H_20	8
10 µM Primer forward	0.5
10 µM Primer reverse	0.5
cDNA Template	1
	20

Stage	Temp (°C)	Time
Holding stage	50	2 min
	95	10 min
Cycling stage 40 repeats	95	15 sec
	60	1 min
Melt Curve stage	95	15 sec
	60	1 min
	95	30 sec
	60	15 sec

Table 6. RT-PCR sample mixture and cycle program (TaqMan method)

Component	(µl)
Platinum Supermix	12.5
HPLC grade H_20	8.5
6 µM Primer forward	0.5
6 µM Primer reverse	0.5
2 µM Primer reverse	0.5
cDNA Template	2.5
	25

Stage	Temp (°C)	Time
Holding stage	50	2 min
	95	10 min
Cycling stage 40 repeats	95	15 sec
	60	1 min

Equation 1. ΔΔCt method for determination of fold mRNA expression

$\Delta C_{t\ sample} = C_{t\ target\ gene} - C_{t\ housekeeping}$

$\Delta C_{t\ control} = C_{t\ target\ gene} - C_{t\ housekeeping}$

$\Delta\Delta C_t = \Delta C_{t\ Sample} - \Delta C_{t\ control}$

Fold expression $= 2^{-\Delta\Delta Ct}$

C_t = Threshold cycle

3.2.14 Protein Isolation

The protein isolation procedure is based on a standardized protocol, which is used in our research laboratory of Children's Hospital Cologne [92].

Protein isolation from tissue is performed in keeping with the following steps:

- Homogenizer tubes were filled with 20 – 50 µL of CHAPS buffer (dependent on the size of the sample) and supplemented with a 1% Halt protease inhibitor cocktail.
- The samples were then homogenized using a mini mortar and afterwards immediately incubated on ice and sonicated (50%, 20 seconds).
- Lysis solution was incubated on ice for one hour and vortexed every 10 minutes to increase protein concentrations.
- The samples were then centrifuged (15 min, 15000 rpm, 4°C) and the supernatant-containing protein was moved to the fresh tube.
- The protein concentration was measured using the bicinchoninic assay (BCA).

BCA assay: To determine the protein concentrations, the Pierce™ BCA Protein Assay Kit (Thermo Fisher Scientific) was used as directed by the manufacturer:

- For each sample and BSA standard series a 1:10 dilution was prepared and duplicated in a 96 well plate (0 mg mL^{-1} up to 2 mg mL^{-1}).
- The Pierce™ BCA Protein Assay Kit (Thermo Fisher Scientific) reagents A and B were mixed in a 1:50 ratio; 200 µL was applied to each well.
- Samples were incubated for 30 minutes at 37°C.
- The absorbance was calculated at 562 nm using the Tecan Infinite® M200 PRO NanoQuant.
- The protein concentrations were determined according to the BSA standard curve.

3.2.15 Western Blot Analysis

Western Blot is used to identify proteins that have been separated by gel electrophoresis based on their size. Subsequently, electrical current is used to promote protein migration to a membrane that can be further processed with particular antibodies of interest. Protein abundance is visualized using secondary antibodies and detecting reagents.

Gel electrophoresis: Sodium dodecyl sulfate (SDS) polyacrylamide gel electrophoresis (PAGE) is one of the most commonly used methods for detection of protein abundance in tissue samples. The amount of SDS bound to the protein, and thus the charge of the complex is approximately proportional to its size. During electrophoresis, negatively charged proteins will migrate towards the positive electrode and will be seperated according to their molecular weights [93].

SDS polyacrylamide gel electrophoresis (PAGE) is performed in keeping with the following steps:

- Samples containing 20µg protein were diluted in 5x SDS-PAGE loading dye and cooked for 10 minutes at 70°C.
- Meanwhile, the running chamber was loaded with 1x Laemmli-buffer, which denature proteins.
- Samples were then loaded on 8-12% SDS PAGE. Stacking and running gel were prepared as depicted in table 7.
- The running gel was run (30 minutes/80 V on running gel, 120 V/3-4 hours on stacking gel) until the visible running border reached the bottom and proteins are separated by size.

Table 7. Preparation of running and separating gels

	Running gel 10 %	**Stacking gel 4 %**
dH_2O	10 ml	3.4 ml
30 % Acryl/Bis	8.25 ml	0.85 ml
1.5 M Tris (pH 8.8)	6.25 ml	---
0.5 M Tris (pH 6.8)	---	0.65 ml
10 % SDS	0.25 ml	0.05 ml
10 % APS	0.25 ml	0.05 ml
TEMED	0.01 ml	0.005 ml

Semi-dry blotting: The transfer of the proteins from the gel to a nitrocellulose membrane is performed through a method called *semi-dry blotting*. In this procedure, the membrane was primed with cold dH_2O (4°C) and with 4 layers of Whatman paper and then incubated in a cold transfer buffer (4°C) for 5 minutes. Subsequently, both the gel and the membrane were placed

between two layers of Whatman paper on each side. The transition of the proteins was carried out for 2 hours with 1.3 mA/cm^2, followed by a Ponceau staining to confirm that the proteins are transferred properly.

Immunodetection of proteins: The membrane was blocked with a blocking solution (5% milk + 2% BSA in TBST) to avoid background signaling. The membrane was then incubated with the primary antibody for 30 minutes at RT followed by overnight incubation at 4°C on a shaker. The next day, the membrane was washed 3 x 10 minutes with TBST followed by incubation with suitable horseradish peroxidase (HRP) conjugated secondary antibody diluted in 5% TBST milk for 1 hour at RT on a shaker. All antibodies were either diluted in 5% BSA in TBST or 5% milk in TBST following the manufacturer's recommendations (Table 8).

Table 8. Antibody dilutions

Antibody	Weight	Dilution	% 5 in	Secondary antibody	Dilution
Surfactant protein C	21 kDa	1:1000	Milk	Goat	1:1000
Aquaporin 5	27 kDa	1:2000	BSA	Rabbit	1:2000
CD31	110-120 kDa	1:1000	Milk	Rabbit	1:2000
VE Cadherin	115 kDa (predicted 87)	1:1000	BSA	Rabbit	1:1000
Alpha smooth muscle actin	43 kDa	1:200	Milk	Mouse	1:1000
STAT3	79,86 kDa	1:3000	Milk	Mouse	1:3000
pSTAT3	79,86 kDa	1:1000	BSA	Rabbit	1:1000
SMAD 2/3	52,60 kDa	1:1000	BSA	Rabbit	1:1000
Caspase 3	17, 19, 35 kDa	1:2000	Milk	Rabbit	1:2000
PAI-1	48 kDa	1:1000	Milk	Rabbit	1:1000
PCNA	36 kDa	1:10000	Milk	Mouse	1:10000

Visualization of protein bands: The samples are soaked in TBST solution after three washing steps with TBST. Labeled protein bands were visualized by using the Chemiluminescence solution (Amersham ECL Prime Western Blotting Detection Reagent Kit), ChemiDoc XRS+ (Bio-Rad Laboratories GmbH), and Image LabTM software (Bio-Rad Laboratories GmbH) according to the manufacturer's instructions.

Stripping: Stripping allows the identification of more than one protein on the same membrane. A βME-containing stripping buffer was added and the membrane was incubated in an H_2O bath for 10-15 minutes at 56°C. βME acts as a reductant of previously applied antibodies to cleave disulfide bonds. The dilution factors and the dilution solutions used for the respective primary and secondary antibodies are shown in section 2.1.4 and primary and secondary antibodies are listed in section 2.1.6.

Evaluation: The quantitative evaluation of western blot analysis was performed using densitometry and the Image Lab™ software (Bio-Rad Laboratories GmbH). Protein band density was measured and expressed as a ratio of protein of interest over the loading control (β-Actin). The statistical evaluation and graphical representation of the obtained protein quantity were carried out using the GraphPad Prism 7 software (GraphPad Software, LLC).

3.3 Statistical Analysis

Statistical analyses were performed on GraphPad Prism 7 software (GraphPad Software, LLC). Statistical significance was calculated using the non-parametric Mann-Whitney U test when two groups were compared or the One-way ANOVA followed by Bonferroni post-test to compare outcomes four groups. Statistical data are presented as mean value ± standard mean error (SEM). Significances were indicated with *$p<0.05$, **$p<0.01$, ***$p<0.001$, and data was graphically represented using GraphPad Prism 7.

4. Results

4.1 Quantitative Structural Analysis

4.1.1 Alveolarization of the Lungs

Hyperoxia adversely affects lung alveolarization and induces experimental BPD. Since MMP-12 plays a significant role in key pathomechanistic processes of BPD, including ECM remodeling composition and inflammation, we hypothesized that loss of MMP-12 may attenuate hyperoxia-induced lung injury and protect from BPD. To test our hypothesis, we used previously established MMP-12 knock-out mice. Newborn WT and $MMP12^{-/-}$ mice were exposed to room air (normoxia) or hyperoxia for 14 days; at the end of 14 days, all mice were transferred into normoxia to recover for another 14 days. At P28, pups were sacrificed and lungs were excised for further analysis. To investigate the effects of MMP-12 on lung morphology and alveolar formation, we stained paraffin sections with H&E. Afterwards, MLI, RAC, ST, and SA were quantified in both WT and $MMP12^{-/-}$ mice as described above.

Prolonged hyperoxia for 14 days after birth caused a marked lung injury. Quantitative histomorphometric changes in the neonatal lungs after hyperoxia comprised increased MLI and SA as well as reduced RAC in both groups WT^{HYX} and $MMP12^{-/-HYX}$ when compared to the control groups WT^{NOX} and $MMP12^{-/-NOX}$, respectively. These changes in alveolar parameters indicate fewer and larger alveoli after hyperoxia. However, $MMP12^{-/-\ HYX}$ were partly protected from hyperoxia when compared to WT^{HYX}. Moreover, $MMP12^{-/-NOX}$ mice showed a significant reduction of ST whereas $MMP12^{-/-HYX}$ mice showed significantly thicker septae compared to WT^{NOX} and WT^{HYX}, respectively. Furthermore, WT^{HYX} had thicker septae compared to WT^{NOX} (Figure 6).

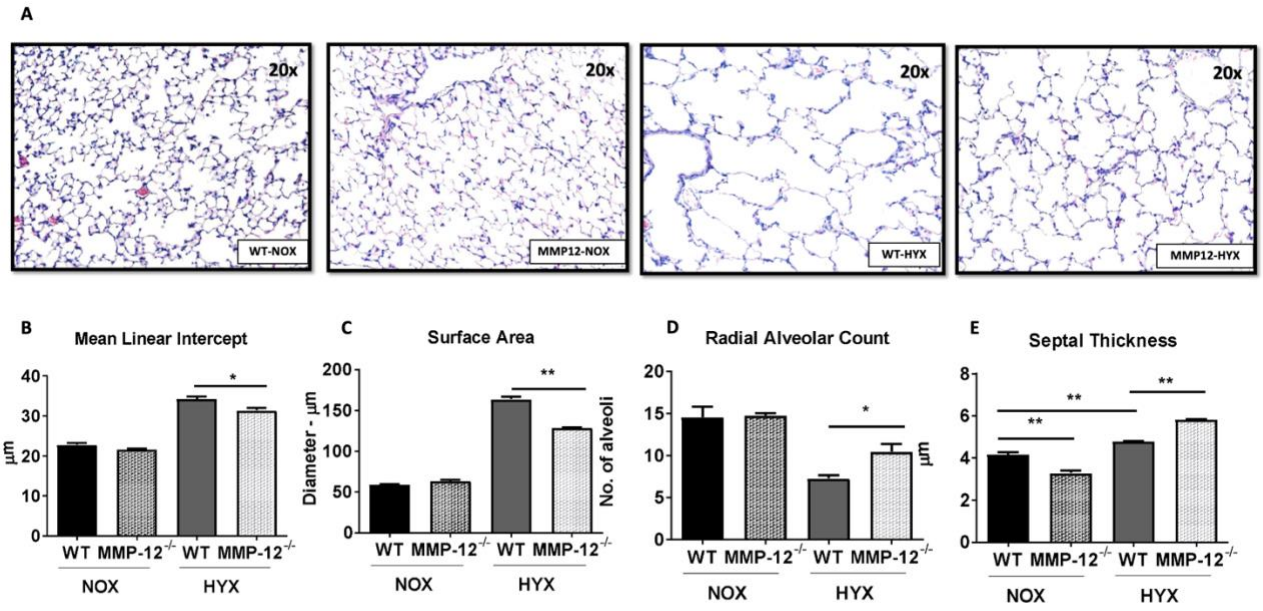

Figure 6. A: Representative images of hematoxylin and eosin (H&E) stained tissue sections showing alveolarization in mice at postnatal day 28 (P28). Wildtype (WT) and MMP-12 knockout mice ($MMP12^{-/-}$) were exposed to hyperoxia (HYX, 85 % O_2) or normoxia (NOX, 21 % O_2) from postnatal day 1 (P1) to P14. Starting from P15 all animals were exposed to 21% O_2 until P28 B-E: Summary data of the quantitative histomorphometric analysis: mean linear intercept (MLI, B), the average surface are of a single alveolus (average surface area; C), radial alveolar count (RAC; D) and septal thickness (E). Mean±SEM; n = 5-7/group; non-parametric Mann-Whitney test: *p<0.05; **p<0.001.

4.1.2 Organization of the Extracellular Matrix

4.1.2.1 Elastic Fibers

To investigate the role of MMP-12 in elastogenesis and alveolar formation, we stained paraffin sections with Hart's stain. Histologic sections revealed an improved alveolar structure as well as a more physiological organization of elastic fibers in $MMP12^{-/-HYX}$ in terms of reduced abnormal deposition, an even accumulation of the fibers as well as localization at the tips of secondary crests. The analysis also showed that loss of MMP-12 promotes elastic fiber production in the lungs of $MMP12^{-/-HYX}$. Elastic fibers are normally found at the tips of the septae, i.e., secondary crests. The amount of secondary crests was significantly increased in $MMP12^{-/-HYX}$ compared to WT^{HYX}. These findings suggest that in the absence of MMP-12 septation and alveolar formation is preserved (Figure 6).

Moreover, abnormal deposition of elastic fibers and structural disorganization in the lung parenchyma was observed in the lungs of WT^{HYX} (Figure 7, F).

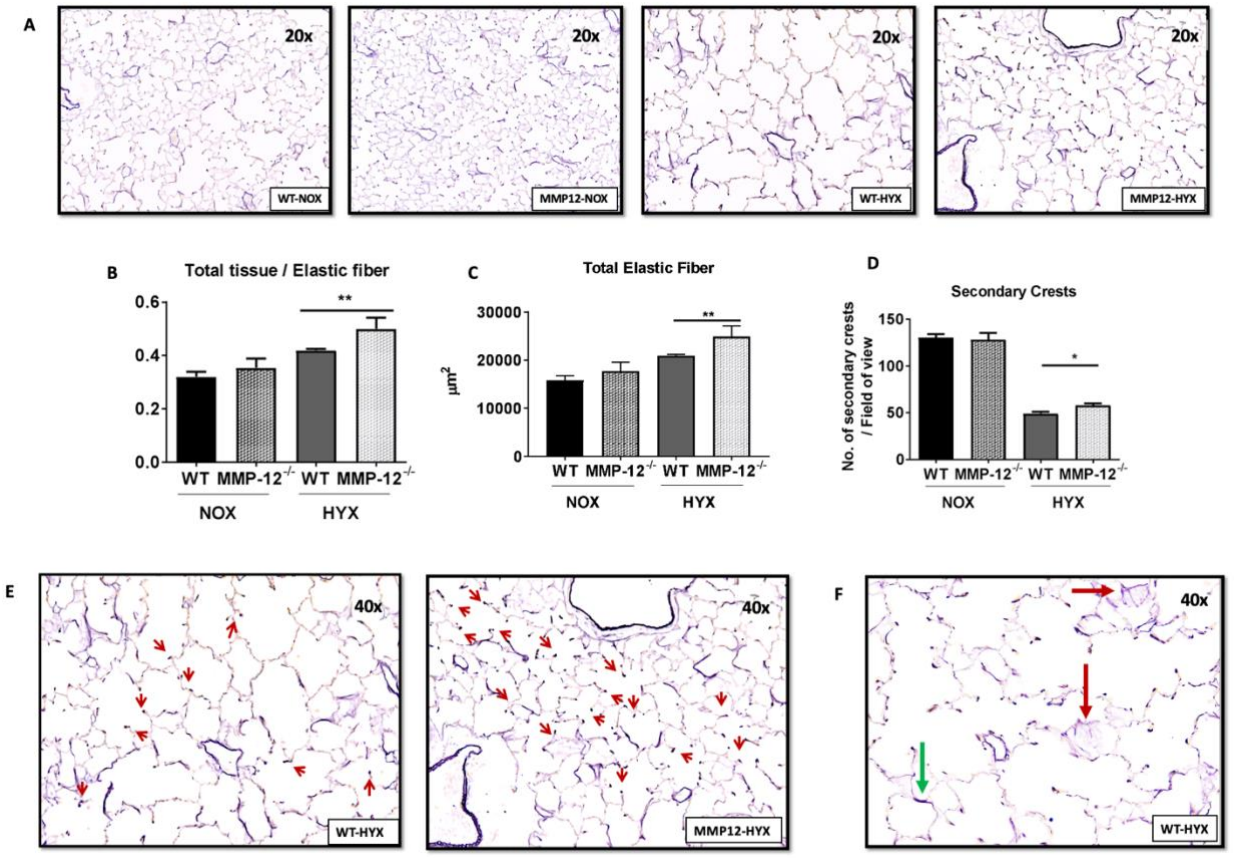

Figure 7. Wildtype (WT) and MMP-12 knockout mice (MMP12$^{-/-}$) were exposed to hyperoxia (HYX, 85 % O_2) or normoxia (NOX, 21 % O_2) from postnatal day 1 (P1) to P14. Starting from P15 all animals were exposed to 21% O_2 until P28 A: Representative images of Hart's-stained tissue sections showing distribution and localization of elastic fibers in mice at postnatal day 28 (P28). B, C: Summary data of the elastic fiber content relative to lung tissue in % (B) and quantitative analysis of elastic fibers per defined area (µm^3) (C). D: Quantitative analysis of secondary crests per field of view. E: High magnification of hyperoxia exposed groups; red arrows indicate elastic fibers at the secondary tips after hyperoxia. F: Representative image of abnormal deposition and organization of elastic fibers (red arrows) and elastin accumulation (green arrow). Mean±SEM; n = 5-7/group; non-parametric Mann-Whitney test: *p<0.05; **p<0.001.

4.1.2.2 Collagen

To investigate the role of MMP-12 in collagen abundance and structure, we stained paraffin sections with PSR. Our results showed an increased amount of collagen in WT^{HYX} compared to MMP12$^{-/-HYX}$. Moreover, total collagen abundance related to alveolar tissue was elevated in the WT^{HYX} compared to MMP12$^{-/-HYX}$ (Figure 8; A, B, C, D). However, the type of collagen cannot be distinguished with PSR. According to previous studies, a specific increase of Collagen I/Collagen III ratio was observed in patients with BPD, as well as an increased level of Collagen IV [11].

The histomorphometric analysis results of collagen were similar to the observation using a polarization microscope. By using this technique, it is possible to observe the collagenization of the lung tissue, in terms of observing the collagen skeleton underneath the tissue as well as their form and thickness. Red, yellow and green colors can be observed showing a decreased abundance of collagen fibers. Collagen distribution and abundance were determined to be similar among $MMP12^{-/-NOX}$ and WT^{NOX}. However, $MMP12^{-/-HYX}$ mice had a skeleton of collagen with thinner and greener fibers and showed fewer accumulation sites than WT^{HYX} mice (figure 8, D).

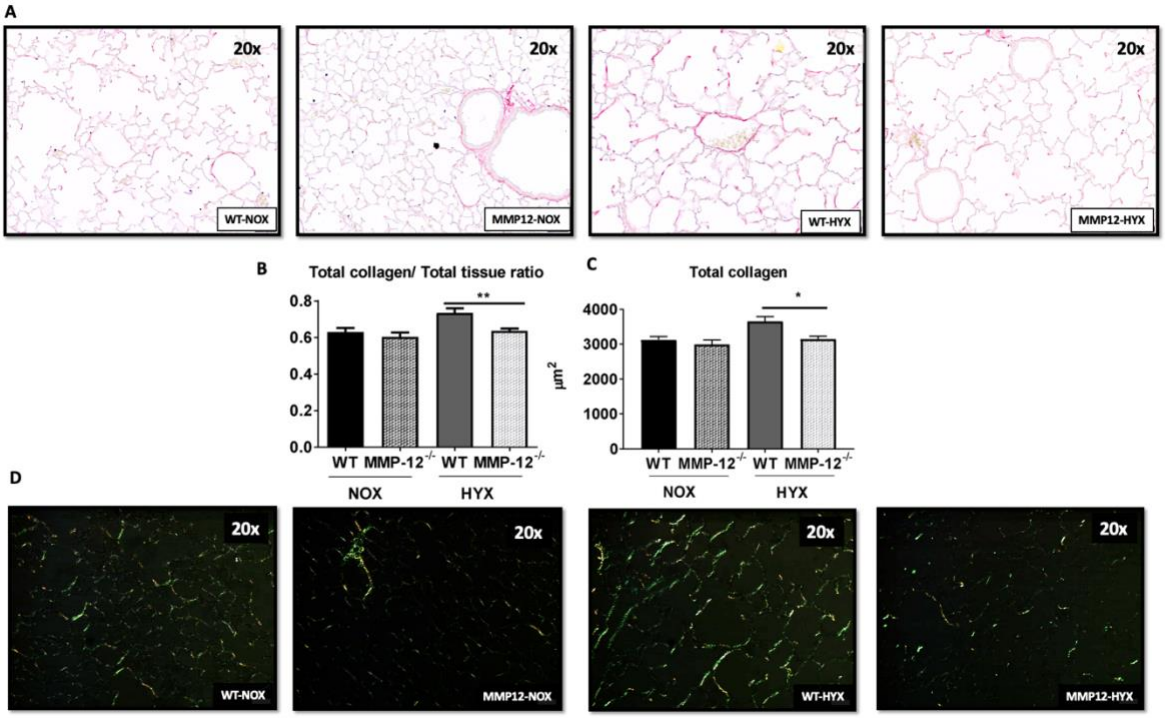

Figure 8. Wildtype (WT) and MMP-12 knockout mice ($MMP12^{-/-}$) were exposed to hyperoxia (HYX, 85 % O_2) or normoxia (NOX, 21 % O_2) from postnatal day 1 (P1) to P14. Starting from P15 all animals were exposed to 21% O_2 until P28 A: Representative images of PSR stained tissue sections showing distribution and localization of collagen in mice at postnatal day 28 (P28). B, C: Summary data of quantitative analysis of collagen content relative to lung tissue in % (B) and of collagen per defined area (μm^3) (C). D: Representative images of PSR stained tissue sections using a polarization microscope showing the distribution of collagen in mice at P28; green and yellow staining indicate collagen abundance. Mean±SEM; n = 5-7/group; non-parametric Mann-Whitney test: *p<0.05; **p<0.001.

4.1.3 Assessment of Inflammation

To identify the number of inflammatory cells in lungs, specific CD68 immuno staining was performed. CD68 is a glycosylated type I membrane protein found in the granules of macrophages and widely used to determine macrophages. The number of macrophages per slide in 20 different areas under 100x magnification was quantified.

Our results showed that loss of MMP-12 inhibited macrophage influx in the neonatal lung, protecting lungs from inflammation under hyperoxia. MMP12$^{-/-HYX}$ mice showed a reduced number of macrophages under hyperoxia suggesting a protective effect of loss of MMP-12 (Figure 9).

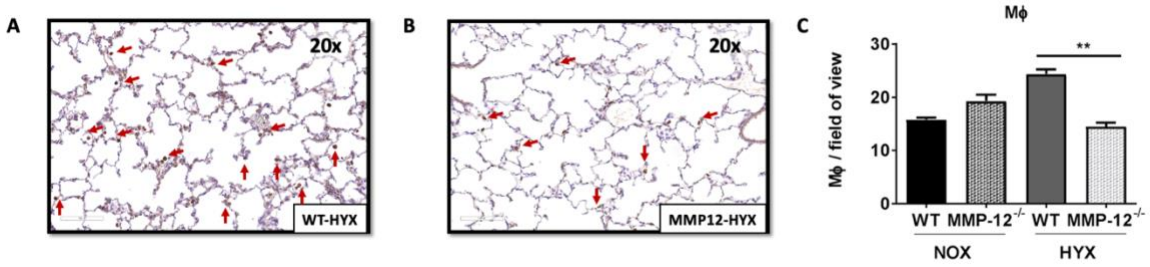

Figure 9. Wildtype (WT) and MMP-12 knockout mice (MMP12 $^{-/-}$) were exposed to hyperoxia (HYX, 85 % O_2) or normoxia (NOX, 21 % O_2) from postnatal day 1 (P1) to P14. Starting from P15 all animals were exposed to 21% O_2 until P28. A, B: Representative of macrophage staining of hyperoxia exposed animals using CD68 as a marker. Red arrows are depicting positively stained cells. C: Quantification data of CD68-positive cells per field of view. Mean±SEM; n = 5-7/group; non-parametric Mann-Whitney test: **p<0.01.

4.1.4 Angiogenesis

The arrested development of the distal lung is associated with impaired angiogenesis. Lungs with BPD show alveolar simplification and significant disruption of the microvascular structure [94]. To investigate the effects of hyperoxia on microvascular growth, vWF staining was performed. The number of microvessels was quantified in two groups: 0-20 μm and 20-100 μm microvessels are quantified per slide in 20 different areas under 10x magnification to determine arrested angiogenesis.

Our data showed that loss of MMP-12 has a positive effect on microvascular structure. MMP12$^{-/-HYX}$ showed a significantly elevated amount of both 0-20μm and 20-100μm vessels within the lung tissue compared to WT^{HYX}.

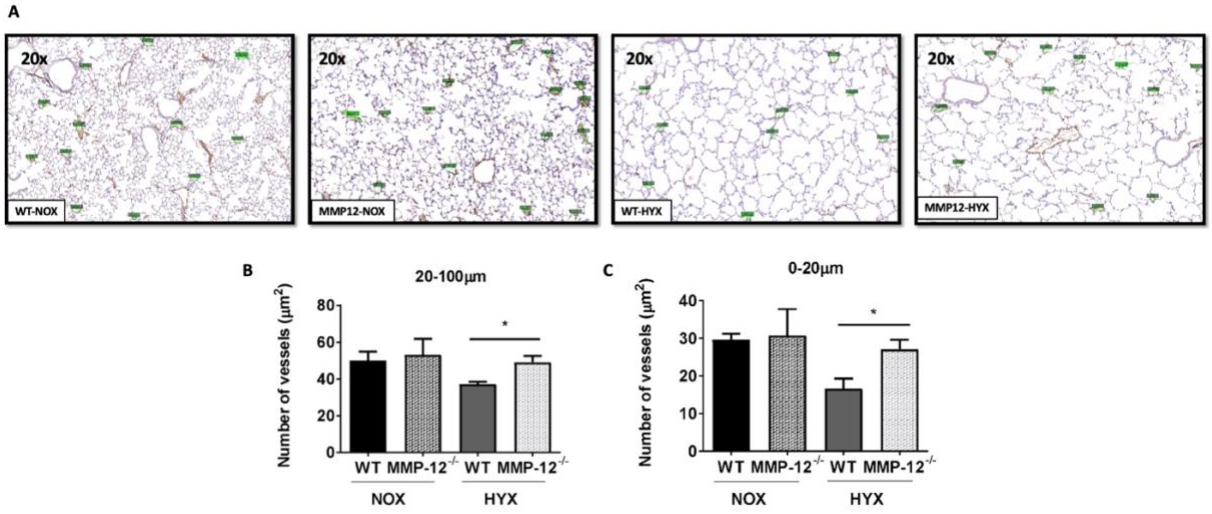

Figure 10. Wildtype (WT) and MMP-12 knockout mice ($MMP12^{-/-}$) were exposed to hyperoxia (HYX, 85 % O_2) or normoxia (NOX, 21 % O_2) from postnatal day 1 (P1) to P14. Starting from P15 all animals were exposed to 21% O_2 until P28. A: Representative images of von Willebrand factor stained tissue sections from mice at P28; green signs indicate microvessels (0-100µm). B, C: microvessel count per μm^2: 20-100 µm (B) and 0-20 µm (C). Mean±SEM; n = 5-7/group; non-parametric Mann-Whitney test: *p<0.05.

4.2 Molecular Studies

4.2.1 Analysis of Alveolar Cellular Composition

To complement our histological findings, we first performed quantitative real-time PCR (qRT-PCR) to determine gene expressions of markers of both AECI and AECII.

4.2.1.1 Surfactant Proteins

Surfactant proteins are chemically heterogeneous proteins that form a complex and play an important role in normal lung development. Both protein and lipid components of these proteins are secreted in AECIIs after being stimulated. Four major types of surfactant proteins have been demonstrated, being surfactant protein-A (SFTPA), SFTPB, SFTPC, and SFTPD. SFPTC is specific for AECII.

Our qRT-PCR data showed an increased gene expression of *Sftpb* and *Sftpc* both in $MMP12^{-/-NOX}$ compared to WT^{NOX} and $MMP12^{-/-HYX}$ compared to WT^{HYX}. However, none of the increased

values were found statistically significant (Figure 11 B, C); most likely due to the recovery of the lungs after 14 days of hyperoxia.

4.2.1.2 Epithelial Markers

Aquaporin 5: Aquaporins are a family of small integral membrane proteins. Aquaporin 5 (*Aqp5*) is a water channel protein that plays a role in the generation of saliva, tears, and pulmonary secretions. *Aqp5* is a marker for AECIs, which are the squamous cells that cover the majority of the gas exchange surface of the lung. Moreover, during EMT, AECIIs can differentiate to AECIs following hyperoxic injury. Our qRT-PCR results showed a decreased expression of *Aqp5* in $MMP12^{-/-HYX}$ compared to WT^{HYX} (Figure 11, E).

E-Cadherin *(Cdh1)*: The cadherin superfamily plays an important role in intracellular adhesiveness and maintenance of the normal tissue architecture in which E-cadherin is the major component. E-cadherin is expressed in epithelial cells, and changes in E-cadherin expression are the prototypical epithelial cell marker of EMT. E-cadherin expression is reduced during EMT in a variety of conditions such as embryonic development, tissue fibrosis, and cancer. Since hyperoxia can induce EMT, we investigated the gene expression of *Cdh1* (E-cadherin) and found no statistically significant difference between the four groups (Figure 11, F).

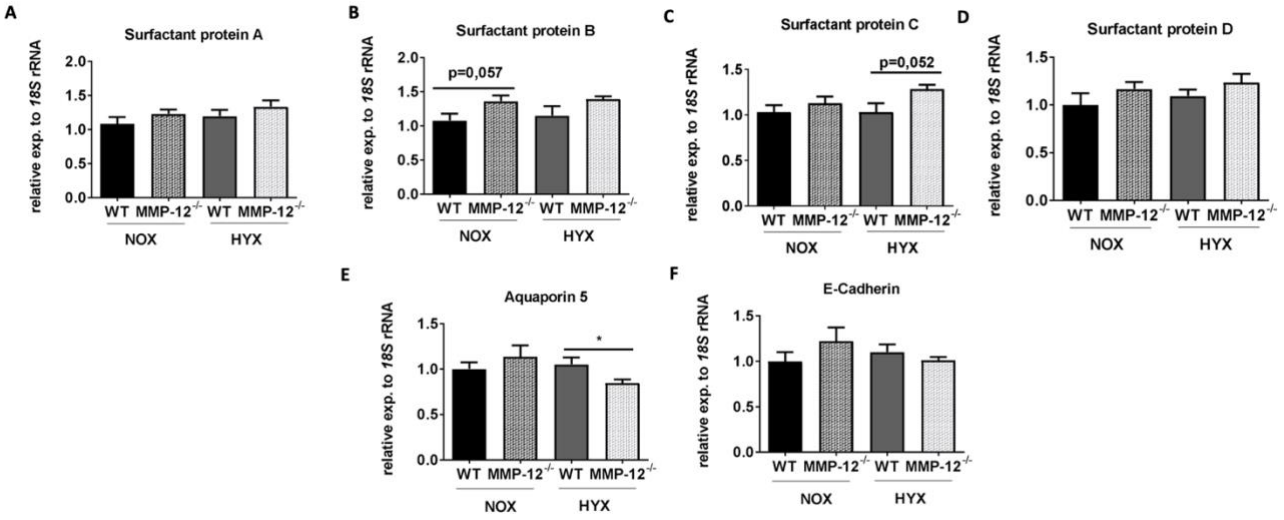

Figure 11. Wildtype (WT) and MMP-12 knockout mice (MMP12$^{-/-}$) were exposed to hyperoxia (HYX, 85 % O_2) or normoxia (NOX, 21 % O_2) from postnatal day 1 (P1) to P14. Starting from P15 all animals were exposed to 21% O_2 until P28, followed by the assessment of gene expression of the surface markers of type one and type two pneumocytes (ACE) using qRT-PCR. A-D: Surface markers of AECI and AECII, surfactant protein *Sftpa*, *Sftpb*, *Sftpc*, *Sftpd*. E: Surface markers of AECI cells, aquaporin 5 (*Aqp5*) . F: epithelial cell marker of epithelial-mesenchymal transition (EMT), E-cadherin (*Cdh1*). Mean±SEM; (n = 10-12/group); non-parametric Mann-Whitney test; *p<0,05; **p<0.01.

4.2.2 Analysis on Extracellular Matrix Composition

Elastin: Firstly, the elastin component of the samples was investigated. Although our histomorphometric data suggested an increase in elastic fibers and elastic fiber/tissue ratio, qRT-PCR results revealed no significant difference in gene expression of elastin (*Eln*) among groups (Figure 12, A).

Collagen: As a second step, collagen type-I (*Col1a1*) and type-III (*Col3a1*) expressions were investigated. The histomorphometric data showed a decreased production of collagen as well as collagen/tissue ratio in MMP12$^{-/-HYX}$ mice. Our qRT-PCR data showed an increased expression of *Col3a1* in MMP12$^{-/-HYX}$ mice compared to WT^{HYX}; the expression of *Col1a1* was not significantly regulated (Figure 12, B, C).

Fibrillin: Fibrillins are elastin-binding proteins. Both fibrillin 1 (*Fbn1*) and fibrillin 2 (*Fbn2*) are important proteins that have crucial part in alveolarization and structural homeostasis. Our qRT-PCR data showed an increased expression of *Fbn2* MMP12$^{-/-NOX}$ compared to WT^{NOX} and no difference in the gene expression of *Fbn1* among the four groups. (Figure 12, D,E).

Fibulin: Fibulin (*Fbln*) proteins promote proper elastic fiber formation via binding elastin. It has been shown that *Fbln5* shows a tendency to rise under hyperoxia. The gene expression of *Fbln5* was increased in WT^{HYX} compared to WT^{NOX}, as well as in $MMP12^{-/-HYX}$ compared to $MMP12^{-/-NOX}$. The gene expression of *Fbln4*, however, was only increased in in $MMP12^{-/-NOX}$ versus WT^{NOX} and not significantly affected by hyperoxia (Figure 12, F, G).

Microfibrillar-associated protein 4: Microfibrillar-associated protein 4 (*Mfap4*) is an extracellular glycoprotein found in elastic fibers. *Mfap4* has been shown to interact with *Fbn1* and promote elastic fiber formation in *in vitro* dermal skin fibroblast cultures. [95]. The qRT-PCR results demonstrated a significant increase in WT^{HYX}, but not in $MMP12^{-/-HYX}$ when compared to WT^{NOX} and $MMP12^{-/-NOX}$, respectively (Figure 12, H).

Plasminogen activator inhibitor-1: Plasminogen activator inhibitor-1 (*Serpine1*) plays an important role in the regulation of ECM degradation. Among the inhibitors of plasminogen activators, *Serpine1* is one of the most important substances whose expression is increased in the process of lung fibrosis. The qRT-PCR data showed a significant increase in both WT^{HYX} compared to WT^{NOX}, whereas hyperoxia only induce a mild, and not significant increase of *Serpine1* in $MMP12^{-/-HYX}$ (Figure 12, I).

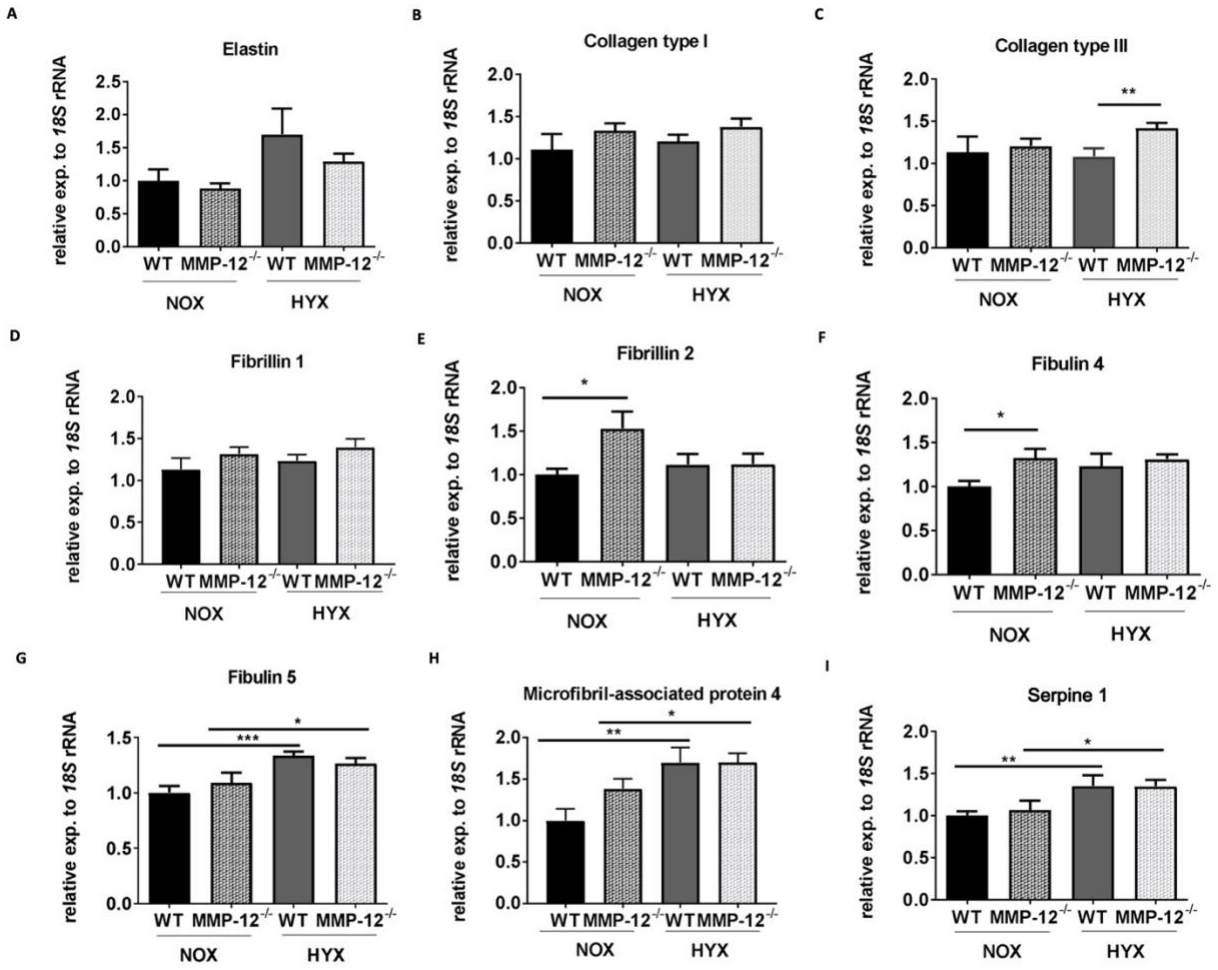

Figure 12. Wildtype (WT) and MMP-12 knockout mice (MMP12$^{-/-}$) were exposed to hyperoxia (HYX, 85 % O_2) or normoxia (NOX, 21 % O_2) from postnatal day 1 (P1) to P14. Starting from P15 all animals were exposed to 21% O_2 until P28, followed by assessment of extracellular matrix components using qRT-PCR [A: Elastin (*Eln*), B: Collagen type I (*Col1a1*), C: Collagen type III (*Col3a1*), D: Fibrillin 1 (*Fbn1*), E: Fibrillin 2 (*Fbn2*), F: Fibulin 4 (*Fbln4*) G: Fibulin 5 (Fbln5), H: Microfibril-associated protein 4 (*Mfap4*) I: Serpine 1 (*Pai1*)]. Mean±SEM; (n = 10-12/group); non-parametric Mann-Whitney test; *p<0,05; **p<0.01.

4.2.3 Analysis on Stromal Markers

Desmin: Desmin is an important structural protein that is thought to be a marker of myofibroblasts and alveolar ring muscles due to its expression in the smooth muscle cells of airways and alveolar ducts [96]. The qRT-PCR results for desmin (*Des*) showed no difference between MMP12$^{-/-HYX}$ and WT^{HYX}. However, the gene expression of *Des* in the MMP12$^{-/-NOX}$ group was significantly higher compared to WT^{NOX}, indicating that loss of MMP-12 might regulate smooth muscle cell characteristics and might thereby affect vascular and bronchial development (Figure 13, A).

Vimentin: Vimentin is a type III intermediate filament protein that serves as the primary cytoskeletal component and is found in mesenchymal cells [97]. Vimentin is often used as a marker of mesenchymally-derived cells or cells undergoing EMT [98]. The qRT-PCR results demonstrated a significant decrease in gene expression of vimentin (*Vim*) in the $MMP12^{-/-HYX}$ group compared to WT^{HYX}. (Figure 13, B).

Alpha-smooth muscle actin (α-SMA): α-SMA, is an actin isoform that is predominant in smooth muscle cells as well as in myofibroblasts, and is involved in fibrogenesis [99]. The elevated expression of ECM proteins has been shown to be associated with an increased number of myofibroblasts, which are α-SMA positive and play a role in fibrosis [14]. Our gene expression analysis revealed an increase in α-SMA (*Acta2*) gene expression in WT^{HYX} when compared to WT^{NOX}. Interestingly, hyperoxia did not affect *Acta2* expression in lungs of $MMP12^{-/-HYX}$ mice (Figure 13, C).

Zinc finger protein 1 (SNAI1): SNAI1, also referred to as Snail, belongs to a family of transcription factors that promote the repression of the adhesion molecule E-cadherin to regulate EMT during embryonic development [100]. The qRT-PCR results demonstrated a mild, but not significant increase of *Snai1* expression in WT^{HYX} compared to WT^{NOX}. Interestingly, *Snai1* gene expression was significantly lower in lungs of the $MMP12^{-/-HYX}$ than in lungs of WT^{HYX} (Figure 13, D).

Zinc finger protein 2 (SNAI2): The encoded protein of the *Snai2* gene, also known as Slug, acts as a transcriptional repressor which plays a role in EMT and has antiapoptotic properties [100]. The qRT-PCR data showed a significant increase in gene expressions in WT^{HYX} compared to WT^{NOX}; in contrast, loss of MMP-12 attenuates hyperoxia-induced *Snai2* mRNA expression. (Figure 13, E).

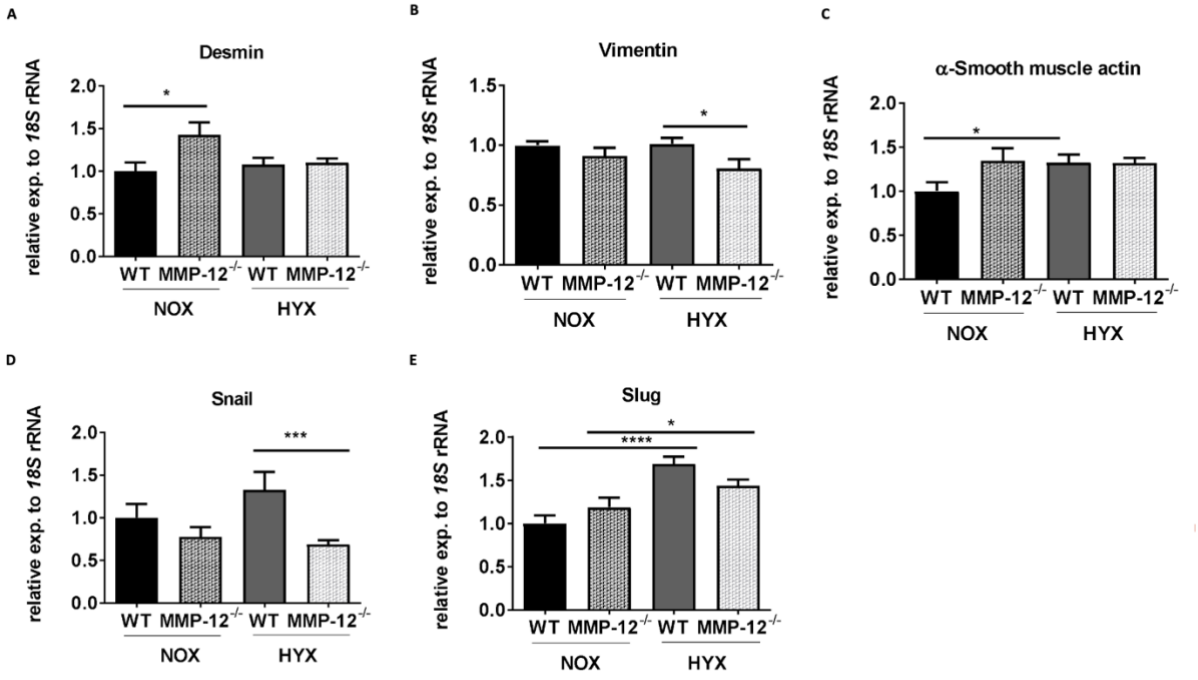

Figure 13: Wildtype (WT) and MMP-12 knockout mice (MMP12$^{-/-}$) were exposed to hyperoxia (HYX, 85 % O_2) or normoxia (NOX, 21 % O_2) from postnatal day 1 (P1) to P14. Starting from P15 all animals were exposed to 21% O_2 until P28, followed by assessment of stromal markers using qRT-PCR. A: Desmin (*Des*) B: Vimentin (*Vim*) C: α-smooth muscle actin (*Acta2*) D: Zinc finger protein 1, Snail (*Snai1*), E: Zinc finger protein 2, Slug (*Snai2*). Mean±SEM; (n = 10-12/group); non-parametric Mann-Whitney test; *p<0,05; **p<0.01.

4.2.4 Analysis of Growth Factors

Connective tissue growth factor (CTGF): CTGF regulates various biological processes (e.g., cell adhesion, myofibroblast activation) associated with fibrogenesis and has been found to promote deposition of several ECM proteins [101]. Moreover, CTGF has been demonstrated to affect various cell types involved in the fibrogenic process, such as epithelial cells, mesenchymal stem cells, and resident fibroblasts [101]. Our qRT-PCR results demonstrated a decrease in *Ctgf* gene expression in the MMP12$^{-/-HYX}$ group compared to MMP12$^{-/-NOX}$ (Figure 14, A).

Vascular endothelial growth factor A (VEGFA): VEGFA is a pluripotent growth factor that influences endothelial cell function in a variety of ways. In adults, VEGFA is also important for lung development and acts as a maintenance factor [102]. The qRT-PCR results showed no significant difference in *Vegfa* expression among the four groups (Figure 14, B).

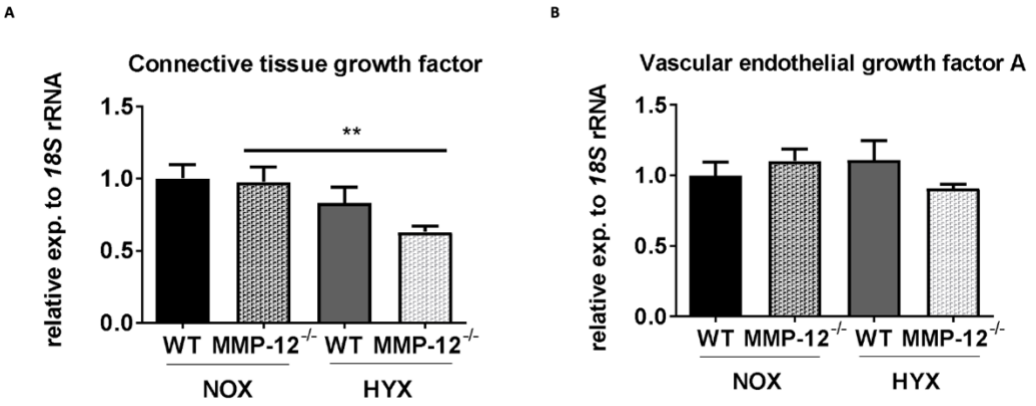

Figure 14. Wildtype (WT) and MMP-12 knockout mice (MMP12$^{-/-}$) were exposed to hyperoxia (HYX, 85 % O_2) or normoxia (NOX, 21 % O_2) from postnatal day 1 (P1) to P14. Starting from P15 all animals were exposed to 21% O_2 until P28, followed by assessment of growth factors [A: Connective tissue growth factor (*Ctgf*), B: Vascular endothelial growth factor A (*Vegfa*)]. Mean±SEM; (n = 10-12/group); non-parametric Mann-Whitney test; *p<0,05; **p<0.01.

4.2.5 Analysis on Macrophage Surface Markers

To determine the inflammatory properties of macrophages, cytokine and chemokine expression pattern of M1-like pro-inflammatory and M2-like anti-inflammatory macrophages were examined among four study groups.

M1-like macrophage markers: For the evaluation of the characteristic markers of M1-like macrophages, C-X-C motif chemokine 10 (*Cxcl10*, IP-10), interleukin 6 (*Il6*), and toll-like receptor 4 (*Tlr4*) were selected and qRT-PCR measurements were performed. The results demonstrated a significant increase of *Cxcl10* gene expression in both WT^{HYX} and MMP12$^{-/-\ HYX}$ when compared to WT^{NOX} and MMP12$^{-/-NOX}$, respectively (Figure 15, A). The expression of *Il6* and *Tlr4* mRNA was neither altered by hyperoxia or Mmp12 knockout.

M2-like macrophage markers: For the evaluation of the classical markers of M2-like macrophages, arginase-1 (*Arg1*), *Il4*, and *Il13* were selected and gene expression was assessed using qRT-PCR. The data only show an increase of *Arg1* gene expression in MMP12$^{-/-HYX}$ when compared to WT^{HYX} (p=0.0503), whereas changes in the expression of *Il4* and *Il13* were insignificant (Figure 15, B).

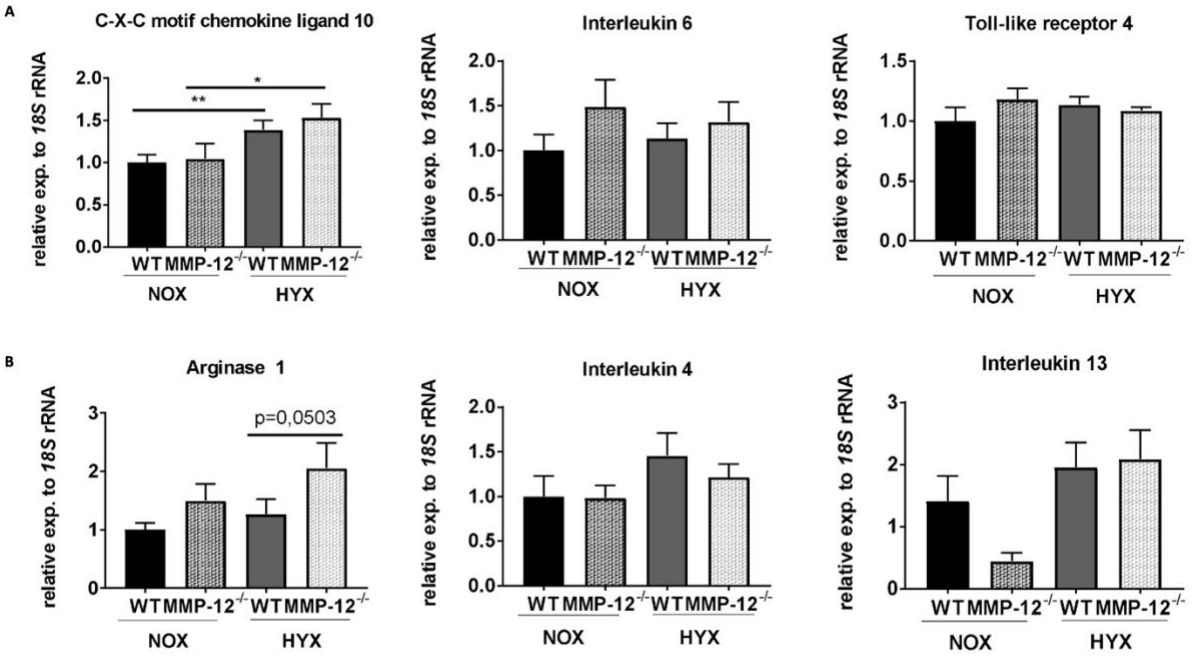

Figure 15. Wildtype (WT) and MMP-12 knockout mice (MMP12$^{-/-}$) were exposed to hyperoxia (HYX, 85 % O_2) or normoxia (NOX, 21 % O_2) from postnatal day 1 (P1) to P14. Starting from P15 all animals were exposed to 21% O_2 until P28, followed by assessment of gene expression of genes characteristic for M1 polarization [A; C-X-C motif chemokine ligand 10 (*Cxcl10).* Interleukin 6 (*Il6*), and toll-like receptor-4 (*Tlr-4*)] and M2 polarization [B; arginase 1 (*Arg1*), Interleukin 4(*Il4*), Interleukin 13 (*Il13*)] using qRT-PCR. Mean±SEM; (n = 10-12/group); non-parametric Mann-Whitney test; *p<0,05; **p<0.01.

4.3 Immunoblot Analysis

4.3.1 Alveolar Structure

Aquaporin-5: Aquaporin-5 (AQP5) is a strong determinant of AECIs [103]. Although being produced more in MMP12$^{-/-NOX}$ compared to WT^{NOX}, this increase was not statistically significant. Hyperoxia did not affect AQP5 protein abundance neither in WT nor MMP12$^{-/-}$ (Figure 16, A).

Surfactant protein-C: SFTPC is primarily produced by AECIIs as an integral membrane precursor (pre-) protein, which is subsequently processed proteolytically and secreted into alveolar space with phospholipids [104]. SFTPC promotes the surface tension-lowering properties of surfactant and also plays a role in regulating inflammation. Assessment of SFTPC using immunoblot showed a significant increase in pre-SFTPC in both MMP12$^{-/-NOX}$ and MMP12$^{-/-HYX}$ group when compared to WT^{NOX} and WT^{HYX}, respectively. Mature SFTPC, however, was only increased in MMP12$^{-/-NOX}$ compared to WT^{NOX} (Figure 16, B).

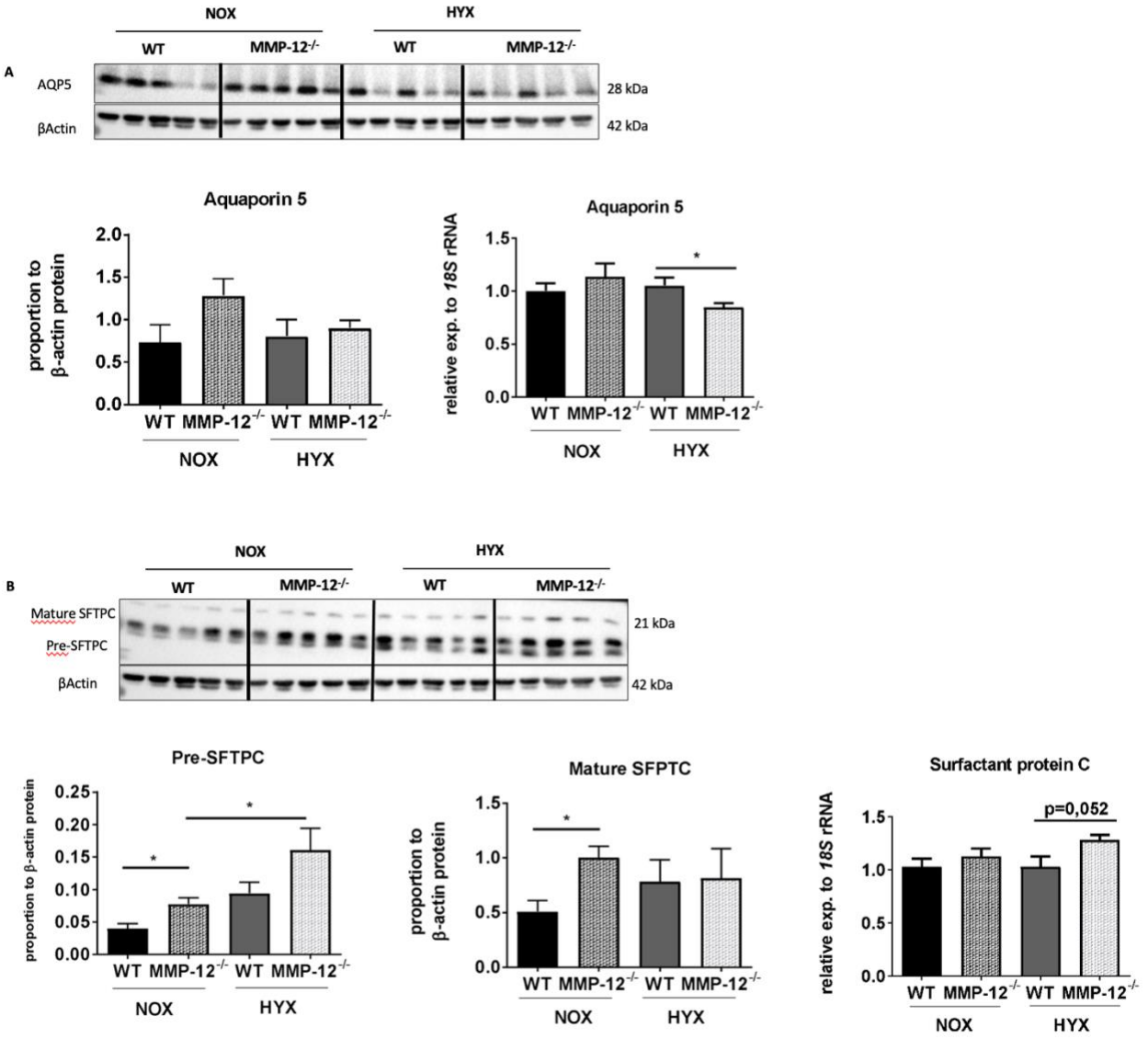

Figure 16. Measurement of protein abundance: Wildtype (WT) and MMP-12 knockout mice (MMP12$^{-/-}$) were exposed to hyperoxia (HYX, 85 % O_2) or normoxia (NOX, 21 % O_2) from postnatal day 1 (P1) to P14. Starting from P15 all animals were exposed to 21% O_2 until P28. Immunoblots show epithelial cell markers at P28; β-actin served as loading control. A: Immunoblot (left) and gene expression (right) of aquaporin 5 protein (AQP5) as a marker of type I alveolar epithelial cells (AECI). B: Immunoblot (left) and gene expression (right) of surfactant protein C (SFTPC) as an indicator of AECII. Mean±SEM; (n = 5/group); non-parametric Mann-Whitney test; *p<0,05; **p<0.01.

4.3.2 Extracellular Matrix Metabolism

Plasminogen activator inhibitor 1: *Serpine1* expression and activation play an important role in the process of lung fibrosis. Although qRT-PCR data showed an increase in the gene expression of *Serpine1* in MMP12$^{-/-HYX}$; immunoblot results demonstrated a significant increase in PAI-1

protein abundance in WT^{HYX} when compared to WT^{NOX} that was significantly attenuated in in $MMP12^{-/-\ HYX}$ (Figure 17).

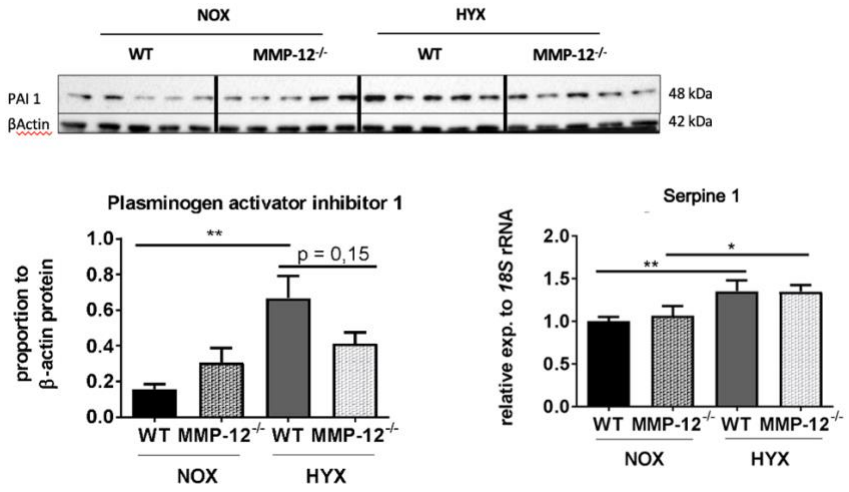

Figure 17. Measurement of PAI-1 protein abundance: Wildtype (WT) and MMP-12 knockout mice ($MMP12^{-/-}$) were exposed to hyperoxia (HYX, 85 % O_2) or normoxia (NOX, 21 % O_2) from postnatal day 1 (P1) to P14. Starting from P15 all animals were exposed to 21% O_2 until P28; β-actin served as the loading control. Immunoblot analysis (left) and gene expression (right) of PAI-1. Mean±SEM; (n = 5/group); non-parametric Mann-Whitney

4.3.3 Mesenchymal and endothelial Markers

Cluster of differentiation 31 (CD31): CD31, also referred to as platelet endothelial cell adhesion molecule 1 (PECAM-1) is expressed in blood cells and vascular cells. PECAM-1 regulates vascular barrier function and also has been reported to mediate leucocyte migration through VE-cadherin [105]. Immunoblots showed a significant increase in the abundance of CD31 in $MMP12^{-/-\ NOX}$ compared to WT^{NOX} (Figure 18, A).

Vascular endothelial (VE) cadherin: VE-cadherin is an essential protein that is required for the maintenance of endothelial cell contacts and also engages in the regulation of certain cellular processes (e.g., cell proliferation, apoptosis) as well as the modulation of VEGF receptor functions [106]. Assessment of VE-Cadherin protein abundance in total lung homogenate using immunoblot showed a significant increase in protein production in $MMP12^{-/-\ NOX}$ compared to WT^{NOX} and to $MMP12^{-/-\ HYX}$ (Figure 18, B).

Alpha-smooth muscle actin (α-SMA): α-SMA is used as a marker for myofibroblasts, which are typically present in all fibrotic tissues or diseases (e.g., granulation tissue, idiopathic pulmonary fibrosis) [107]. Having qRT-PCR results revealing an increase in *Acta2* gene expression in the

MMP12$^{-/-HYX}$ group; no statistically significant difference was found among the four groups via immunoblotting (Figure 18, C).

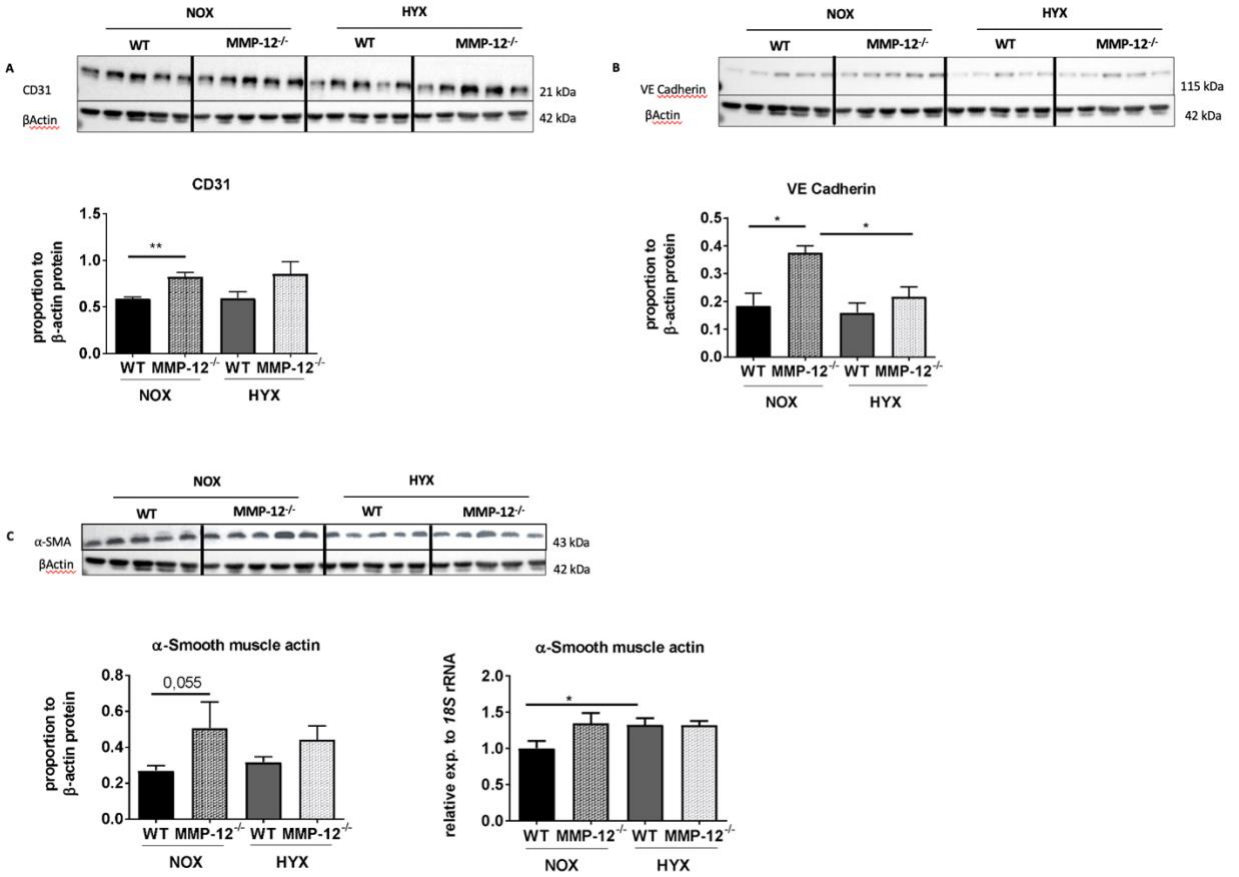

Figure 18. Measurement of protein abundance: Wildtype (WT) and MMP-12 knockout mice (MMP12$^{-/-}$) were exposed to hyperoxia (HYX, 85 % O_2) or normoxia (NOX, 21 % O_2) from postnatal day 1 (P1) to P14. Starting from P15 all animals were exposed to 21% O_2 until P28. Immunoblots show stromal markers at P28; β-actin served as loading control. A: Immunoblot of CD31 protein as an indicator of endothelial cells, B: VE-Cadherin a regulator of endothelial cell integrity, C: Immunoblot (left) and gene expression (right) of αSMA as a marker of myofibroblasts. Mean±SEM; (n = 5/group); non-parametric Mann-Whitney test; *p<0,05; **p<0.01

4.3.4 Transcription Factors

Signal transducer and activator of transcription 3 (STAT3): Signal transducer and activator of transcription 3 (STAT3) is a transcription factor, functioning similarly to STAT1, and known as an intracellular mediator of inflammatory cytokines, including IL-6 [108]. Immunoblot results showed significant decrease in the protein abundance of both STAT3 and pSTAT3 in MMP12$^{-/-HYX}$ compared to MMP12$^{-/-NOX}$; while no difference in their activation ratio (pSTAT3/STAT3) was determined among four groups (Figure 19, A).

Mothers against decapentaplegic homolog 2/3 (SMAD2/3): Mothers against decapentaplegic homolog 2 (SMAD2) is a transcription factor that mediates the signal of the TGFβ, and thus plays a role in the regulation of multiple cellular processes, such as cell proliferation, differentiation, or apoptosis [109]. Immunoblot results demonstrated a significant decrease in SMAD2 protein in MMP12$^{-/-HYX}$ compared to MMP12$^{-/-NOX}$ (Figure 19, B). Immunoblot for pSMAD2 and 3 did not yield any conclusive results and is therefore not depicted.

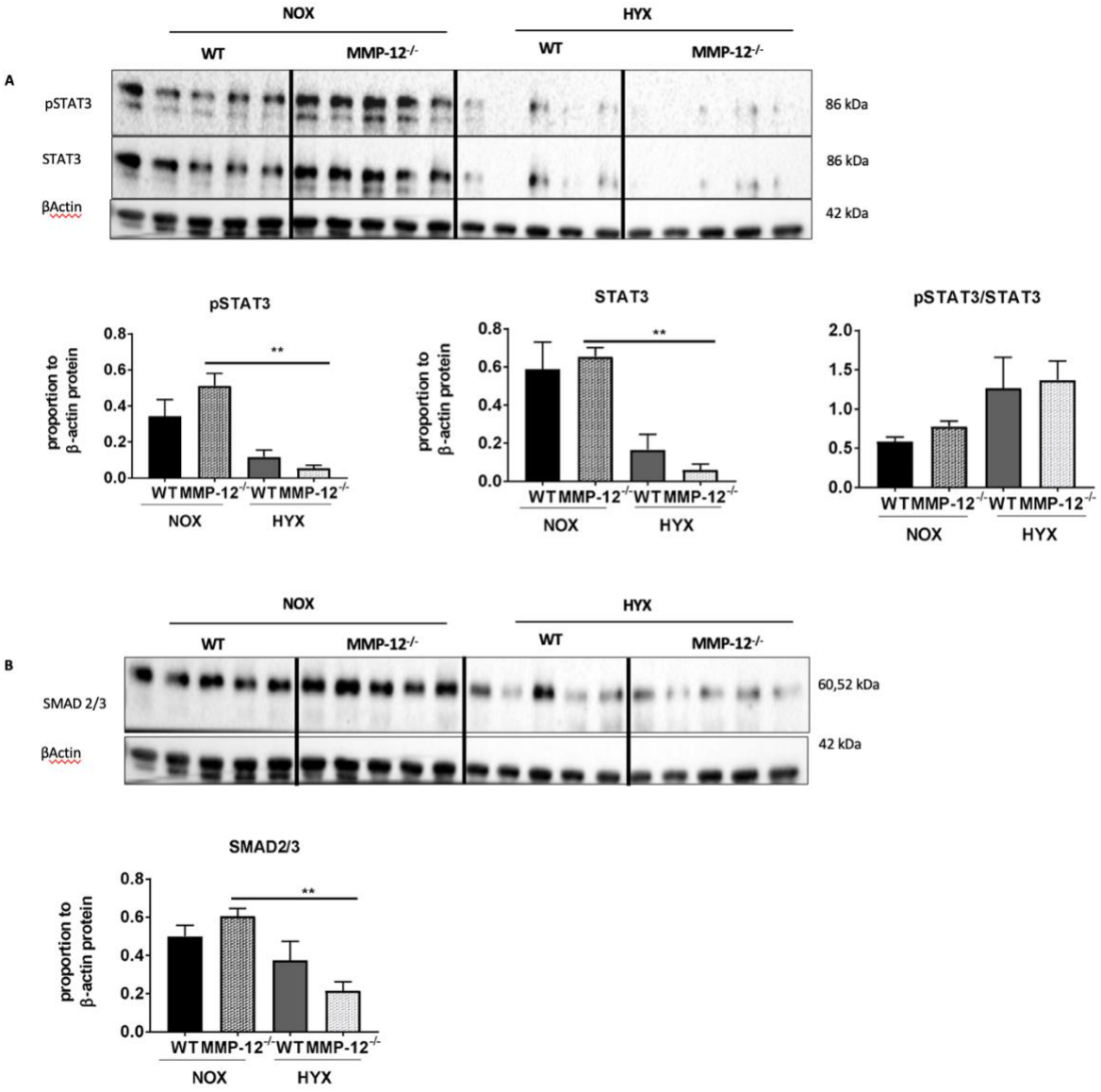

Figure 19. Measurement of protein abundance: Wildtype (WT) and MMP-12 knockout mice (MMP12$^{-/-}$) were exposed to hyperoxia (HYX, 85 % O_2) or normoxia (NOX, 21 % O_2) from postnatal day 1 (P1) to P14. Starting from P15 all animals were exposed to 21% O_2 until P28. Immunoblots show transcription factors at P28; β-actin served as loading control. A: Phosphorylated and total STAT3 (pSTAT3, STAT3); densitometric summary data show pSTAT3 relative to total STAT3 (pSTAT3/STAT3). B: SMAD2/3. Mean±SEM; (n = 5/group); non-parametric Mann-Whitney test; *p<0,05; **p<0.01.

4.3.5 Proteins Regulating Cell Cycle and DNA Metabolism

Proliferating cell nuclear antigen (PCNA): Proliferating cell nuclear antigen (PCNA) has a key role in nucleic acid metabolism and cell replication [110]. Immunoblot results showed no significant difference among the four groups (Figure 20, A).

Caspase-3: Caspases are central components of the machinery responsible for apoptosis. In the apoptotic cell, cleavage of caspase-3 executes cell death via cytoskeletal and nuclear protein degradation and causing DNA fragmentation [111]. Immunoblot results revealed no marked difference in Caspase 3 abundance between WT and MMP12$^{-/-}$. (Figure 20, B).

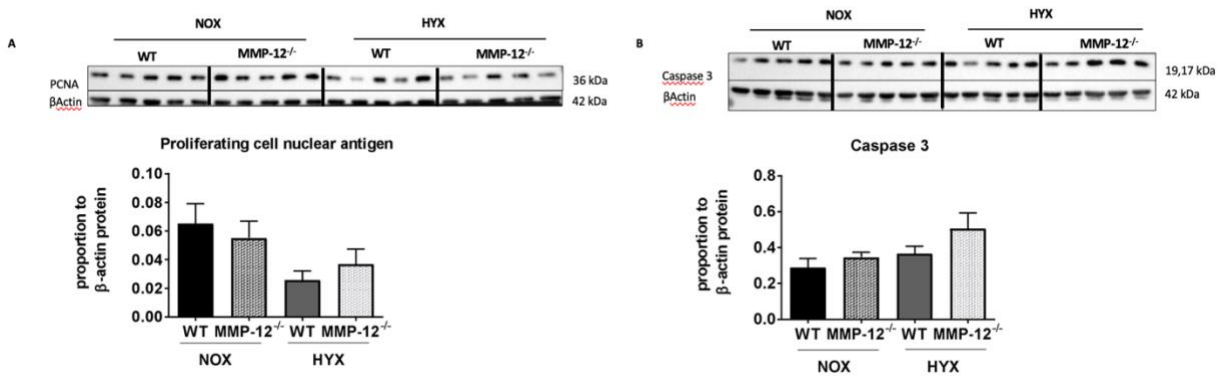

Figure 20. Measurement of protein abundance: Wildtype (WT) and MMP-12 knockout mice (MMP12$^{-/-}$) were exposed to hyperoxia (HYX, 85 % O_2) or normoxia (NOX, 21 % O_2) from postnatal day 1 (P1) to P14. Starting from P15 all animals were exposed to 21% O_2 until P28. Immunoblots show proteins that regulate cell cycle and DNA metabolism. A: Proliferating cell nuclear antigen (PCNA) B: Caspase 3. Mean±SEM; (n = 5/group); non-parametric Mann-Whitney test; *p<0,05; **p<0.01.

5. Discussion

Premature newborns frequently develop respiratory adaptive disorders as a result of their immature lungs, requiring medical interventions such as oxygen support or mechanical ventilation. However, these respiratory supportive measures potentially have serious consequences for the developing lung. Although the impact of hyperoxia on lung development has been extensively studied over the last decades, no definitive pathomechanism has been identified yet. Previous studies showed that hyperoxia leads to a reduced number of alveoli and an increased alveolar wall thickness [112,113] due to excessive inflammation, apoptosis of alveolar cells and fibrotic changes [26,32]. These pathological conditions limit the normal development of the preterm lung, thus contributing to the phenotype of BPD.

The development of the lung is not completed at birth and continues throughout infancy which is the last stage of lung development known as 'the alveolar stage'. In this phase of lung development, formation of the alveoli and the pulmonary vascular bed takes place, and the gas-air exchange surface maturates [114]. Premature infants are at an increased risk of developing BPD due to the interruption of normal lung development before the alveolar stage. As a result of this interruption, morphological changes such as fewer alveoli with enlarged air spaces, decreased radial alveolar count and number of secondary crests as well as thinner interstitia are observed [115]. Both old and new BPD exhibit reduced alveolar formation, decreased lung growth and increased pulmonary vascular resistance, resulting in structural changes similar to those seen in emphysema and COPD, thereby emerging as a growing risk factor for adult chronic lung diseases [112,116]

As previously described, MMP-12 is upregulated in epithelial cells under pathological conditions, such as hyperoxia, and the overexpression of MMP-12 has been linked to inflammation-induced lung remodeling [117]. The damaged lung tissue triggers an inflammatory response that ultimately accelerates the process. These morphological changes and arrest of alveolar growth are associated with diminished pulmonary vasculature which has been implicated in the pathogenesis of BPD [118].

The underlying mechanism by which MMP-12 contributes to the pathology of neonatal chronic lung disease has not yet been established. MMPs play critical roles in the normal turnover of connective tissue during morphogenesis, tissue development, wound healing, and reproduction [119] as well as regulation of inflammation and innate immunity by activating, deactivating, or altering

the activity of signaling cytokines, chemokines, and receptors [120]. Since these are key processes disrupted in lungs with clinical or experimental BPD, the overall goal of the present study was to gain a deeper understanding of the functional role of MMP-12 in hyperoxia-induced lung injury as a model for BPD. This was investigated in a murine model of hyperoxia-induced neonatal lung damage. In order to investigate whether MMP-12 plays a role in the pathogenesis of the lungs after hyperoxia damage, MMP-12 deficient mice [81], as described previously, were used [121].

In brief, the goal of this study was to test if loss of MMP-12 using a genetic modified mouse protects from hyperoxia-induced arrest of alveolar and microvascular formation, and matrix remodeling.

Loss of MMP-12 promotes alveolarization

Numerous studies demonstrated that hyperoxia results in a reduced radial alveolar count, increased alveolar surface area, and increased alveolar septal thickness [113,122]. This phenomenon was also shown in our present animal model. At P28, significant quantitative histomorphological differences were evident between the lungs of WT^{NOX} and WT^{HYX}. The group of WT mice exposed to hyperoxia had a significantly higher MLI and septal thickness than the WT mice maintained under normoxia. Moreover, the average alveolar surface area of a single alveolus was three-fold higher and the radial alveolar count was reduced by 50% in WT^{HYX} when compared to WT^{NOX}, similar to previous data in the literature [123,124].

Although the role of MMP-12 has been studied in various diseases and conditions (e.g., emphysema, cigarette smoke exposure, asthma, chronic obstructive pulmonary disease) little is known about the regulation of MMP-12 in the context of BPD [117,125]. Consistent with our hypothesis that loss of MMP-12 is protective, we observed an attenuation of hyperoxia-induced lung growth arrest in the $MMP\text{-}12^{-/-}$ group. Specifically, the RAC was higher and the MLI as well as the average alveolar surface area of a single alveolus were significantly lower in $MMP\text{-}12^{-/-}$ mice after hyperoxia than in WT^{HYX} mice. These histomorphometric findings suggest that global knockout of MMP-12 reduces lung injury by mitigating the pathological impact of prolonged exposure to oxygen on alveolar growth.

While MMPs are well-known for their function in ECM degradation and turnover, recent studies showed that MMPs also play a role in immunity and repair [126]. In our study, we showed that global

knockout of MMP-12 improves lung morphology, highlighting the importance of MMP-12 in lung development. These data could also indicate that down regulation of MMP-12 might promote tissue regeneration. Nevertheless, further studies are necessary to understand the precise molecular and cellular mechanisms by which blockage of MMP-12 activity is protective for lung development.

Although it was not the primary goal of this study, it is noteworthy the results of our direct comparison of the histological structure of mouse lungs between WT- and MMP-12-deficient mice under normoxia. We observed no significant difference when the MLI, RAC and average alveolar surface are of MMP-12$^{-/-}$ were compared to WT mice, illustrating a similar lung development consistent with other studies [127,128]. Interestingly, MMP-12$^{-/-}$ mice had significantly reduced septal thickness compared to WT mice even though the opposite, i.e., increased ST on MMP12$^{-/-HYX}$ compared to WT^{HYX}, was detected in the hyperoxia group.

These data demonstrate a remarkable difference in ST at physiologic and pathologic oxygen exposure when MMP-12 is not present. Similarly, in another study in which guinea pigs were chronically exposed to smoke, animals treated with MMP-12 inhibitors had a decreased mean airway wall thickness. Also, similar to our findings, treated animals showed a significant protection in airspace size as well as surface to volume ratio [129], indicating that they were protected from small airway remodeling. A separate study is required to understand how the mechanisms by which MMPs regulate airway remodeling.

MMP-12 deficiency promotes the expression of surfactant proteins and might protect type II alveolar epithelial cells from hyperoxia.

Changes in epithelial cell function lead to a wide range of acute and chronic lung diseases, as epithelial cells are both a target of injury and a key regulator of disease and lung repair [130]. AECIIs play an important role in normal pulmonary function, such as synthesis and secretion of surfactant and regeneration of the alveolar epithelium. The data derived from western blotting and qRT-PCRs might indicate an improved homeostasis and survival of AECIIs. For example, both surfactant protein B and C gene (*Sftpb* and *Sftpc*) expression were significantly increased MMP-12$^{-/-}$ mice, especially under hyperoxia. SFTPC, in particular, is a specific marker for AECIIs [104] whereas SFTPB is required for pulmonary function at birth. It is known that mutation in the *Sftpb* causes SFTPB deficiency, leading to a type of respiratory failure in newborns [131]. Moreover,

animal experiments show that mice lacking SFTPB die of respiratory distress shortly after birth, despite having normal pulmonary structure [132]. Additionally, we also observed that hyperoxia reduced the expression of *Aqp5*, a surface marker of AECI. Since AECIIs are progenitor cells in the normal lung that allow regeneration of the alveolar epithelium via differentiation into AECIs, reduced expression of *Aqp5* can be possibly due to apoptosis of AECI and/or reduced differentiation of AECII to AECI in MMP-12 deficient mice compared to WT.

Interestingly, we observed a significant increase in the abundance of Caspase-3, a critical enzyme involved in programmed cell death (apoptosis). This finding may be associated with a possible loss of AECIs, as indicated by the reduced expression of *Aqp5* as mentioned above. In the literature findings are contradictory: While some studies demonstrate a link between caspase-3 activation and increased cell death in the presence of hyperoxia [133], others do not [134,135]. Further assessment of cleaved caspase 3, which is indicative of active apoptotic signaling, is necessary to better define the relationship between loss of MMP-12 and apoptosis.

Loss of MMP-12 promotes blood vessel formation

Early observations show that, alveolar capillary formation and alveolar epithelial growth occur concurrently, resulting in the formation of a thin air-blood barrier [1]. However, as a result of hyperoxia with subsequent inflammation, premature infants with BPD have a disrupted pulmonary vasculature with abnormal alveolar development. This compromised parenchymal architecture impairs gas exchange and contributes to cardiopulmonary morbidity beyond the neonatal period and infancy.

To determine the effects of loss of MMP-12 on microvascular formation, vWF staining was performed and microvessels (0-20µm and 20-100µm) were quantified. We observed a significant preservation of microvascular growth in MMP-12$^{-/-}$ mice exposed to hyperoxia when compared to WT mice. These quantitative histomorphometric data support the aforementioned literature [34]. Development of pulmonary hypertension, another significant feature of BPD, however, could not be evaluated using this staining method.

In addition to the histological findings, gene expression of *Vegfa* was examined. Previous studies demonstrate that the lung epithelium of the infants with BPD contains little or no *Vegf* gene expression and their pulmonary vasculature lacks VEGF receptors [136]. Moreover, administration

of VEGF reduces the adverse effects of hyperoxia and promote alveolarization [137]. Although no significant changes were observed in the gene expression of *Vegfa* among four groups, protein abundance of VE-Cadherin, which is an endothelial cell marker and a modulator of VEGF, was significantly higher in both $MMP12^{-/-NOX}$ and $MMP12^{-/-HYX}$, compared to WT^{NOX} and WT^{HYX}, respectively. Furthermore, we have found an increase in the protein abundance of CD31, another marker used to determine pulmonary microvasculature, in $MMP12^{-/-NOX}$ compared to WT^{NOX}. Both of these findings are consistent with a previous study conducted on infants who died with BPD [138], who showed decreased expression of respective markers.

Our present data strongly suggest that loss of MMP-12 promotes microvascular growth. However, as previously discussed, the expression of *Vegfa* might be unaltered in WT and $MMP12^{-/-}$ after hyperoxia due to the recovery in normoxia after P14. Further studies are necessary to understand the factors that promote and direct angiogenesis as well as the relationship between the alveolar and vascular development in the lung.

Loss of MMP-12 reduces macrophage influx into the lung and alleviates inflammation

Based on previous clinical and experimental studies [34,35,138], we hypothesized next that the disruption of normal alveolar and capillary growth was related to an excessive inflammatory response with an imbalance of pro- and anti-inflammatory cytokines, chemokines and growth factors. As BPD develops, an influx of inflammatory cells to the injured lung tissue and a consequent increase in TGF-β secretion are observed [16]. TGF-β is involved in mechanisms that regulate the expression and activity of some MMPs, including MMP-12 [139]. Our data indicate that the upregulation of MMP-12 mediates the influx of macrophages to the inflamed lung tissue, which subsequently causes a further damage and triggers the inflammatory response, therebey accelerating the lung damage.

To determine the effects of loss of MMP-12 on inflammatory processes, CD68 staining was performed and the number of macrophages were quantified. Interestingly, $MMP\text{-}12^{-/-}$ mice were protected from the significant macrophage influx observed in WT mice after hyperoxia, which is in line with a prior study [140]. Intriguingly though, the number of macrophages was slightly, but not significantly higher in $MMP\text{-}12^{-/-NOX}$ mice than in WT^{NOX} mice. This finding, however, does not refer to which macrophage subtype might be predominantly present in WT and $MMP12^{-/-}$ mice. For

example, MMP12 could possibly be involved in macrophage polarization and therefore favor M2-like anti-inflammatory macrophages. Direct evaluation of M1-like and M2-like macrophages, however, was not possible with the immune staining applied in our study. For this reason, gene expression of M1-like and M2-like macrophage markers were examined. Interestingly, M1-like pro-inflammatory *Cxcl10* was significantly increased in both MMP12$^{-/-HYX}$ and WT^{HYX} mice regardless the genetic background, whereas no difference was noted for *Il6* and *Tlr4* expression. On the other hand, we observed an upregulation of the M2-like anti-inflammatory marker *Arg1* in MMP12$^{-/-}$ mice under hyperoxia and normoxia when compared to the respective WT controls. Specifically, the increase in *Arg1* expression was increased in MMP-12$^{-/-HYX}$ compared to WT^{HYX} (p=0,0503). This outcome is consistent with previous research, showing the capability of murine alveolar macrophages expressing high levels of *Arg1* as part of their polarization toward an alternative activation state [141]. This process was triggered in particular by IL-4 and IL-13, two other M2-like macrophage markers, whose expression, however, was not significantly altered in our study in MMP12$^{-/-HYX}$ [142].

Recent findings show that a continuous activation of IL-6/STAT3 signalling in AECIIs induces inflammation as well as development of bronchoalveolar adenocarcinoma [143]. Moreover, a recent study from our laboratory demonstrated that prolonged exposure to hyperoxia induces cytokine-driven inflammation and significantly activates IL-6-STAT3-SOCS3 signalling in lungs of newborn mice, resulting in impaired alveolarization and decreased dynamic compliance [78]. Based on these findings, we further investigated if the loss of MMP-12 affects the IL-6/STAT3 pathway in our animal model.

We observed a reduction in the abundance of both pSTAT3 and STAT3 in MMP12$^{-/-HYX}$ compared to MMP-12$^{-/-NOX}$. Moreover, despite being increased, pSTAT3/STAT was insignificant in MMP12$^{-/-HYX}$ compared to MMP-12$^{-/-NOX}$. A similar pattern in the abundance of STAT3, pSTAT3 and pSTAT3/STAT was observed in WT^{HYX} compared to WT^{NOX}, neither of which was significant. This finding indicates that the STAT3 machinery is downregulated in hyperoxia regardless of the genetic background of the mice, and our data contradicts the previously mentioned findings in the literature [78,143] . Surprisingly, there is also evidence that STAT3 overexpression protects the lung from oxygen-induced lung injury by decreasing MMP production, preventing neutrophil influx into the lung, and promoting surfactant protein and lipid synthesis to maintain alveolar structure [144]. In conclusion, in order to gain a better understanding of STAT3 signaling and its functional impact in neonatal lung injury, it is necessary to conduct more in-depth research on this protein and its

functions, as its activity is closely related to many cytokines (e.g., IL-6, IL-11) as well as growth factors (e.g., TGF-α, epithelial growth factor).

Although both the lung structure (e.g., alveolar formation, vascularization) and number of macrophages evidently pointed out the inflammatory response and showed the adverse effect of hyperoxia on lungs of WT mice, some inconsistent results were observed in the gene expression experiments. A putative explanation of this discrepancy might be the transfer of the mice to normoxia after exposure to hyperoxia from P1 to P14 for recovery until P28. Here, in normoxia between P14 - P28 the gene expression pattern might normalize and differences between WT and MMP12-/- as well as normoxia and hyperoxia might reverse, whereas the histopathological changes remain salient.

Loss of MMP-12 significantly promotes the formation of elastic fibers

The deposition of elastic fibers in the tips of forming alveolar septa shows that elastogenesis plays an important role in alveolar septal formation [30]. Previous studies prove that hyperoxia disrupts the physiological assembly of elastic fibers [11,47]. Disrupted alveolarization or impaired lung function as seen in BPD could thus be attributed to distorted and dysfunctional elastic fibers.

In animal models of BPD, it has been demonstrated that elastic fibers are located in the alveolar walls, rather than in the tips of alveolar septa, and exhibit *brush-like* structure [11]. We hypothesized, that this mislocalization could be due to increased *Eln* gene expression, and therefore changes in the synthesis and assembly of elastic fiber production, together with disrupted cross-linking with collagen, all of which affect elastic fiber localization and deposition in the alveolar septae [11,46].

To determine whether MMP-12 has an effect on the formation of elastic fibers, we stained elastic fibers and quantified their absolute content as well as relative to the lung tissue. We observed a significant increase in the absolute elastic fiber content in both the WT^{HYX} and MMP-$12^{-/-HYX}$ mice under direct microscopy. Additionally, elastic fibers relative to total alveolar tissue was significantly higher in both WT^{HYX} and MMP-$12^{-/-HYX}$ mice. Statistically, $MMP12^{-/-HYX}$ exhibited a higher absolute elastic fiber content and ratio of total tissue/elastic fibers than the WT^{HYX}. Next, we quantified secondary crests, where elastic fibers are typically localized (at the tips) and are crucial in secondary septation. While the quantitative analysis revealed a reduction of secondary crests in both WT and $MMP12^{-/-}$ mice under hyperoxia, we found a partial protection in $MMP12^{-/-HYX}$

compared to WT^{HYX}. This finding is particularly important because, as previously shown [11,12], elastic fiber deposition at the tips of secondary alveolar crests highlight the importance of elastin's role in the formation of new alveoli. Final histomorphometric analysis, consistent with the organization of secondary crests, revealed a more organized assembly of elastic fibers in $MMP12^{-/-HYX}$ compared to WT^{HYX} under direct microscopy. In summary, our findings suggest that changes in elastic fiber synthesis and assembly, in combination with their localization and deposition in the alveolar septae, quality of the elastic fibers are intimately linked to MMP12. These findings are in line with previous research and confirm the profound effect of oxygen on alveolar formation and elastogenesis [11,46].

Because the regulation of the synthesis or breakdown of elastic fiber components by MMP-12 cannot be demonstrated using histomorphometry, the gene expression of elastic fiber-associated genes and proteins involved in the formation of elastic fibers were examined subsequently. In detail, hyperoxia significantly increased the gene expression *Fbln5* in lungs of WT and $MMP12^{-/-}$ mice after hyperoxia. Moreover, the expression of *Mfap4*, whose loss is associated with spontaneous alveolar enlargement [145], is also increased in both $MMP12^{-/-HYX}$ and WT^{HYX}. Increased expression of *Fbln5*, and *Mfap4* in WT^{HYX} can be attributed to hyperoxia-induced increased elastic fiber production. However, further analysis of the enzymes involved in the assembly, such as lysyl oxidases, should be studied in the future. Interestingly, we determined an upregulation of *Fbln4* and *Fbn2* in lungs of $MMP12^{-/-NOX}$ compared to WT^{NOX}. All of these proteins, which are required for the formation, organization, maintenance, and stabilization of elastic fibers and other ECM structures, showed different expression patterns. However, interestingly, the *Eln* gene expression was not markedly altered despite the increase in elastic fiber content in both WT^{HYX} and $MMP12^{-/-HYX}$ mice. This promiscuous data suggests that even though the synthesis and the assembly of elastic fibers are influenced by both hyperoxia and loss of MMP-12, marked difference in the expression of the relevant genes could not be detected, possibly due to the change in extrinsic factors (i.e., transfer from hyperoxia to oxygen concentration of 21%) after P14. These findings highlight that evaluation of gene expression could point out different results, if performed during or right after the injury, which is of great importance for the interpretation of the outcome. Our current findings cannot explain the controversial results regarding the expression of elastogenesis- associated genes in hyperoxia-induced lung injury and the role of MMP-12 in its pathophysiology.

Loss of MMP-12 prevents pathological fibrosis

Hyperoxia-induced lung injury is characterized by disrupted matrix remodeling, inflammation favoring fibrosis, and an increase in septal thickness. According to previous studies, circulating fibrocytes act as mesenchymal progenitor cells that are capable of migrating to the lung and differentiate into fibroblasts or myofibroblasts as a response to inflammation. Both of these cells are the main producers of collagen and elastin, and contribute to fibrotic changes that occur during wound healing [146,147].

To determine whether MMP-12 has an effect on collagen production, we stained collagen and quantified collagen proportions in lung tissue. We observed a significant increase in the collagen content of WT^{HYX} mice compared to WT^{NOX}. $MMP12^{-/-HYX}$, however, were partly protected from a significant increase of total collagen amount after hyperoxia. When WT^{NOX} and $MMP12^{-/-NOX}$ were compared, a similar collagen content was determined in both groups. In $MMP12^{-/-HYX}$, however, total collagen amount was similar to those of WT^{NOX} and $MMP12^{-/-NOX}$ and, more importantly, significantly less than WT^{HYX}. Moreover, we demonstrated that the amount of collagen related to total alveolar tissue was significantly lower in $MMP12^{-/-HYX}$ compared to WT^{HYX}, indicating that pathological fibrosis is attenuated. Our subsequent evaluation using polarization microscope further strengthened our conclusion. Although we have not quantified collagen abundance, we found that $MMP\text{-}12^{-/-HYX}$ mice had less fibrotic remodeling compared to WT^{HYX}, which was also similar to WT^{NOX} and $MMP12^{-/-NOX}$.

Because the regulation of collagen synthesis or breakdown, as well as the effect of MMP-12 cannot be demonstrated using histomorphometry, we next examined gene expressions of collagen and fibrosis-associated genes and proteins. Previous research indicates a distinct increase in the collagen I/collagen III ratio in individuals with BPD [11,47]. Although we could not differentiate different types of collagens through histomorphometry and staining, we found that the gene expression of *Col3a1* was significantly increased in $MMP\text{-}12^{-/-HYX}$ mice when compared to WT^{HYX}, which might possibly indicate that loss of MMP-12 prevents disrupted breakdown of collagen fibers under hyperoxia. We did not observe a similar increasing pattern in the expression of *Col1a1*. This illustrates that the increased collagen I/collagen III ratio in BPD could be possibly reversed by loss of MMP-12.

Numerous pulmonary diseases are characterized by the coagulation cascade with intra-alveolar fibrin deposition, and the plasminogen activator/plasmin system plays a critical role in ECM deposition leading to fibrosis. PAI-1, physiologic inhibitor of plasminogen activators, is required for proper ECM degradation [148]. In certain lung diseases, such as acute respiratory distress syndrome (ARDS) and sarcoidosis, decreased fibrinolytic activity is associated with an increase in *Serpine1* expression as well as RDS and BPD in preterm infants [149,150]. Given the neat collagen distribution and the attenuated fibrosis in MMP12$^{-/-HYX}$ when compared to WT^{HYX}, a decreased expression of *Serpine1* would be expected. However, we did not observe this in our experiment. The gene expression of *Serpine1* was increased in both WT^{HYX} and MMP12$^{-/-HYX}$ when compared to WT^{NOX} and MMP12$^{-/-NOX}$, respectively. However, protein abundance of PAI-1 was significantly lower in MMP12$^{-/-HYX}$ when compared to WT^{HYX}. In summary, these data suggest a possible anti-fibrotic effect of MMP12 deficiency in hyperoxia-induced lung injury.

Loss of MMP-12 prevents activation of TGF-β signaling and epithelial mesenchymal transition

TGF-β expression that is balanced and timed correctly is critical for embryonic and fetal lung development. Previous studies showed that in genetically modified animal models activation of TGF-β generates epithelial-mesenchymal interactions and adversely regulates lung branching morphogenesis and alveolarization. On the other hand, TGF- β and its target genes *Ctgf* as well as *Serpine1* are important in fibrotic tissue remodeling through promotion of fibroblast proliferation and matrix synthesis [151]. Consistently, we also found a decrease in *Ctgf* gene expression in MMP12$^{-/-HYX}$ mice, which could explain the orderly distribution of collagen and possibly reduced fibrosis in their lungs.

Collectively, our findings suggest that loss of MMP-12 prevents pro-fibrotic processes and possibly EMT by preventing a significant increase of *Snail* and *Slug* mRNA expression in MMP12$^{-/-HYX}$ compared to MMP12$^{-/-NOX}$ that is seen in WT mice after hyperoxia. While the slight reduction in the gene expression of E-cadherin was not notable, expression of vimentin, which is an abundant cytoskeletal protein in cells of mesenchymal origin, was significantly reduced in MMP12$^{-/-HYX}$ compared to WT^{HYX}. This finding is particularly important as presence of vimentin has been associated with increased invasiveness of fibroblasts whereas its inhibition is protective against fibrotic injuries [152].

It is well-known that fibroblasts transdifferentiate into myofibroblasts upon activation, resulting in excessive collagen deposition and tissue remodeling [153]. We found no difference in the expression of *Acta2*, which is a marker of myofibroblasts, in either MMP12$^{-/-NOX}$, or MMP12$^{-/-HYX}$. *Acta2* expression was induced in WT^{HYX} compared to WT^{NOX}. Concurrently, the production and deposition were significantly higher in in WT^{HYX} compared to MMP12$^{-/-HYX}$. Interestingly, the abundance of SMA was almost significant (i.e., p= 0,055) in MMP12$^{-/-NOX}$ compared to WT^{NOX}. Although neither group showed pathological fibrosis, histological quantification revealed a discrepancy in the thickness of alveolar septae between MMP12$^{-/-}$ mice (i.e., significantly thin septa in MMP12$^{-/-\ NOX}$ and significantly thick septa in MMP12$^{-/-HYX}$ when compared to WT^{NOX} and WT^{HYX}, respectively). Given that MMP activity is required for the balance of ECM synthesis and degradation, and that MMP gain- or loss-of-function alleles exhibit defects in branching organs [154], it is possible that loss of MMP-12 is associated with fibroblast to myofibroblast transformation, influencing ECM dynamics and resulting in divergent septal formation under different levels of oxygen exposure.

Another consequence of overexpression of TGF-β is the morphological, pathological, and biochemical changes in the postnatal period leading to epithelial-derived alveolar elastogenesis or negatively regulated alveolarization. The downstream effects of TGF-β are mediated by a protein superfamily known as SMADs. Upon their activation in response to TGF-β, the phosphorylated SMAD2 and SMAD3 in the cytoplasm promote the expression of several profibrotic genes, including *Col1a1* and *Col3a1* [155] *Serpine1* [156], *Ctgf* [157], and *Mmp*s [158] . In our study, we demonstrated a significant reduction in protein abundance of SMAD in MMP12$^{-/-HYX}$ compared to MMP12$^{-/-NOX}$, which can in part explain the group's improved alveolar architecture with less remarkable fibrosis. In contrast, a recent study on renal tubular epithelial cells concluded that overexpression of SMAD2 reduced TGF-β-induced SMAD3 signaling, and thus ECM production and fibrosis [159]. Therefore, our finding is currently insufficient to deduce the precise mechanism by which SMAD2 acts on fibrosis, especially because the abundance of SMAD3 was not examined. Additional research is required to fully understand the function of TGF-β/SMAD2/3 signaling in MMP12$^{-/-}$ mice exposed to hyperoxia.

Conclusion

Current knowledge indicates that BPD is a complex disease of multiple etiologies in which MMP-12 could play an important role. In this study, we demonstrate a significant effect MMP-12 deficiency on alveolar and microvascular formation, enabling lung growth under hyperoxia. Additionally, we have shown that loss of MMP-12 reduces inflammation in neonatal lungs exposed to hyperoxia. Based on our present study, these beneficial effects in MMP12$^{-/-}$ mice are most likely related to (1) attenuated macrophage influx and inflammatory response as well as (2) reduced profibrotic processes which collectively improves alveolar structure through facilitating alveolar and vascular formation. Clearly, a significant outcome of this study was our finding of how collagen and elastic fiber production and organization are influenced by MMP12. Specifically, MMP12$^{-/-}$ mice exhibited a less abnormal elastic fiber deposition and pathological fibrosis using collagen content as an indicator. This attenuated matrix remodeling in MMP12$^{-/-}$ after hyperoxia combined with improved pulmonary angiogenesis enabled alveolar growth and ultimately the formation of a more functional air-blood barrier. Finally, we demonstrated that loss of MMP-12 could possibly prevent the activation of TGF-β signaling and the expression of *Serpine1*, *Snail* and *Slug*. These findings together with decreased expression of *Ctgf* and *Vim*, suggest that MMP-12 deficiency might also prevent EMT.

Collectively, our data demonstrate that loss of MMP12 has an anti-inflammatory and anti-fibrotic effect, enabling alveolar and microvascular growth in neonatal lungs with hyperoxia-induced lung injury as a model of BPD. Based on these data, we conclude that MMP-12 constitutes a promising pharmacological target to treat BPD.

6. References:

1. Schittny JC. Development of the lung. *Cell Tissue Res* 2017; 367(3): 427-44.
2. Joshi S, Kotecha S. Lung growth and development. *Early Hum Dev* 2007; 83(12): 789-94.
3. Jeffrey PK. The development of large and small airways. *Am J Respir Crit Care Med* 1998; 157(5 Pt 2): S174-80.
4. Barkauskas CE, Cronce MJ, Rackley CR, et al. Type 2 alveolar cells are stem cells in adult lung. *J Clin Invest* 2013; 123(7): 3025-36.
5. Desai TJ, Brownfield DG, Krasnow MA. Alveolar progenitor and stem cells in lung development, renewal and cancer. *Nature* 2014; 507(7491): 190-4.
6. Smith LJ, McKay KO, van Asperen PP, Selvadurai H, Fitzgerald DA. Normal development of the lung and premature birth. *Paediatr Respir Rev* 2010; 11(3): 135-42.
7. Mammoto A, Mammoto T. Vascular Niche in Lung Alveolar Development, Homeostasis, and Regeneration. *Front Bioeng Biotechnol* 2019; 7: 318.
8. Schittny JC, Mund SI, Stampanoni M. Evidence and structural mechanism for late lung alveolarization. *Am J Physiol Lung Cell Mol Physiol* 2008; 294(2): L246-54.
9. Shi W, Xu J, Warburton D. Development, repair and fibrosis: what is common and why it matters. *Respirology* 2009; 14(5): 656-65.
10. Li DY, Brooke B, Davis EC, et al. Elastin is an essential determinant of arterial morphogenesis. *Nature* 1998; 393(6682): 276-80.
11. Mizikova I, Morty RE. The Extracellular Matrix in Bronchopulmonary Dysplasia: Target and Source. *Front Med (Lausanne)* 2015; 2: 91.
12. Mecham RP. Elastin in lung development and disease pathogenesis. *Matrix Biol* 2018; 73: 6-20.
13. Warburton D, El-Hashash A, Carraro G, et al. Lung organogenesis. *Curr Top Dev Biol* 2010; 90: 73-158.
14. Klingberg F, Hinz B, White ES. The myofibroblast matrix: implications for tissue repair and fibrosis. *J Pathol* 2013; 229(2): 298-309.
15. Rehan VK, Torday JS. The lung alveolar lipofibroblast: an evolutionary strategy against neonatal hyperoxic lung injury. *Antioxid Redox Signal* 2014; 21(13): 1893-904.
16. Oak P, Hilgendorff A. The BPD trio? Interaction of dysregulated PDGF, VEGF, and TGF signaling in neonatal chronic lung disease. *Mol Cell Pediatr* 2017; 4(1): 11.
17. Herriges JC, Yi L, Hines EA, et al. Genome-scale study of transcription factor expression in the branching mouse lung. *Dev Dyn* 2012; 241(9): 1432-53.
18. Mendelson CR. Role of transcription factors in fetal lung development and surfactant protein gene expression. *Annu Rev Physiol* 2000; 62: 875-915.
19. Saito A, Horie M, Nagase T. TGF-beta Signaling in Lung Health and Disease. *Int J Mol Sci* 2018; 19(8).
20. Thebaud B, Ladha F, Michelakis ED, et al. Vascular endothelial growth factor gene therapy increases survival, promotes lung angiogenesis, and prevents alveolar damage in hyperoxia-induced lung injury: evidence that angiogenesis participates in alveolarization. *Circulation* 2005; 112(16): 2477-86.
21. Suki B, Bates JH. Extracellular matrix mechanics in lung parenchymal diseases. *Respir Physiol Neurobiol* 2008; 163(1-3): 33-43.
22. Loffek S, Schilling O, Franzke CW. Series "matrix metalloproteinases in lung health and disease": Biological role of matrix metalloproteinases: a critical balance. *Eur Respir J* 2011; 38(1): 191-208.
23. O'Dwyer DN, Gurczynski SJ, Moore BB. Pulmonary immunity and extracellular matrix interactions. *Matrix Biol* 2018; 73: 122-34.

24. Pasha AB, Chen XQ, Zhou GP. Bronchopulmonary dysplasia: Pathogenesis and treatment. *Exp Ther Med* 2018; 16(6): 4315-21.
25. Mowitz ME, Ayyagari R, Gao W, Zhao J, Mangili A, Sarda SP. Health Care Burden of Bronchopulmonary Dysplasia Among Extremely Preterm Infants. *Front Pediatr* 2019; 7: 510.
26. Thebaud B, Goss KN, Laughon M, et al. Bronchopulmonary dysplasia. *Nat Rev Dis Primers* 2019; 5(1): 78.
27. Organisation WH. WHO: Preterm birth fact sheet. 19 February 2018. https://www.who.int/news-room/fact-sheets/detail/preterm-birth (Last accessed on 12.04.2022)
28. Siffel C, Kistler KD, Lewis JFM, Sarda SP. Global incidence of bronchopulmonary dysplasia among extremely preterm infants: a systematic literature review. *J Matern Fetal Neonatal Med* 2021; 34(11): 1721-31.
29. Coalson JJ, Winter VT, Siler-Khodr T, Yoder BA. Neonatal chronic lung disease in extremely immature baboons. *Am J Respir Crit Care Med* 1999; 160(4): 1333-46.
30. Bourbon J, Boucherat O, Chailley-Heu B, Delacourt C. Control mechanisms of lung alveolar development and their disorders in bronchopulmonary dysplasia. *Pediatr Res* 2005; 57(5 Pt 2): 38R-46R.
31. Hadchouel A, Franco-Montoya M, Delacourt C. Altered lung development in bronchopulmonary dysplasia. *Birth defects research Part A, Clinical and molecular teratology* 2014; 100 3: 158-67.
32. Alejandre-Alcazar MA, Kwapiszewska G, Reiss I, et al. Hyperoxia modulates TGF-beta/BMP signaling in a mouse model of bronchopulmonary dysplasia. *Am J Physiol Lung Cell Mol Physiol* 2007; 292(2): L537-49.
33. Mach WJ, Thimmesch AR, Pierce JT, Pierce JD. Consequences of hyperoxia and the toxicity of oxygen in the lung. *Nurs Res Pract* 2011; 2011: 260482.
34. Alvira CM. Aberrant Pulmonary Vascular Growth and Remodeling in Bronchopulmonary Dysplasia. *Front Med (Lausanne)* 2016; 3: 21.
35. Niedermaier S, Hilgendorff A. Bronchopulmonary dysplasia - an overview about pathophysiologic concepts. *Mol Cell Pediatr* 2015; 2(1): 2.
36. Raoul W, Chailley-Heu B, Barlier-Mur AM, Delacourt C, Maitre B, Bourbon JR. Effects of vascular endothelial growth factor on isolated fetal alveolar type II cells. *Am J Physiol Lung Cell Mol Physiol* 2004; 286(6): L1293-301.
37. Davies PL, Spiller OB, Beeton ML, Maxwell NC, Remold-O'Donnell E, Kotecha S. Relationship of proteinases and proteinase inhibitors with microbial presence in chronic lung disease of prematurity. *Thorax* 2010; 65(3): 246-51.
38. Watterberg KL, Carmichael DF, Gerdes JS, Werner S, Backstrom C, Murphy S. Secretory leukocyte protease inhibitor and lung inflammation in developing bronchopulmonary dysplasia. *J Pediatr* 1994; 125(2): 264-9.
39. Fielding CA, McLoughlin RM, McLeod L, et al. IL-6 regulates neutrophil trafficking during acute inflammation via STAT3. *J Immunol* 2008; 181(3): 2189-95.
40. Cathcart JM, Banach A, Liu A, Chen J, Goligorsky M, Cao J. Interleukin-6 increases matrix metalloproteinase-14 (MMP-14) levels via down-regulation of p53 to drive cancer progression. *Oncotarget* 2016; 7(38): 61107-20.
41. Tasaka S, Inoue K, Miyamoto K, et al. Role of interleukin-6 in elastase-induced lung inflammatory changes in mice. *Exp Lung Res* 2010; 36(6): 362-72.
42. Greenlee KJ, Werb Z, Kheradmand F. Matrix metalloproteinases in lung: multiple, multifarious, and multifaceted. *Physiol Rev* 2007; 87(1): 69-98.
43. Tatler AL, Jenkins G. TGF-beta activation and lung fibrosis. *Proc Am Thorac Soc* 2012; 9(3): 130-6.
44. Roach KM, Feghali-Bostwick C, Wulff H, Amrani Y, Bradding P. Human lung myofibroblast TGFbeta1-dependent Smad2/3 signalling is Ca(2+)-dependent and regulated by KCa3.1 K(+) channels. *Fibrogenesis Tissue Repair* 2015; 8: 5.

45. Chen SJ, Yuan W, Lo S, Trojanowska M, Varga J. Interaction of smad3 with a proximal smad-binding element of the human alpha2(I) procollagen gene promoter required for transcriptional activation by TGF-beta. *J Cell Physiol* 2000; 183(3): 381-92.
46. Mizikova I, Ruiz-Camp J, Steenbock H, et al. Collagen and elastin cross-linking is altered during aberrant late lung development associated with hyperoxia. *Am J Physiol Lung Cell Mol Physiol* 2015; 308(11): L1145-58.
47. Mascaretti RS, Mataloun MM, Dolhnikoff M, Rebello CM. Lung morphometry, collagen and elastin content: changes after hyperoxic exposure in preterm rabbits. *Clinics (Sao Paulo)* 2009; 64(11): 1099-104.
48. Kaarteenaho-Wiik R, Paakko P, Herva R, Risteli J, Soini Y. Type I and III collagen protein precursors and mRNA in the developing human lung. *J Pathol* 2004; 203(1): 567-74.
49. Thibeault DW, Mabry SM, Ekekezie, II, Zhang X, Truog WE. Collagen scaffolding during development and its deformation with chronic lung disease. *Pediatrics* 2003; 111(4 Pt 1): 766-76.
50. Margraf LR, Tomashefski JF, Jr., Bruce MC, Dahms BB. Morphometric analysis of the lung in bronchopulmonary dysplasia. *Am Rev Respir Dis* 1991; 143(2): 391-400.
51. Pierce RA, Albertine KH, Starcher BC, Bohnsack JF, Carlton DP, Bland RD. Chronic lung injury in preterm lambs: disordered pulmonary elastin deposition. *Am J Physiol* 1997; 272(3 Pt 1): L452-60.
52. Salton F, Ruaro B, Confalonieri P, Confalonieri M. Epithelial-Mesenchymal Transition: A Major Pathogenic Driver in Idiopathic Pulmonary Fibrosis? *Medicina (Kaunas)* 2020; 56(11).
53. Deshmukh AP, Vasaikar SV, Tomczak K, et al. Identification of EMT signaling cross-talk and gene regulatory networks by single-cell RNA sequencing. *Proceedings of the National Academy of Sciences* 2021; 118(19): e2102050118.
54. Xu J, Lamouille S, Derynck R. TGF-beta-induced epithelial to mesenchymal transition. *Cell Res* 2009; 19(2): 156-72.
55. Willis BC, Borok Z. TGF-beta-induced EMT: mechanisms and implications for fibrotic lung disease. *Am J Physiol Lung Cell Mol Physiol* 2007; 293(3): L525-34.
56. Pain M, Bermudez O, Lacoste P, et al. Tissue remodelling in chronic bronchial diseases: from the epithelial to mesenchymal phenotype. *Eur Respir Rev* 2014; 23(131): 118-30.
57. Wendt MK, Allington TM, Schiemann WP. Mechanisms of the epithelial-mesenchymal transition by TGF-beta. *Future Oncol* 2009; 5(8): 1145-68.
58. Willis BC, duBois RM, Borok Z. Epithelial origin of myofibroblasts during fibrosis in the lung. *Proc Am Thorac Soc* 2006; 3(4): 377-82.
59. Hirani D, Alvira CM, Danopoulos S, et al. Macrophage-derived IL-6 trans-signaling as a novel target in the pathogenesis of bronchopulmonary dysplasia. *European Respiratory Journal* 2021: 2002248.
60. Auten RL, Jr., Mason SN, Tanaka DT, Welty-Wolf K, Whorton MH. Anti-neutrophil chemokine preserves alveolar development in hyperoxia-exposed newborn rats. *Am J Physiol Lung Cell Mol Physiol* 2001; 281(2): L336-44.
61. Geissmann F, Manz MG, Jung S, Sieweke MH, Merad M, Ley K. Development of monocytes, macrophages, and dendritic cells. *Science* 2010; 327(5966): 656-61.
62. Arora S, Dev K, Agarwal B, Das P, Syed MA. Macrophages: Their role, activation and polarization in pulmonary diseases. *Immunobiology* 2018; 223(4-5): 383-96.
63. Syed MA, Bhandari V. Hyperoxia exacerbates postnatal inflammation-induced lung injury in neonatal BRP-39 null mutant mice promoting the M1 macrophage phenotype. *Mediators Inflamm* 2013; 2013: 457189.
64. Groneck P, Götze-Speer B, Speer CP, Oppermann M, Eiffert H. Association of pulmonary inflammation and increased microvascular permeability during the development of bronchopulmonary dysplasia: a sequential analysis of inflammatory mediators in respiratory fluids of high-risk preterm neonates. *Pediatrics* 1994; 93(5): 712-8.

65. Cox TR, Erler JT. Remodeling and homeostasis of the extracellular matrix: implications for fibrotic diseases and cancer. *Dis Model Mech* 2011; 4(2): 165-78.
66. Scheau C, Badarau IA, Costache R, et al. The Role of Matrix Metalloproteinases in the Epithelial-Mesenchymal Transition of Hepatocellular Carcinoma. *Anal Cell Pathol (Amst)* 2019; 2019: 9423907.
67. Shapiro SD, Hartzell WO, Senior RM. 136 - Macrophage elastase. In: Barrett AJ, Rawlings ND, Woessner JF, eds. Handbook of Proteolytic Enzymes (Second Edition). London: Academic Press; 2004: 540-4.
68. Lanone S, Zheng T, Zhu Z, et al. Overlapping and enzyme-specific contributions of matrix metalloproteinases-9 and -12 in IL-13-induced inflammation and remodeling. *J Clin Invest* 2002; 110(4): 463-74.
69. Molet S, Belleguic C, Lena H, et al. Increase in macrophage elastase (MMP-12) in lungs from patients with chronic obstructive pulmonary disease. *Inflamm Res* 2005; 54(1): 31-6.
70. Joos L, He JQ, Shepherdson MB, et al. The role of matrix metalloproteinase polymorphisms in the rate of decline in lung function. *Hum Mol Genet* 2002; 11(5): 569-76.
71. Houghton AM, Quintero PA, Perkins DL, et al. Elastin fragments drive disease progression in a murine model of emphysema. *J Clin Invest* 2006; 116(3): 753-9.
72. Hunninghake GM, Cho MH, Tesfaigzi Y, et al. MMP12, lung function, and COPD in high-risk populations. *N Engl J Med* 2009; 361(27): 2599-608.
73. Warner RL, Lukacs NW, Shapiro SD, et al. Role of metalloelastase in a model of allergic lung responses induced by cockroach allergen. *Am J Pathol* 2004; 165(6): 1921-30.
74. Hautamaki RD, Kobayashi DK, Senior RM, Shapiro SD. Requirement for macrophage elastase for cigarette smoke-induced emphysema in mice. *Science* 1997; 277(5334): 2002-4.
75. Churg A, Zhou S, Wright JL. Series "matrix metalloproteinases in lung health and disease": Matrix metalloproteinases in COPD. *Eur Respir J* 2012; 39(1): 197-209.
76. Morris DG, Huang X, Kaminski N, et al. Loss of integrin alpha(v)beta6-mediated TGF-beta activation causes Mmp12-dependent emphysema. *Nature* 2003; 422(6928): 169-73.
77. Wang X, Inoue S, Gu J, et al. Dysregulation of TGF-beta1 receptor activation leads to abnormal lung development and emphysema-like phenotype in core fucose-deficient mice. *Proc Natl Acad Sci U S A* 2005; 102(44): 15791-6.
78. Hirani D, Alvira CM, Danopoulos S, et al. Macrophage-derived IL-6 trans-signaling as a novel target in the pathogenesis of bronchopulmonary dysplasia. *Eur Respir J* 2021.
79. Will JP, Hirani D, Thielen F, et al. Strain-dependent effects on lung structure, matrix remodeling, and Stat3/Smad2 signaling in C57BL/6N and C57BL/6J mice after neonatal hyperoxia. *Am J Physiol Regul Integr Comp Physiol* 2019; 317(1): R169-R81.
80. Aristorena M, Gallardo-Vara E, Vicen M, et al. MMP-12, Secreted by Pro-Inflammatory Macrophages, Targets Endoglin in Human Macrophages and Endothelial Cells. *Int J Mol Sci* 2019; 20(12).
81. Shipley JM, Wesselschmidt RL, Kobayashi DK, Ley TJ, Shapiro SD. Metalloelastase is required for macrophage-mediated proteolysis and matrix invasion in mice. *Proc Natl Acad Sci U S A* 1996; 93(9): 3942-6.
82. Hsia CC, Hyde DM, Ochs M, Weibel ER, Structure AEJTFoQAoL. An official research policy statement of the American Thoracic Society/European Respiratory Society: standards for quantitative assessment of lung structure. *Am J Respir Crit Care Med* 2010; 181(4): 394-418.
83. Cardiff RD, Miller CH, Munn RJ. Manual hematoxylin and eosin staining of mouse tissue sections. *Cold Spring Harb Protoc* 2014; 2014(6): 655-8.
84. Segnani C, Ippolito C, Antonioli L, et al. Histochemical Detection of Collagen Fibers by Sirius Red/Fast Green Is More Sensitive than van Gieson or Sirius Red Alone in Normal and Inflamed Rat Colon. *PLoS One* 2015; 10(12): e0144630.

85. Dinger K, Kasper P, Hucklenbruch-Rother E, et al. Early-onset obesity dysregulates pulmonary adipocytokine/insulin signaling and induces asthma-like disease in mice. *Sci Rep* 2016; 6: 24168.
86. Emery JL, Mithal A. The number of alveoli in the terminal respiratory unit of man during late intrauterine life and childhood. *Arch Dis Child* 1960; 35: 544-7.
87. Alcazar MA, Boehler E, Rother E, et al. Early postnatal hyperalimentation impairs renal function via SOCS-3 mediated renal postreceptor leptin resistance. *Endocrinology* 2012; 153(3): 1397-410.
88. Shahzad S, Afzal M, Sikandar S, Afzal I. Polymerase Chain Reaction. *Genetic Engineering - A Glimpse of Techniques and Applications* 2020.
89. Navarro E, Serrano-Heras G, Castano MJ, Solera J. Real-time PCR detection chemistry. *Clin Chim Acta* 2015; 439: 231-50.
90. Espy MJ, Uhl JR, Sloan LM, et al. Real-time PCR in clinical microbiology: applications for routine laboratory testing. *Clin Microbiol Rev* 2006; 19(1): 165-256.
91. Valasek MA, Repa JJ. The power of real-time PCR. *Adv Physiol Educ* 2005; 29(3): 151-9.
92. Alejandre Alcázar MA, Boehler E, Amann K, et al. Persistent changes within the intrinsic kidney-associated NPY system and tubular function by litter size reduction. *Nephrology Dialysis Transplantation* 2011; 26(8): 2453-65.
93. Mahmood T, Yang PC. Western blot: technique, theory, and trouble shooting. *N Am J Med Sci* 2012; 4(9): 429-34.
94. Speer CP. Inflammation and bronchopulmonary dysplasia: a continuing story. *Semin Fetal Neonatal Med* 2006; 11(5): 354-62.
95. Pilecki B, Holm AT, Schlosser A, et al. Characterization of microfibrillar-associated protein 4 (MFAP4) as a tropoelastin-and fibrillin-binding protein involved in elastic fiber formation. *Journal of Biological Chemistry* 2016; 291(3): 1103-14.
96. Lindahl P, Karlsson L, Hellstrom M, et al. Alveogenesis failure in PDGF-A-deficient mice is coupled to lack of distal spreading of alveolar smooth muscle cell progenitors during lung development. *Development* 1997; 124(20): 3943-53.
97. Eriksson JE, Dechat T, Grin B, et al. Introducing intermediate filaments: from discovery to disease. *J Clin Invest* 2009; 119(7): 1763-71.
98. Mendez MG, Kojima S, Goldman RD. Vimentin induces changes in cell shape, motility, and adhesion during the epithelial to mesenchymal transition. *FASEB J* 2010; 24(6): 1838-51.
99. Annegowda VM, Devi HU, Rao K, Smitha T, Sheethal HS, Smitha A. Immunohistochemical study of alpha-smooth muscle actin in odontogenic cysts and tumors. *J Oral Maxillofac Pathol* 2018; 22(2): 188-92.
100. Garg M. Epithelial-mesenchymal transition - activating transcription factors - multifunctional regulators in cancer. *World J Stem Cells* 2013; 5(4): 188-95.
101. Lipson KE, Wong C, Teng Y, Spong S. CTGF is a central mediator of tissue remodeling and fibrosis and its inhibition can reverse the process of fibrosis. *Fibrogenesis & Tissue Repair* 2012; 5(1): S24.
102. Voelkel NF, Vandivier RW, Tuder RM. Vascular endothelial growth factor in the lung. *Am J Physiol Lung Cell Mol Physiol* 2006; 290(2): L209-21.
103. King LS, Nielsen S, Agre P. Aquaporins in complex tissues. I. Developmental patterns in respiratory and glandular tissues of rat. *Am J Physiol* 1997; 273(5): C1541-8.
104. Conkright JJ, Bridges JP, Na CL, et al. Secretion of surfactant protein C, an integral membrane protein, requires the N-terminal propeptide. *J Biol Chem* 2001; 276(18): 14658-64.
105. Arif N, Zinnhardt M, Nyamay'Antu A, et al. PECAM-1 supports leukocyte diapedesis by tension-dependent dephosphorylation of VE-cadherin. *EMBO J* 2021; 40(9): e106113.
106. Vestweber D. VE-cadherin: the major endothelial adhesion molecule controlling cellular junctions and blood vessel formation. *Arterioscler Thromb Vasc Biol* 2008; 28(2): 223-32.

107. Holm Nielsen S, Willumsen N, Leeming DJ, et al. Serological Assessment of Activated Fibroblasts by alpha-Smooth Muscle Actin (alpha-SMA): A Noninvasive Biomarker of Activated Fibroblasts in Lung Disorders. *Transl Oncol* 2019; 12(2): 368-74.
108. Zhong Z, Wen Z, Darnell JE, Jr. Stat3: a STAT family member activated by tyrosine phosphorylation in response to epidermal growth factor and interleukin-6. *Science* 1994; 264(5155): 95-8.
109. Xu L. Regulation of Smad activities. *Biochim Biophys Acta* 2006; 1759(11-12): 503-13.
110. Kelman Z. PCNA: structure, functions and interactions. *Oncogene* 1997; 14(6): 629-40.
111. Elmore S. Apoptosis: a review of programmed cell death. *Toxicol Pathol* 2007; 35(4): 495-516.
112. Alejandre-Alcazar MA, Shalamanov PD, Amarie OV, et al. Temporal and spatial regulation of bone morphogenetic protein signaling in late lung development. *Dev Dyn* 2007; 236(10): 2825-35.
113. Coalson JJ. Pathology of new bronchopulmonary dysplasia. *Semin Neonatol* 2003; 8(1): 73-81.
114. Copland I, Post M. Lung development and fetal lung growth. *Paediatr Respir Rev* 2004; 5 Suppl A: S259-64.
115. Jónsson B, Tullus K, Brauner A, Lu Y, Noack G. Early increase of TNFα and IL-6 in tracheobronchial aspirate fluid indicator of subsequent chronic lung disease in preterm infants. *Archives of Disease in Childhood-Fetal and Neonatal Edition* 1997; 77(3): F198-F201.
116. Davidson LM, Berkelhamer SK. Bronchopulmonary Dysplasia: Chronic Lung Disease of Infancy and Long-Term Pulmonary Outcomes. *J Clin Med* 2017; 6(1).
117. Qu P, Du H, Wang X, Yan C. Matrix metalloproteinase 12 overexpression in lung epithelial cells plays a key role in emphysema to lung bronchioalveolar adenocarcinoma transition. *Cancer Res* 2009; 69(18): 7252-61.
118. Choi CW, Kim BI, Kim HS, Park JD, Choi JH, Son DW. Increase of interleukin-6 in tracheal aspirate at birth: a predictor of subsequent bronchopulmonary dysplasia in preterm infants. *Acta Paediatr* 2006; 95(1): 38-43.
119. Cui N, Hu M, Khalil RA. Biochemical and Biological Attributes of Matrix Metalloproteinases. *Prog Mol Biol Transl Sci* 2017; 147: 1-73.
120. Page-McCaw A, Ewald AJ, Werb Z. Matrix metalloproteinases and the regulation of tissue remodelling. *Nat Rev Mol Cell Biol* 2007; 8(3): 221-33.
121. Kopf M, Baumann H, Freer G, et al. Impaired immune and acute-phase responses in interleukin-6-deficient mice. *Nature* 1994; 368(6469): 339-42.
122. Choi CW, Kim BI, Hong JS, Kim EK, Kim HS, Choi JH. Bronchopulmonary dysplasia in a rat model induced by intra-amniotic inflammation and postnatal hyperoxia: morphometric aspects. *Pediatr Res* 2009; 65(3): 323-7.
123. Mehats C, Franco-Montoya ML, Boucherat O, et al. Effects of phosphodiesterase 4 inhibition on alveolarization and hyperoxia toxicity in newborn rats. *PLoS One* 2008; 3(10): e3445.
124. Wang H, Jafri A, Martin RJ, et al. Severity of neonatal hyperoxia determines structural and functional changes in developing mouse airway. *Am J Physiol Lung Cell Mol Physiol* 2014; 307(4): L295-301.
125. Suzuki R, Miyazaki Y, Takagi K, Torii K, Taniguchi H. Matrix metalloproteinases in the pathogenesis of asthma and COPD: implications for therapy. *Treat Respir Med* 2004; 3(1): 17-27.
126. Fingleton B. Matrix metalloproteinases as regulators of inflammatory processes. *Biochimica et Biophysica Acta (BBA)-Molecular Cell Research* 2017; 1864(11): 2036-42.
127. Bozyk PD, Bentley JK, Popova AP, et al. Neonatal periostin knockout mice are protected from hyperoxia-induced alveolar simplication. *PLoS One* 2012; 7(2): e31336.
128. Jin Y, Liu Y, Nelin LD. Deficiency of cationic amino acid transporter-2 protects mice from hyperoxia-induced lung injury. *Am J Physiol Lung Cell Mol Physiol* 2019; 316(4): L598-L607.

129. Churg A, Wang R, Wang X, Onnervik PO, Thim K, Wright JL. Effect of an MMP-9/MMP-12 inhibitor on smoke-induced emphysema and airway remodelling in guinea pigs. *Thorax* 2007; 62(8): 706-13.
130. Crosby LM, Waters CM. Epithelial repair mechanisms in the lung. *Am J Physiol Lung Cell Mol Physiol* 2010; 298(6): L715-31.
131. Mason RJ, Dobbs LG. 8 - Alveolar Epithelium and Pulmonary Surfactant. In: Broaddus VC, Mason RJ, Ernst JD, et al., eds. Murray and Nadel's Textbook of Respiratory Medicine (Sixth Edition). Philadelphia: W.B. Saunders; 2016: 134-49.e5.
132. Whitsett JA. Surfactant homeostasis: composition and function of pulmonary surfactant lipids and proteins. Fetal and Neonatal Physiology: Elsevier; 2017: 798-808. e1.
133. Dieperink HI, Blackwell TS, Prince LS. Hyperoxia and apoptosis in developing mouse lung mesenchyme. *Pediatr Res* 2006; 59(2): 185-90.
134. Pagano A, Donati Y, Métrailler I, Argiroffo CB. Mitochondrial cytochrome c release is a key event in hyperoxia-induced lung injury: protection by cyclosporin A. *American Journal of Physiology-Lung Cellular and Molecular Physiology* 2004.
135. Guthmann F, Wissel H, Schachtrup C, et al. Inhibition of TNFalpha in vivo prevents hyperoxia-mediated activation of caspase 3 in type II cells. *Respir Res* 2005; 6: 10.
136. Meller S, Bhandari V. VEGF levels in humans and animal models with RDS and BPD: temporal relationships. *Exp Lung Res* 2012; 38(4): 192-203.
137. McGillick EV, Orgeig S, Morrison JL. Structural and molecular regulation of lung maturation by intratracheal vascular endothelial growth factor administration in the normally grown and placentally restricted fetus. *J Physiol* 2016; 594(5): 1399-420.
138. Bhatt AJ, Pryhuber GS, Huyck H, Watkins RH, Metlay LA, Maniscalco WM. Disrupted pulmonary vasculature and decreased vascular endothelial growth factor, Flt-1, and TIE-2 in human infants dying with bronchopulmonary dysplasia. *Am J Respir Crit Care Med* 2001; 164(10 Pt 1): 1971-80.
139. Krstic J, Santibanez JF. Transforming growth factor-beta and matrix metalloproteinases: functional interactions in tumor stroma-infiltrating myeloid cells. *ScientificWorldJournal* 2014; 2014: 521754.
140. Shipley JM, Wesselschmidt RL, Kobayashi DK, Ley TJ, Shapiro SD. Metalloelastase is required for macrophage-mediated proteolysis and matrix invasion in mice. *Proceedings of the National Academy of Sciences* 1996; 93(9): 3942-6.
141. Munder M, Eichmann K, Modolell M. Alternative metabolic states in murine macrophages reflected by the nitric oxide synthase/arginase balance: competitive regulation by CD4+ T cells correlates with Th1/Th2 phenotype. *J Immunol* 1998; 160(11): 5347-54.
142. Yu H, Yoo PK, Aguirre CC, et al. Widespread expression of arginase I in mouse tissues. Biochemical and physiological implications. *J Histochem Cytochem* 2003; 51(9): 1151-60.
143. Li Y, Du H, Qin Y, Roberts J, Cummings OW, Yan C. Activation of the signal transducers and activators of the transcription 3 pathway in alveolar epithelial cells induces inflammation and adenocarcinomas in mouse lung. *Cancer Res* 2007; 67(18): 8494-503.
144. Lian X, Qin Y, Hossain SA, et al. Overexpression of Stat3C in Pulmonary Epithelium Protects against Hyperoxic Lung Injury. *The Journal of Immunology* 2005; 174(11): 7250-6.
145. Pilecki B, Holm AT, Schlosser A, et al. Characterization of Microfibrillar-associated Protein 4 (MFAP4) as a Tropoelastin- and Fibrillin-binding Protein Involved in Elastic Fiber Formation. *J Biol Chem* 2016; 291(3): 1103-14.
146. Madala SK, Edukulla R, Schmidt S, Davidson C, Ikegami M, Hardie WD. Bone marrow-derived stromal cells are invasive and hyperproliferative and alter transforming growth factor-alpha-induced pulmonary fibrosis. *Am J Respir Cell Mol Biol* 2014; 50(4): 777-86.
147. Lo CY, Michaeloudes C, Bhavsar PK, et al. Increased phenotypic differentiation and reduced corticosteroid sensitivity of fibrocytes in severe asthma. *J Allergy Clin Immunol* 2015; 135(5): 1186-95 e1-6.

148. Liu RM. Oxidative stress, plasminogen activator inhibitor 1, and lung fibrosis. *Antioxid Redox Signal* 2008; 10(2): 303-19.
149. Cederqvist K, Siren V, Petaja J, Vaheri A, Haglund C, Andersson S. High concentrations of plasminogen activator inhibitor-1 in lungs of preterm infants with respiratory distress syndrome. *Pediatrics* 2006; 117(4): 1226-34.
150. Ince DA, Atac FB, Ozkiraz S, et al. The role of plasminogen activator inhibitor-1 and angiotensin-converting enzyme gene polymorphisms in bronchopulmonary dysplasia. *Genet Test Mol Biomarkers* 2010; 14(5): 643-7.
151. Bartram U, Speer CP. The role of transforming growth factor beta in lung development and disease. *Chest* 2004; 125(2): 754-65.
152. Surolia R, Li FJ, Wang Z, et al. Vimentin intermediate filament assembly regulates fibroblast invasion in fibrogenic lung injury. *JCI Insight* 2019; 4(7).
153. Frangogiannis NG. Fibroblast-Extracellular Matrix Interactions in Tissue Fibrosis. *Curr Pathobiol Rep* 2016; 4(1): 11-8.
154. Lu P, Takai K, Weaver VM, Werb Z. Extracellular matrix degradation and remodeling in development and disease. *Cold Spring Harb Perspect Biol* 2011; 3(12).
155. Verrecchia F, Chu ML, Mauviel A. Identification of novel TGF-beta /Smad gene targets in dermal fibroblasts using a combined cDNA microarray/promoter transactivation approach. *J Biol Chem* 2001; 276(20): 17058-62.
156. Dennler S, Itoh S, Vivien D, ten Dijke P, Huet S, Gauthier JM. Direct binding of Smad3 and Smad4 to critical TGF beta-inducible elements in the promoter of human plasminogen activator inhibitor-type 1 gene. *EMBO J* 1998; 17(11): 3091-100.
157. Chen Y, Blom IE, Sa S, Goldschmeding R, Abraham DJ, Leask A. CTGF expression in mesangial cells: involvement of SMADs, MAP kinase, and PKC. *Kidney Int* 2002; 62(4): 1149-59.
158. Leivonen SK, Ala-Aho R, Koli K, Grenman R, Peltonen J, Kahari VM. Activation of Smad signaling enhances collagenase-3 (MMP-13) expression and invasion of head and neck squamous carcinoma cells. *Oncogene* 2006; 25(18): 2588-600.
159. Meng XM, Huang XR, Chung AC, et al. Smad2 protects against TGF-beta/Smad3-mediated renal fibrosis. *J Am Soc Nephrol* 2010; 21(9): 1477-87.

7. Appendix

7.1 Index of Tables

7.2 Index of Figures